DIFFERENT ACID SYSTEMS INTERACTIONS WITH SAND AND CERAMIC PROPPANTS USED IN GRAVEL-PACKED AND FRACTURED WELLS

A Dissertation

by

AHMED ISSAM ELSAYED SALAMA ASSEM

Submitted to the Office of Graduate and Professional Studies of
Texas A&M University
in partial fulfillment of the requirements for the degree of

DOCTOR OF PHILOSOPHY

Chair of Committee,	Hisham A. Nasr-El-Din
Committee Members,	Stephen A. Holditch
	Jerome J. Schubert
	Mahmoud M. El-Halwagi
Head of Department,	A. Daniel Hill

August 2017

Major Subject: Petroleum Engineering

ABSTRACT

Proppants are solid particles, extensively used in hydraulic fracturing operations. These materials possess specific mechanical strength indispensable in keeping induced fractures open, resulting in up-surged well production.

Proppants have different parameters including density, mechanical strength, internal porosity, shape, sieve distribution, and most importantly acid resistance.

The acid resistance of the fracturing proppants, defined as the stability and suitability of proppants when they come into contact with different acids, is an important property. Numerous acids are used during the hydraulic fracturing process to remove the scale and clays affecting the fracture conductivity. Inopportunely, these acids adversely affect the proppants already existing in the fracture. The industry measures the acid solubility of proppants according to the API RP 19C/ISO 13503-2 standard. However, it fails to give any guidance on the anticipated final effect of acid dissolution on the mechanical performance of the tested proppants.

This study investigates different factors affecting the interactions of different acid systems with sand and ceramic proppants under downhole conditions. Solubility experiments were conducted using translucent and aging cells at temperatures up to 350°F. The effects of varying acid system, temperature, soaking time, static, and dynamic conditions were examined. The supernatant of solubility tests was analyzed with Fluorine Nuclear Magnetic Resonance (^{19}F-NMR) to identify the reaction products. Total key cations' concentrations were measured using Inductively Coupled Plasma Optical

Emission Spectroscopy (ICP-OES). Proppants were then analyzed by X-ray fluorescence (XRF) and X-ray diffraction (XRD) to detect their mineral composition. After performing solubility tests, the residual solids were then dried and analyzed using Scanning Electron Microscopes (SEMs) with Energy Dispersive X-ray Spectroscopy (EDS) capabilities. Moreover, the effects of acid dissolution on the mechanical performance of proppants were also tested using an automated load frame.

Experimental results show that monocrystalline sand proppants are soluble in regular mud acid (12.0 wt% HCl, 3.0 wt% HF), with a maximum recorded solubility of 10.0 wt%. Clay-based ceramic proppants are also soluble in mud acid, with much higher acid solubility compared to sand proppants. Proppant pack shows more compaction for clay-based proppants than that of sand proppants prior to and after acid exposure. Bauxitic ceramic proppants have a minimal solubility of 0.5 wt% in 10.0 wt% HCl. The proppant, however, is readily soluble in different mud acid solutions, reaching up to 56.0 wt% dissolution in some extreme cases. The higher solubility of ceramic proppants is attributed to HF attack at the grain boundaries.

Understanding the effects of various acids on natural and synthetic proppants will improve production capabilities by promoting the design of acidizing regimens recommended during hydraulic fracturing operations.

DEDICATION

I dedicate this dissertation to my family for their continuous support and encouragement.

ACKNOWLEDGEMENTS

I would like to thank my committee chair, Dr. Hisham A. Nasr-El-Din, for his continuous encouragement, guidance, and support throughout my time at Texas A&M University. I would like to extend my appreciation to Dr. Stephen A. Holditch, Dr. Jerome J. Schubert, and Mahmoud M. El-Halwagi for serving as committee members. Thanks also go to my friends and colleagues in our big research group, Ms. Gia Alexander for proofreading our work, and the department faculty and staff for making my time at Texas A&M University a pleasant experience. I also want to extend my gratitude to Saint-Gobain Proppants for the support and my appreciation to the McNew Research Laboratory for granting permission to utilize their load frames.

Finally, thanks to my father and mother for their encouragement, patience, and love.

CONTRIBUTORS AND FUNDING SOURCES

Contributors

This work was supervised by a dissertation committee consisting of Professor Hisham A. Nasr-El-Din, Professor Stephen A. Holditch, and Associate Professor Jerome J. Schubert of the Department of Petroleum Engineering and Professor Mahmoud M. El-Halwagi of the Department of Chemical Engineering.

The microstructure analysis and crushing test data for Chapter II were provided by Mr. Raphael Herskovits of Saint-Gobain Proppants.

All other work conducted for the dissertation was completed by the student, under the advisement of Professor Hisham A. Nasr-El-Din of the Department of Petroleum Engineering.

Funding Sources

This work was made possible in part by Saint-Gobain Proppants under Grant Number 28-402305-00001.

NOMENCLATURE

EDS	Energy Dispersive X-ray Spectroscopy
^{19}F-NMR	Fluorine Nuclear Magnetic Resonance
HDC	High-Density Ceramic
HSP	High-Strength Proppant
ICP-OES	Inductively Coupled Plasma Optical Emission Spectrometry
ISP	Intermediate-Strength Proppant
LRC	Liquid Resin Coating
LDC	Low-Density Ceramic
RCP	Resin Coated Proppant
RPM	Revolution per Minute
SEM	Scanning Electron Microscope
Na_3-HEDTA	Trisodium Salt of N-(Hydroxyethyl)-Ethylenediaminetriacetic Acid
UHSP	Ultra-High Strength Proppant
XRD	X-ray Diffraction
XRF	X-ray Fluorescence

TABLE OF CONTENTS

Page

LIST OF FIGURES

Page

LIST OF TABLES

Page

CHAPTER I

INTRODUCTION AND LITERATURE REVIEW

Introduction

Hydraulic Fracturing in Unconventional Resources

Hydraulic fracturing is a well stimulation technique that increases well productivity by creating highly conductive fractures, or channels, in the reservoir rocks[1]. This process normally involves injecting a fluid at rates and pressures high enough to break the formation. Proppant slurries are then pumped into these induced fractures to keep them open where the hydrocarbons production increases significantly. The process combines the interactions of different fluid properties including pressure, viscosity, and leakoff characteristics coupled with the elastic properties of the rock (Brown et al. 2000).

The first fracturing treatment designed for well stimulation was done in the Hugoton gas field in July of 1947. Hydraulic fracturing was elected for that well because of its poor deliverability and lack of productivity. This pioneered an idea about the potential benefits of fracturing compared to acidizing (Gidley et al. 1989).

Hydraulic fracturing is an unparalleled stimulation technique used in the extraction of unconventional energy prospects including, but not limited to, tight sands reservoirs, coalbed methane, and shale gas reservoirs. This can be attributed to the higher depletion rates of oil and gas reserves compared with the discovery of new ones (Zahid et al. 2007).

---

[1] This dissertation follows the style of *SPE Journal.*

These resources have been present since the beginning of time, but their commercial development did not commence until the 1970s when significant natural gas demand increased simultaneously with improvements in completion technologies.

Tight reservoirs are not analogous to one another. For instance, reservoirs can be found in shallow or deep formations, low or high temperature, and in single or multiple layers. As a result, a unique hydraulic fracturing treatment should be meticulously designed and then applied to the different types of reservoirs (Holditch 2006).

Controlling fracture initiation and propagation is of crucial importance to the success of the treatment. Accordingly, multistage fracturing in the openhole, with liners and ball-actuated sliding sleeve systems, is used as an alternative to single-stage fracturing. **Fig. I-1** shows an example of multistage fracturing in the middle Bakken formation.

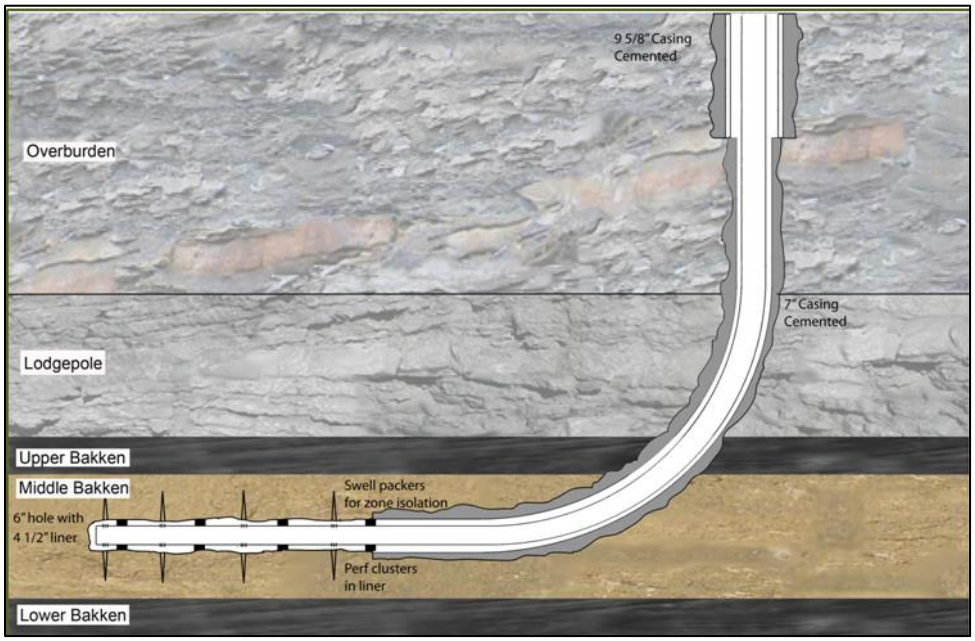

Fig. I- 1— A schematic of a multistage fracture in the middle Bakken formation (Source: EERC).

Gravel-Packed Wells

During drilling operations, formation sand is produced from the breakdown of different lithology. Formation strength stems from the degree of cementation, which took place during rock diagenesis. Gravel packing is a technique which excludes formation sand from the produced fluids. A specific-sized gravel is placed into the well mimicking a downhole filter. This procedure prevents sand from entering the wellbore without hindering fluid production. Gravel packs are performed in both openhole and inside casings. However, the cased hole gravel packing shown in (**Fig. I-2**) is more common as it encounters fewer complications with drilling and completion operations (Penberthy and Echols 1993). The chief objective of gravel packing is to produce high volumes of sand-free fluids for a longer period of time.

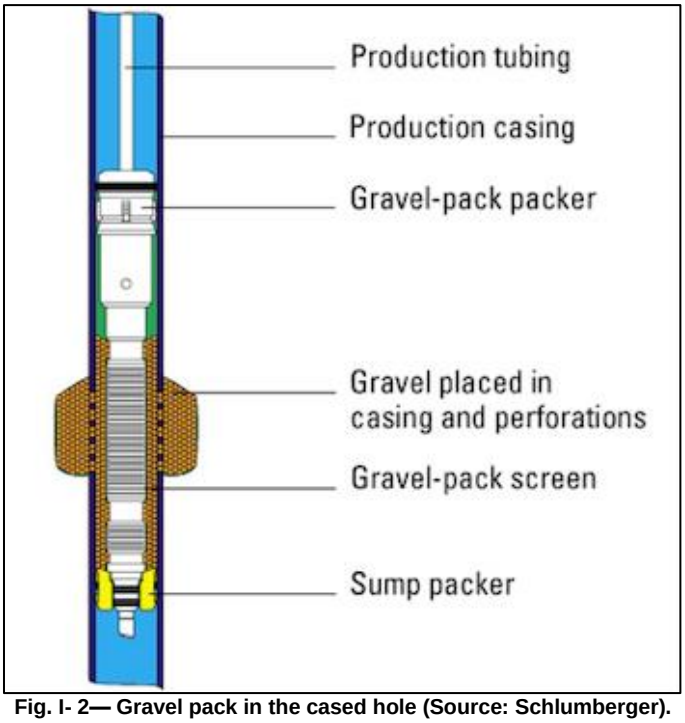

Fig. I- 2— Gravel pack in the cased hole (Source: Schlumberger).

Stanley et al. 2000 reported countless gravel-packed wells worldwide since the technique is reliable and cost-effective for removing formation damage.

According to Penberthy and Cope 1980, sand-filled perforations are the main restriction to flow causing sand plugging to the perforations; they should be avoided to achieve maximum productivity. One way to do so is by pressure-packing the gravel through the perforation so that the permeability of the gravel in the perforation is high enough to prevent sand production.

In 1974, Saucier showed that in order to minimize pack impairment and sand production, the ratio of pack median grain size to formation median grain size should be between 5 and 6. Also, the author noticed that increasing the size and the density of the perforations increased inherent productivity.

Literature Review

A propping agent is placed in the fractures to keep them open after the pressure is released. According to Hellmann et al. 2014, numerous materials are used as proppants including walnut hulls, natural sand, glass, resin-coated sand, and ceramic proppants, i.e., sintered bauxite, clay-based proppants, and fused zirconia. Silica sand 'Frac sand' is principally a graded high-silica content type of quartz sand. The sand typically used in hydraulic fracturing operations is usually processed to achieve a better performance. Not to mention, it is also favored owing to its competitive prices against its counterparts. Processing sand includes, but is not limited to extracting, crushing, cleaning, drying, and grading procedures. There are two main types of sand proppants, chiefly white and brown.

Brown sand contains high concentrations of impurities making it a lower grade and cheaper (Liang et al. 2016).

Using sand proppants is sometimes not the ideal option. In an attempt to enhance hydraulic fracturing conductivity, a resin coated proppant (RCP) type was introduced. The technology is also extended to glass beads and ceramic proppants. To avoid proppant flowback, in practice there are two main advantages for using resins: (1) coating the proppant, which traps broken grain particles inside the envelope, and (2) connecting individual resin grains. These benefits protect the proppants from being crushed, prevent sand production, and resist their embedment in soft formations. Because of the aforementioned reasons, RCP is usually used in tail-in fracturing (Sinclair et al. 1983; Nguyen et al. 1998). Nevertheless, RCP's drawbacks include low softening temperatures and/or low degradation temperatures since the coating material is made of temperature-sensitive polymers.

RCP can be either pre-coated with resin or coated at the well site by liquid resin coating (LRC) systems (Nguyen et al. 1998; Underdown et al. 1980). The coating can either be pre-cured or curable. In the pre-cured RCP case, the resin is applied on silica sand and no further curing will occur downhole. However, in the case of curable RCP, curing is allowed by shutting the well off after the fracturing treatment (Liang et al. 2016). RCP performance depends on resin material properties. The resin material is supposed to crosslink, which disallows melting or flowing when heated. However, softening can still occur at temperatures higher than the Glass Transition Temperature (T_g). Above T_g, the

cured resin changes from a rigid state to more of a compliant state which can be detrimental to the RCP strength (Liang et al. 2016).

Epoxy resins are considered one of the most commonly used resins in coating proppants. These include furan, polyesters, vinyl esters, and polyurethane (Zoveidavianpoor and Gharibi 2015). Specifically, the epoxy polymers are primarily used due to their excellent heat and chemical resistance coupled with mechanical strength. Similarly, furan resins have great heat and water resistance. However, these types of polymers do not provide enough mechanical strength. Moreover, below temperatures of 250°F, polyurethane provides great mechanical strength, good heat and chemical resistance (Davis and Devereux 2007).

The development of deep reservoirs, with high closure pressures of 20,000 psi and above, is a big challenge. Conventional proppants such as sand proppants do not provide the required conductivity (Palisch et al. 2015). Synthetic ceramic proppants were also introduced to the oil industry, displayed in (**Fig. I-3**). Ceramic proppants are typically produced from either bauxite or clay-based sources. Both minerals contain aluminosilicates at different concentrations, more than 70 wt% Al_2O_3 for bauxite minerals while between 40 and 60 wt% for clay minerals (Fuss et al. 2008).

Fig. I- 3— Different types of proppants (Source: Hexion).

Closure stress changes negatively affect proppants. These cyclic stresses, affecting proppants downhole, can cause their failure. Events in the life of the well, including shut-ins due to workovers and connections to a pipeline, lead to cyclic changes in fracture closure stresses (Terracina et al. 2010). In fact, stress changes cause proppant shifts and/or rearrangements, thus decreasing fracture width and generating fines within the proppant pack (Rickards et al. 1998).

Proppant embedment occurs, especially in soft formations. When embedment increases in the proppant pack, the fracture width decreases during these stress cycles (Lacy et al. 1998).

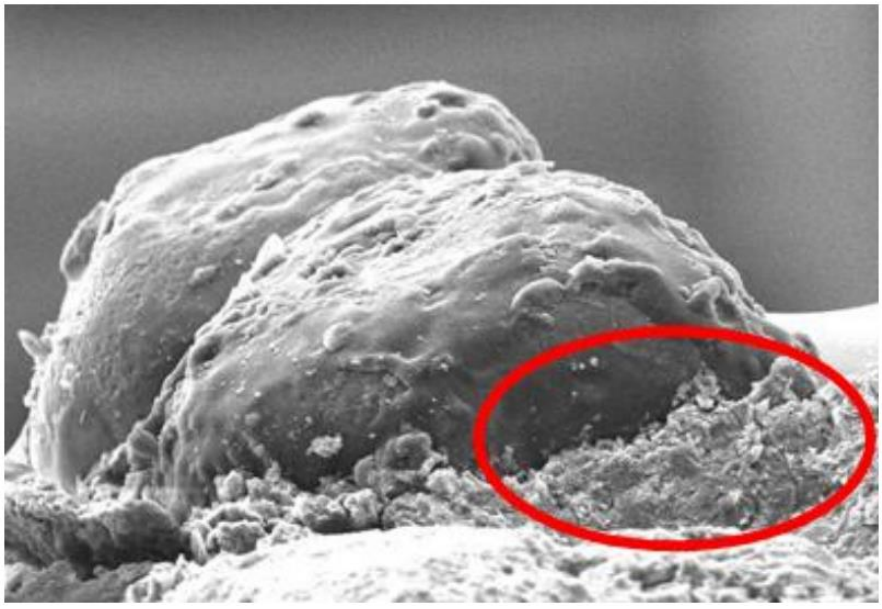

Fig. I- 4— SEM Photo (x514) of formation fines spalling (circled) due to grain embedment (Source: Terracina et al. 2010).

Proppant flowback also causes a reduction in the reservoir productivity shown in (**Fig. I-5**). As previously mentioned, RCPs have grain-to-grain bonding, eliminating proppant flowback. Consequently, a consolidated proppant pack forms in the fracture. The grain-to-grain bonding occurs under different reservoir temperatures and closure stresses (Terracina et al. 2010). Compared to other proppant types, RCPs are more effective in preventing proppant flowback and increasing production (Browne and Wilson 2003).

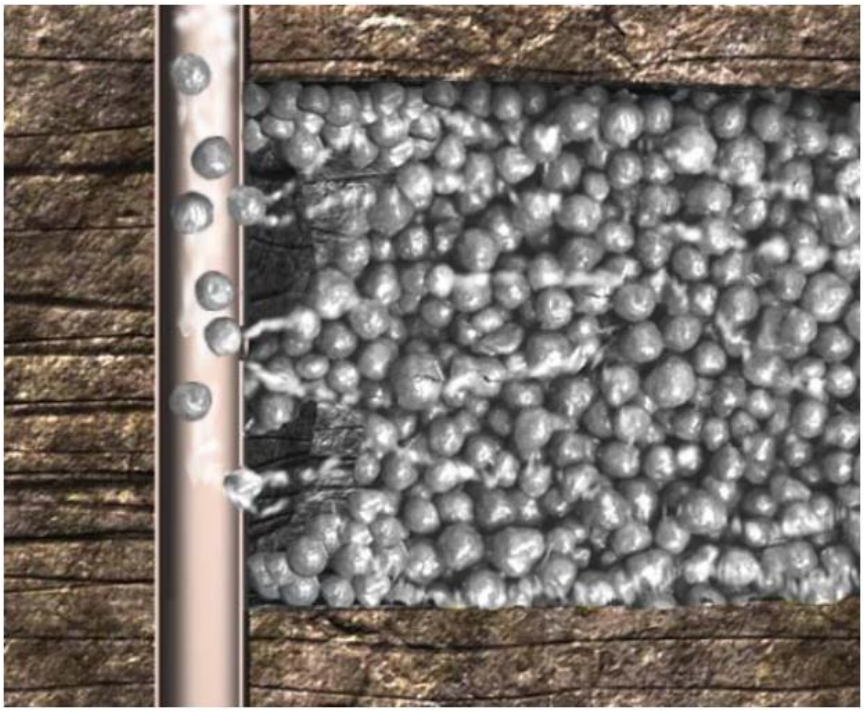

Fig. I- 5— Proppant flowback from the fracture into the wellbore can affect placed proppant (Source: Terracina et al. 2010).

Choosing the proper propping agent depends on all of the aforementioned factors (Terracina et al. 2010). Taking these aspects into account helps to design a successful fracturing job. Moreover, applying good practices and comparing results with public data helps with the proppant selection.

Variable sources or supply points can result in mining anomalies, i.e., size and mineralogical variations. Like any other manufactured product, proppants have some defects. Particle-size and mineral content differences produce deficiencies and contradict widely-accepted published data (Freeman et al. 2009).

Moreover, processing issues including temperature, cooling, resin content, and personnel can adversely affect proppant performance. Transportation abuse of proppant occurs when proppant is transferred multiple times during returns or its movement

between well sites. Pneumatic-discharge pressure can excessively worsen proppant returns. Shortage of available trucking, lack of supervision, and/or driver inexperience can lead the trucking personnel to expedite proppant delivery.

Foreign materials including other proppants, grains, grass, and scale can be introduced as contaminants anywhere along the supply chain during moving, transporting, and shipping proppants. These supply chain issues can adversely affect proppant flow capacity (Stephenson et al. 2003).

All of the previously mentioned issues can severely impact optimum proppant quality and performance.

However, pre-fracturing inspection minimizes these contamination issues. Furthermore, pneumatic handling of proppants can generate fines, affecting their performance. Therefore, collecting a representative sample of all proppants is crucial in evaluating the effectiveness of the fracturing job. Sometimes, on-site testing shows different results compared to public data tested in the laboratory. Conducting these tests, especially before massive jobs, has been proven to reduce the risks of job failures and ensure good results (Freeman et al. 2009).

Proppants have several important properties. These include internal porosity, density, strength, sieve distribution, roundness, and sphericity. Internal interconnected porosity can be defined as the percentage of the pore volume (void volume space) over the total volume of the porous proppant particle. Internal porosity can produce weak points in the proppant structure.

When wells are put back on production, stresses tend to close the fractures that are created and confine the placed proppant. The mechanical strengths of proppants are essential or else, the closure stresses will crush the proppants, creating fines that reduce the permeability and conductivity of the proppant pack. The maximum effective closure stress acting upon the proppant can be described as the difference between the bottomhole fracturing pressure and bottomhole producing pressure (Gulbis and Hodge 2000).

The closure stress depends on different operations performed to the well. For instance, during flowback and testing, the bottomhole producing pressure is usually held constant at low values to increase production rates. Low bottomhole pressure leads to increasing stresses and potentially maximizing proppant crushing. The same situation can also occur when flowing pressure at the perforations is low because, at that time, the fracture gradient is maximized.

Generally, proppants with high strength are more expensive. Strength comparisons between various proppant types are presented in (**Fig. I-6**). Sand proppants can withstand closure stresses up to 6,000 psi. On the other hand, RCPs can handle closure stresses that are less than 8,000 psi. Moreover, Intermediate-strength proppant (ISP) closure stresses can be greater than 5,000 psi, but less than 10,000 psi. Finally, high-strength proppant (HSP) can handle stresses greater than 10,000 psi (Gulbis and Hodge 2000).

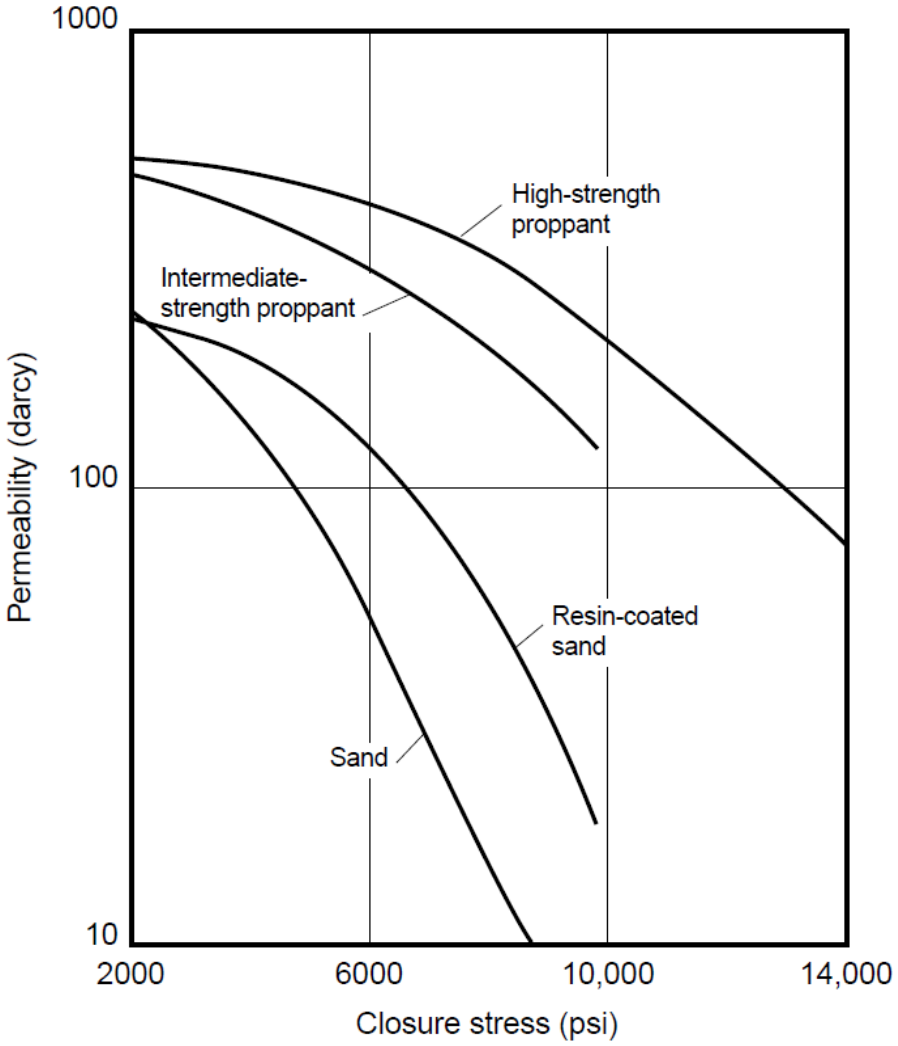

Fig. I- 6— Strength comparison of various types of proppants (Source: Gulbis and Hodge 2000).

Density (apparent specific gravity) is the weight per unit volume of the particles, including the internal porosity. Apparent specific gravity values are determined by the Archimedes method of liquid (water in specific) displacement according to the API RP 60 standard. Based on specific gravity values, there are three main types of proppants: high, intermediate density, and light weight proppants. High-density proppants constitute those having an apparent specific gravity greater than 3.4 g/cm^3. Intermediate density proppants,

on the other hand, are those having apparent specific gravity values between 3.1 and 3.4 g/cm^3. Finally, light weight proppants are those which have an apparent specific gravity less than 3.0 g/cm^3 (Lehman and Cannan 2015). Higher density ceramic proppants (HDC) can provide higher strength while maintaining a higher fracture conductivity when subjected to stress. Low-density ceramic (LDC) produces a fracture that is 30% thicker compared to HDC, despite placing the same weight of the proppant into the fracture. At low stresses, LDC has a better performance than its HDC counterpart because of the width effect (Palisch and Saldungaray 2013).

Sieve distribution represents the size distribution of proppants used and is always defined by a specific range. Usually, 90% of the proppant sample should be within the designated size range. **Table I-1** presents different sieve sizes (proppant particle sizes). In fact, proppant sizes used in fracturing have a max-to-min ratio of 2, as recommended by API. Examples of these include, but are not limited to, 20/40, 30/50, and 40/70 mesh. Sample grading plays an important role in the results of long-term conductivity tests, where stress on proppant is applied and maintained for a duration of 50 hours. Typically, the coarser the proppant sample, the higher the conductivity value (Belyadi et al. 2016).

Sieve Designation		
Standard Sieve Opening, µm	Alternative, Mesh No.	Nominal Sieve Opening, in.
850	20	0.0331
710	25	0.0278
600	30	0.0234
500	35	0.0197
425	40	0.0165
355	45	0.0139
300	50	0.0117
250	60	0.0098
212	70	0.0083
180	80	0.007
150	100	0.0059
125	120	0.0049
106	140	0.0041
90	170	0.0035
75	200	0.0029
63	230	0.0025
53	270	0.0021
45	325	0.0017
38	400	0.0015
32	450	0.0012
25	500	0.001
20	635	0.0008

Table I- 1– Nominal dimensions of standard test sieves (Adapted from ASTM specification E-11).

Roundness and sphericity are similar properties used to characterize the quality of proppants. Roundness merely defines how smooth proppant particles are i.e., the relative sharpness of grains corners. Particle roundness is a direct measure of the distance traveled and the damage done by mishandling during transportation. So, a flat grain can be round, even if it is not spherical. On the other hand, particle sphericity is a measure of how round the particle is (closer to a spherical shape). Sphericity is influenced by several environmental factors, such as erosion, transportation, and depositional patterns. Flat particles would travel differently compared to spherical ones. API recommends that both

proppants' roundness and sphericity values should be at least 0.6. Roundness and sphericity definitions are given by Eqs. I-1 and 2, respectively.

Roundness = (Average Radius of Corners and Edges/Radius of The Maximum Inscribed Circle) . …… (I-1)

Sphericity = $\sqrt[3]{}$ (The Volume of a Particle/The Volume of The Circumscribing Sphere) . …… (I-2)

All of the previously mentioned properties can highly affect fracture conductivity. It can be described as the product of the width of the created fracture and the permeability of the proppant remaining in the fracture.

The composition and microstructure of proppants determine their chemical stability. Ceramic proppants consist of three major phases: corundum, mullite, and silica. These phases are chemically robust as they show different affinities towards HCl and HF.

Silica has a known solubility in HF (Tso and Pask 1982; Liang and Readey 1987). The solubility of corundum and mullite in HF and mud acid are also well documented in the literature. They are relatively inert towards HCl attack, but only corundum is relatively inert towards HF (Grosheva and Mironov 1974). Amorphous SiO_2 or the more general silicate glasses are soluble in HF (Liang and Readey 1987). While crystalline SiO_2 dissolution rates are two to three times slower than those of their amorphous compounds, silicate alumina glasses exhibit dissolution rates that are two to ten times faster than amorphous silica. The dissolution of mullite in HF is lower than crystalline SiO_2 but generally higher than that of corundum (Grosheva and Mironov 1974).

Also, the alumina ceramics' resistance to corrosion/acid dissolution is affected by material purity. Mikeska and Bennison (1999) showed that, in ceramics, the weight measurements and microstructure analysis indicated that HF attacks silicate-based boundaries. Although silica and aluminum have similar dissolution reactions, the rates are different depending on the physical structure. They stated that presence of different oxides could affect the corrosion resistance. Adding MgO at an equimolar ratio with SiO_2 increased the resistance by removing the silicate film at the boundaries by defect compensation mechanism. On the other hand, adding CaO and Na_2O showed little or no effect on corrosion rate. Wu et al. 2013 showed that the presence of silica above 1,000 ppm is detrimental, causing the formation of a silicate-rich glassy phase that can be easily attacked by mineral acids. The poor acid resistance of ceramic proppant mainly results from silicon compounds in the raw material.

Unlike other acids, HF has a special ability to react with silica and silicates, making it an essential component in sandstone acidizing treatments. HF is a weak acid, as it is incapable of keeping reaction products in solution. That is why mud acid was introduced to the oil industry. Despite the significant advancements made in the area of acidizing, treatment success rates have remained fairly low (Nitters et al. 2000). This can be attributed to the precipitation reactions following the dissolution reaction, which requires additional consideration when designing sandstone treatments (Ziauddin 2016). Acid treatment, using mud acid, was reported in fractured and gravel-packed wells for cleanup purposes (Roberts et al. 1990). The filed treatment showed that ceramic proppant was severely attacked by the acid. In 1988, Cheung recommended using mud acids cautiously

in deep wells because they drastically affect the mechanical properties of bauxite. The author mentioned that the contact time between acid-proppant systems should be minimized, or using these acids should be avoided altogether. The size distribution did not change; i.e., more than 90% of the treated proppant retained its original size. On the contrary, gravel-packed wells, with fines generation problems, were successfully treated with a combination of mud acids and clay acid treatments. Moreover, other acid systems containing HF proved effective and economic in removing fines and improving production (Svendsen et al. 1992; Stanley et al. 2000). Welch and Hossaini, 1996, stated that mud acid treatment showed high weight loss, but the compressive strength was minimally affected. Thomas and Suhy (1979) also showed that using fluoboric acid improved the fracture and pack permeability when injected into the propping agents. During hydrolysis, hydrofluoric acid and hydroxyfluoboric acids were released, which reacted with and stabilized the fines generated in the pack. Aluminosilicates are acid-sensitive and their dissolution in the mud acid mixtures, which is a function of their crystalline structure, is usually accompanied by amorphous silica precipitation (Hartman et al. 2006). Other factors affecting the reaction kinetics are acid additives, which can increase acid viscosity or adsorb to the rock surface or both (Nasr-El-Din 2016).

Mud acid—containing HCl—causes problems, including decomposition of clays and precipitation of fluosilicates. Additionally, calcium and magnesium fluorides can precipitate if carbonates are present. Chelating agents, shown in **Fig. I-7**, are aminopolycarboxylic acids which are capable of binding with metal atoms. These acids can replace HCl in mud acid systems or can be used as standalone acids to enhance

permeability (Mahmoud et al. 2011). Also, organic acids, including formic acid (HCOOH), can be used as a preflush or with the main HF stage as an alternative for HCl, in the conventional mud acid system. These weak acids work well at elevated temperatures (Yang et al. 2012).

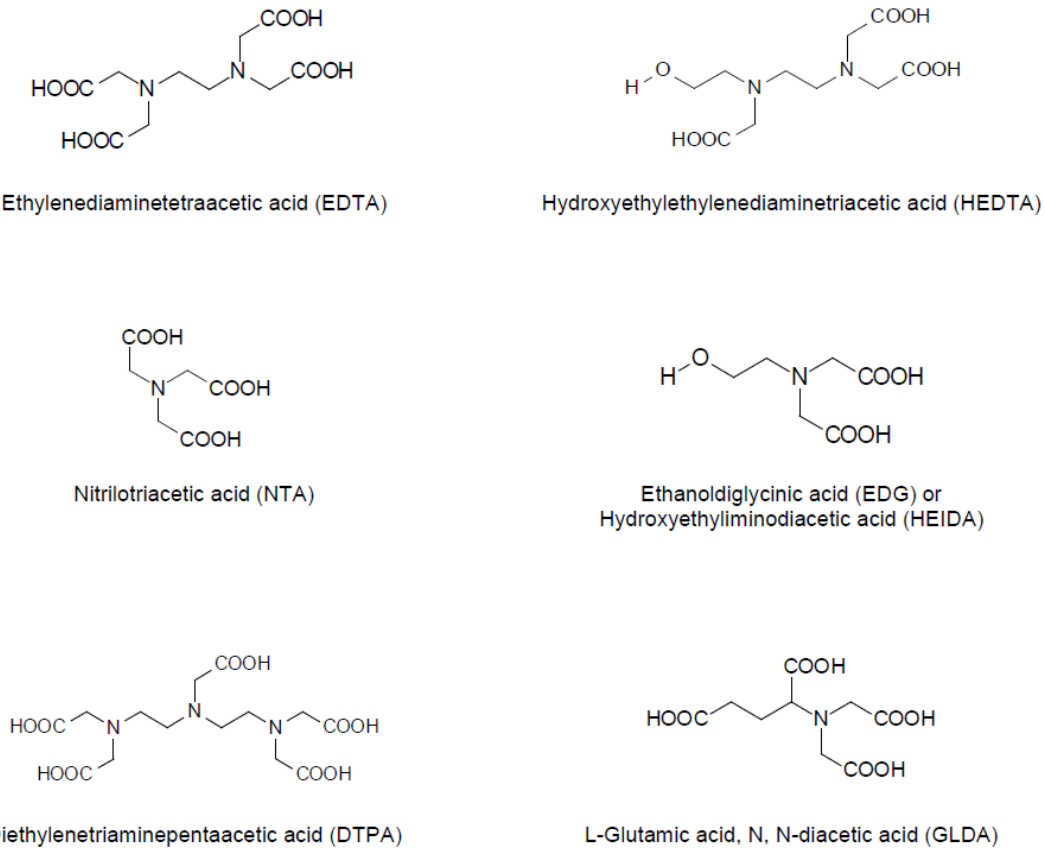

Fig. I- 7— Structures of different chelating agents commonly used in the oil industry.

Fines can migrate and get trapped in the gravel pack. When plugged with these precipitates or formation fines, the gravel pack permeability diminishes, resulting in lower formation productivity (Ravensbergen et al. 2004). Moreover, using water causes some formation damage problems in sensitive layers (Gaurav et al. 2012). The wastewater can

cause dissolution and fines generation, thus impairing the gravel pack via mechanical shearing or loss of coatings. Generating residual solids and filter cake with polymers while using large quantities of water can cause significant damage.

A high-strength proppant may increase the chance of forming fines, which negates its competitive advantage compared to other proppant types. Coating proppants with a hydrophobic film reduces the chemical reaction that results in compaction. Extending the coating to the formation provides the best protection against geochemical reactions (Raysoni and Weaver 2013). The differences in composition between the formation and the alumina-based proppant pack can also generate and/or migrate fines. Proppants can either gain or lose mass depending on the different compositions of both the formation and the proppant (**Fig. I-8**) (Weaver et al. 2010). In addition, fines can be correlated to proppant compaction, which can be defined as the ratio between the current proppant pack height and the initial one, (Stephens et al. 2007). The loss in fracture conductivity can be attributed to proppant degradation. Furthermore, at elevated reservoir temperatures, diagenetic chemistry can occur. A rapid loss in the porosity of the proppant pack due to chemical interactions can take place when exposed to higher temperatures and stresses.

These fluid-fluid and proppant-formation incompatibilities can adversely affect fracture conductivity. The resultant crystalline and amorphous aluminosilicate minerals can fill the pack porosity (Weaver et al. 2007). These factors will further diminish fracture conductivity (Weaver et al. 2007; Weaver and Nguyen 2010).

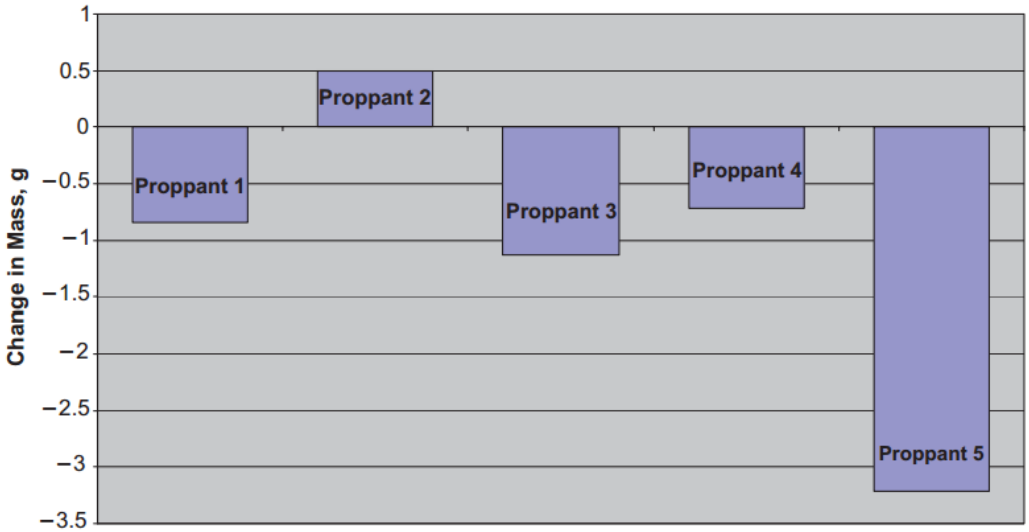

Fig. I- 8— Proppant mass changes during diagenesis testing (Source: Weaver et al. 2010).

The above-mentioned problems are addressed using special chemicals. Gelled water yields wider and shorter fractures, whereas slickwater fracturing results in a longer and skinnier outcome. Slickwater can easily transport light weight proppants. The proppant conductivity decreases with an increase in confining pressure. The conductivity decreases going from a partial monolayer, proppant concentration of 0.07 lbm/ft^2, to monolayer, the concentration of proppant between 0.09 and 0.14 lbm/ft^2, then it increases with increasing proppant concentrations (Gaurav et al. 2012). Owing to the aforementioned reasons, implementing an acid treatment is frequently recommended, in some cases, after placing the proppant in the fracture.

Fuss et al. (2008) showed that while all types of ceramic proppants showed acid solubility lower than 7% under API conditions, their mechanical performance was not proportional to the measured acid solubility number. Post-acid treatment, bauxite-based proppants displayed no change in their mechanical performance, whereas clay-based

proppants experienced substantial degradation. The authors then established that the loss in proppant weight did not necessarily imply a loss of mechanical integrity or proppant conductivity. Crush strength also depends on proppant quality, which may vary. Palisch et al. 2015 stated that ultra-high strength proppant (UHSP) displayed a uniform microstructure, good roundness, and sphericity, and exhibits good conductivity at high closure pressures. Moreover, its acid solubility and erosivity are very low.

In order to select the right proppant, researchers should conduct rigorous quality control and compatibility measures (Weaver et al. 2007; Raysoni and Weaver 2013). Likewise, statistical procedures, where the sample can be tested to determine whether its behavior is unique or is a part of a homogenous distribution, is important in the selection process. These assessments should be implemented when evaluating crush resistance tests to ensure sound results (Stephens et al. 2006). Single-grain crush strength test is used to characterize proppant strength before and after diagenesis. Having reliable data from this test assists in a better understanding of the long-term effects of these mechanical and chemical processes.

Research Problem and Objectives

Previous work reported a narrow spectrum of tests. Some studies investigated the solubility of different proppants at relatively low temperatures without examining its effects on crush resistance (Roberts et al. 1990). Others studied both the solubility and compressive strength of gravel pack. Out of this pool, some showed a direct relationship between solubility and compressive strength (Cheung 1988) while others stated that the

solubility did not produce a concerning compressive strength loss (Welch and Hossaini 1996). Moreover, some results showed that the other HF systems showed promising results in removing fines without negatively affecting the gravel pack (Svendsen et al. 1992; Stanley et al. 2000).

Therefore, the focal objectives of this study are to:

(1) Examine the different factors affecting the acid solubility for sand and ceramic proppants under downhole conditions.

(2) Determine whether there is a relationship between acid solubility and crush resistance.

By completing the above objectives, this research will provide a better selection of proppants used in hydraulic fracturing operations and gravel packing treatments established using experimental work.

CHAPTER II

SOLUBILITY OF SILICATE PROPPANTS IN REGULAR MUD ACID[2]

Experimental Studies

Materials

The HCl solutions were prepared using 36.5 wt% HCl, obtained from Mallinckrodt. The corrosion inhibitor, which was quaternary ammonium compound-based, was obtained from a local service company. The mud acid solutions were prepared using HCl and ammonium biflouride (NH_4HF_2). The deionized water that was used throughout the experiments was obtained from a purification water system with a resistivity of 18.2 MΩ.cm at room temperature. Ottawa sand and clay-based proppant samples were obtained from a local service company. **Table II-1** gives the mineral composition for these proppants.

Mineral	Concentration, wt%	
	Sand Before	Clay-based before
Quartz	>99.00	-
Mullite	-	86.69
Cristobalite	-	13.31
Corundum	-	-

Table II- 1– Mineral composition for different proppants used in the study.

[2] Reprinted with permission from "Mud-Acid Interactions with Sand and Clay-Based Ceramic Proppants Used in Gravel-Packed and Fractured Wells" by Assem, A. I., Nasr-El-Din, H. A., Fuss T. et al. 2017. *SPE Prod & Oper* **32** (2): 196–207, Copyright 2017 by Society of Petroleum Engineers.

Equipment

Aging cells with teflon liners were used to study the reaction between different mud acid solutions and proppants. The cell is a pressure vessel that enables samples to be subjected to temperatures higher than the boiling point of water (above 212°F) and still be maintained in a liquid state. The cells were used for both static and dynamic temperature exposure modes in a roller oven. These liners are suitable for temperatures above 300°F. They also protect steel aging cells from corrosion. The samples were pressurized by nitrogen gas (N_2).

The pH values for spent acid samples were measured. The total concentrations of key cations in the supernatant of solubility tests were measured with the ICP-OES technique. The fluoride complexes in the spent acids were analyzed by ^{19}F-NMR spectroscopy by use of an NMR spectrometer tuned to 300 MHz. 7-cm NMR tubes with deuterated water (D_2O) provided a reference lock to the samples. ^{19}F-NMR chemical shifts were recorded in ppm relative to boron trifluoride etherate by use of the same amount of trichlorofluoromethane as an internal reference standard. Together with the standard NMR, 5 mm polytetrafluoroethylene/fluorinated ethylene polypropylene copolymer tube liners were used to avoid HF reactions with glass. All ^{19}F-NMR measurements were carried out at 75°F.

A crush resistance cell with a 2-in. diameter was used to study the proppants before and after acid exposure. The cell is made of M42 steel with a Rockwell Hardness of 64. A balance recorded the specimen mass to a resolution of ±1 mg. An optical size analyzer measures the size distribution of proppant samples before and after compaction. XRD and

XRF analyses were done for some proppant samples. SEM was used on polished cross sections of both original and acid corroded proppants for microstructure analysis. Also, compositional mapping was performed on polished cross-sections. A different SEM with EDS was also used to determine the elemental analysis of residual solids and crushed proppant samples before and after the acid reaction.

Procedures

Acid Preparation

The regular mud acid solutions were prepared by mixing the corrosion inhibitor with the deionized water, NH_4HF_2, and HCl for at least 15 minutes.

Proppant Preparation

Sieve analysis was conducted for different types of proppants. For consistency, particles of -20+40 mesh size were chosen for all of the aging cell experiments. The sphericity and roundness of proppants were examined in accordance to the API RP 19C/ISO 13503-2 standard. A Zeiss Axiophot optical microscope was used to acquire images of the proppant particles. These images were visually compared to the Krumbein/Sloss diagram (**Fig. II-1**). **Fig. II-2** shows a sample of these photos for different proppants. Both the Ottawa sand and clay-based proppant samples showed good sphericity and roundness with values of approximately (0.7/0.9) and (0.9/0.7), respectively. Sand proppant had a better roundness, while clay-based proppant had a better sphericity. **Table II-2** gives the results of sphericity and roundness (smoothness) analyses.

Proppant Type	Size, µm	Sphericity	Roundness
Sand	425-850	0.7	0.9
Clay-based	425-850	0.9	0.7

Table II- 2– Sphericity and roundness of proppants used in aging cell tests.

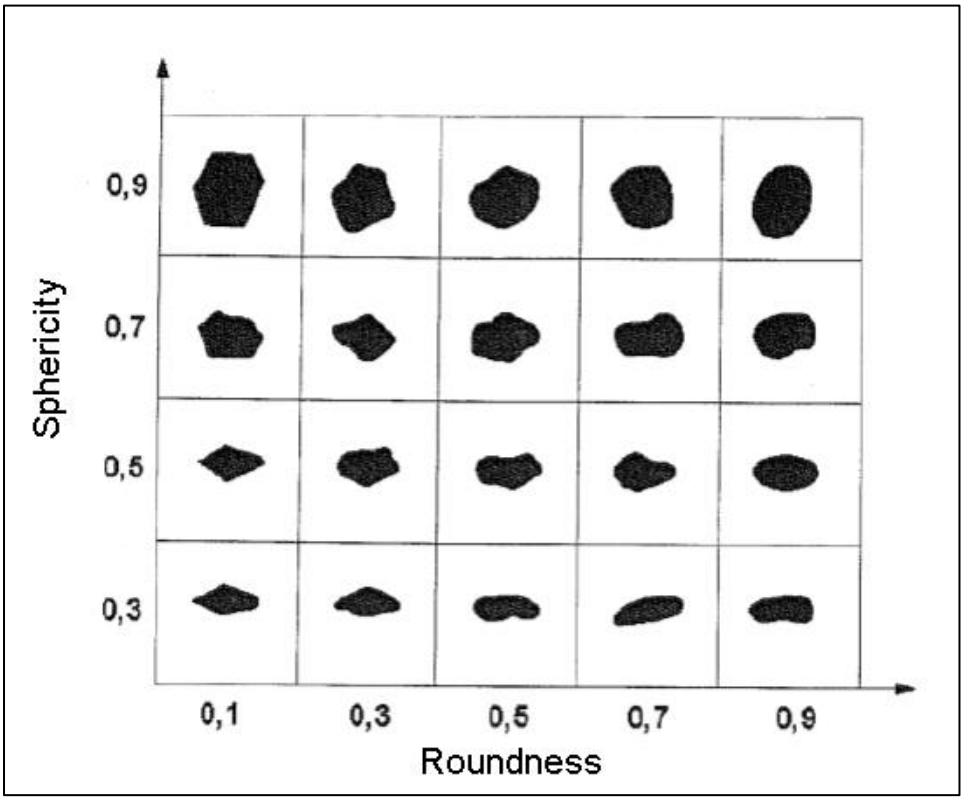

Fig. II- 1— Krumbein/Sloss diagram for visual assessment of sphericity and roundness (The API RP 19C/ISO 13503-2 standard).

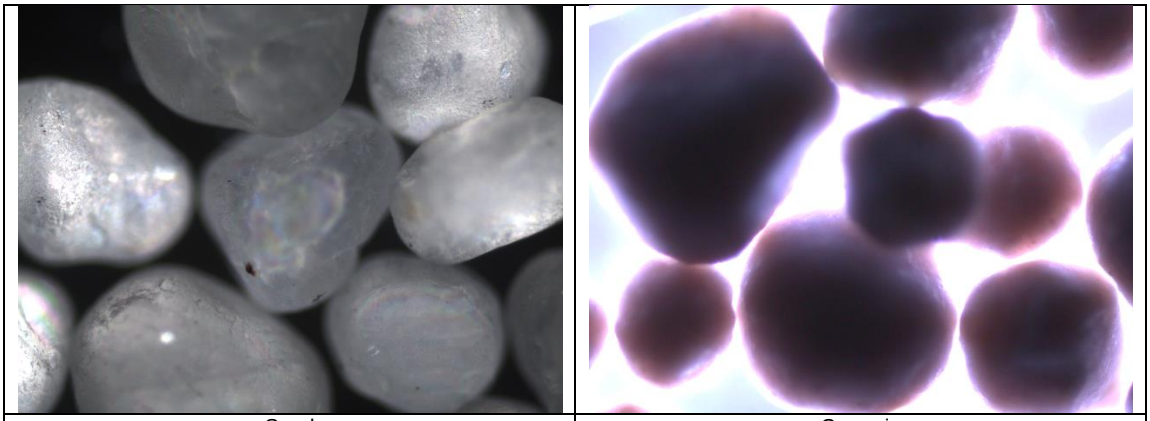

Fig. II- 2— Zeiss Axiophot optical microscope image at 50x magnification of a proppant sample (425–850 µm).

Aging Cell

Sand and clay-based proppant solubility tests in regular mud acid solutions were conducted using the aging cells described in the equipment section. The cells were used for both static and dynamic temperature exposure modes in a roller oven.

Results and Discussion

API Solubility Test

More than 30 experiments were conducted; the collected samples were needed for the crush resistance tests subsequently conducted. Five grams of different proppants were weighed and dried. The proppant was added to plastic beakers containing 100 cm^3 of the regular mud acid solution at room temperature. The beaker was placed in a 66°C (150°F) water bath for 30 minutes without stirring. **Table II-3** gives the average proppant solubility results at 150°F. For the sand proppant type, 0.48 wt% was dissolved while for the clay-based type, a value of 2.39 wt% was achieved. A standard deviation for both

sand and clay-based proppants were found to be 0.007 and 0.015, respectively. However, both proppants showed less than 5.0 wt% weight loss, which meets the industry standards.

Proppant Type	T, °F	Dissolved Proppant, wt%	Standard Deviation
Sand	150	0.48	0.007
Clay-based	150	2.39	0.015

Table II- 3– Average results of API solubility tests for different proppants*.
*The experiments for each proppant were repeated more than thirty times to collect enough sample for crushing tests.

Aging Cell Experiments

Experiments Under Static Conditions

Twenty-five grams of the proppants were used with 200 g of regular mud acid. Several experiments were conducted to study the solubility at different acid soaking times, ranging between 1 and 6 hours at 250-300°F. These experiments were done to simulate soaking conditions where acid diffusion is neglected. Some of the experiments were repeated as many as three times to ensure reproducibility of results. The solutions were then filtered, and the remaining proppants were washed thoroughly with deionized water to remove residual acid. Finally, they were dried at 250°F for at least five hours. The retained weight was then measured. **Tables II-4** and **II-5** summarize the average aging cell results.

For sand and clay-based proppants, acid soaking times of 1, 3, and 6 hours were used. Proppant weights before and after the experiments were tabulated in grams and a percentage of the weight dissolved was calculated.

Soaking Time, hrs	T, °F	Weight Before, g	Weight After, g	Dissolved Proppant, wt%
1		25	24.90	0.40
3	250	25	24.59	1.64
6		25	24.17	3.32
1		25	24.86	0.58
3	300	25	24.53	1.88
6		25	24.06	3.78

Table II- 4– Average results of aging cell experiments for sand proppant at different soaking times under static conditions with regular mud acid*.

*The original sample was -20+40 mesh size standard distribution.

Soaking Time, hrs	T, °F	Weight Before, g	Weight After, g	Dissolved Proppant, wt%
1		25	23.77	4.90
3	250	25	22.84	8.66
6		25	21.49	14.04
1		25	23.73	5.07
3	300	25	21.61	13.56
6		25	21.43	14.28

Table II- 5– Average results of aging cell experiments for clay-based proppant at different soaking times under static conditions with regular mud acid.

Samples of supernatant from solubility tests were analyzed using ICP-OES. **Figs. II-3** through **5** show the concentrations of key elements in the samples after each experiment at 250 and 300°F for sand and clay-based proppants, respectively. The clay-based proppant samples showed high concentrations of aluminum and silicon and small amounts of iron and titanium. Both sets of results show that the solubility increased with increasing temperature. The clay-based proppant samples showed higher total elements' concentration compared to those measured from the sand experiments, indicative of a higher fraction of proppant solubility in acid. However, the amount of silicon dissolved in

clay-based proppants was comparable to that of sand. In clay-based proppants, although the crystals might be somewhat resistant to acid corrosion, HF attacked both silica and mullite ($3Al_2O_3.2SiO_2$), especially at grain boundaries, causing the higher dissolution.

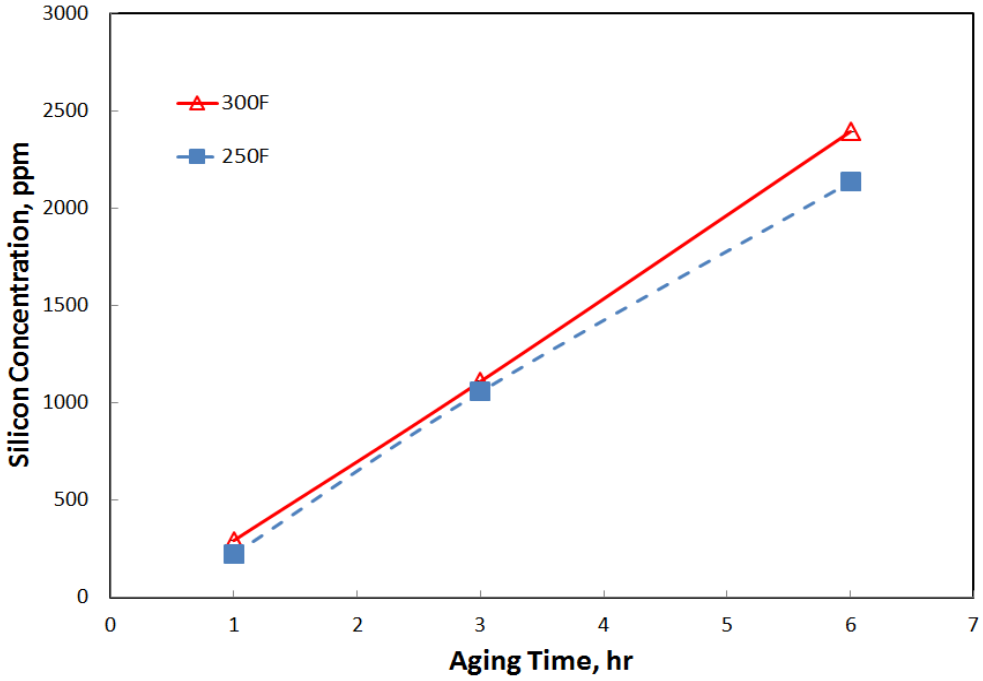

Fig. II- 3— Ion concentration in the supernatant of solubility tests after interaction with sand proppant for different soaking times under static conditions at 250 and 300°F.

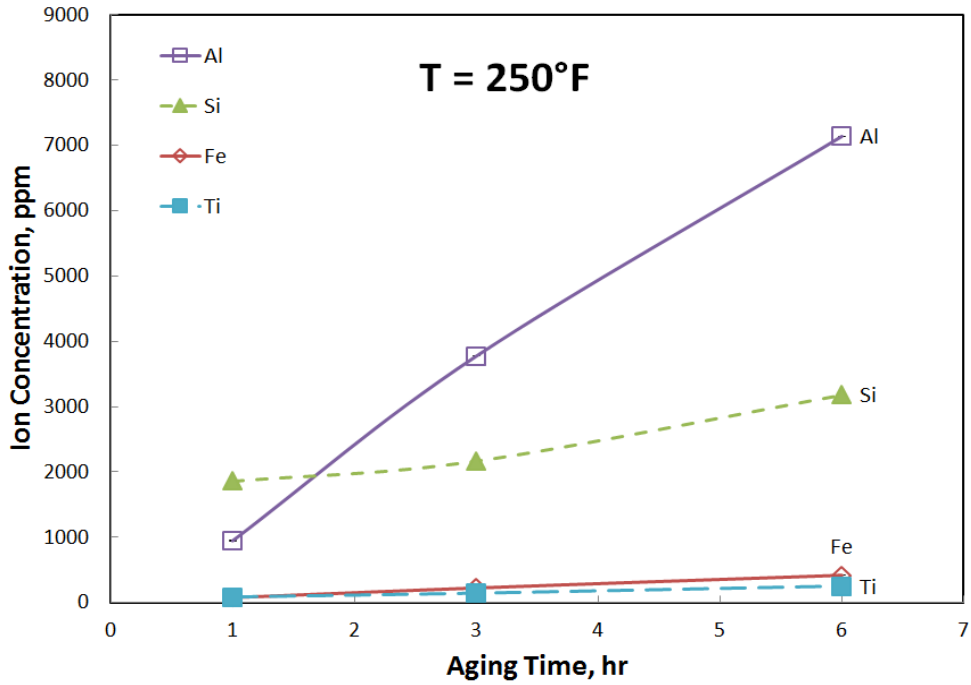

Fig. II- 4— Ion concentration in the supernatant of solubility tests after interaction with clay-based proppant for different soaking times at 250°F under static conditions.

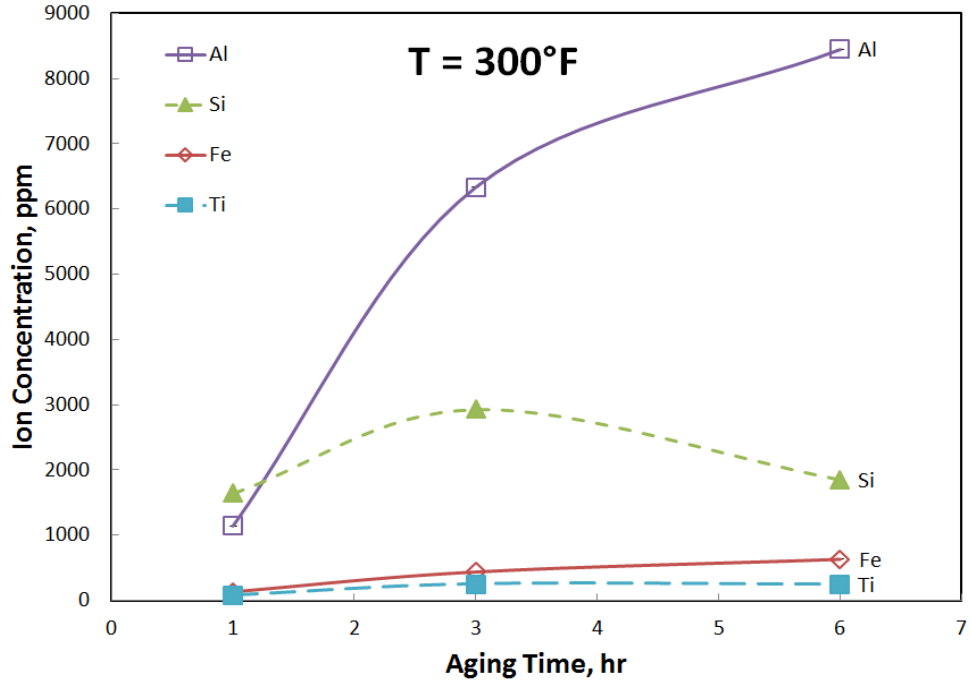

Fig. II- 5— Ion concentration in the supernatant of solubility tests after interaction with clay-based proppant for different soaking times at 300°F under static conditions.

Fig. II-6 shows the dissolved proppant as a function of soaking time for sand and clay-based proppants. The dissolution rate is greater for clay-based proppants; thus, the clay-based proppant weight loss is more significant. The maximum solubility for sand proppant was less than 4.0 wt%; however the clay-based proppant solubility reached 14.0 wt% at 300°F. Unlike the dissolution at 250°F, the rate at which the proppant dissolved decreased after 3 hours at 300°F. This can be attributed to the precipitation of silica gel, which decelerates the reaction (Tso and Pask 1982), confirmed by the decrease of silicon concentration observed in the supernatant of solubility tests. Reasons for that significant loss of proppant mass will be discussed later in the microstructure analysis section.

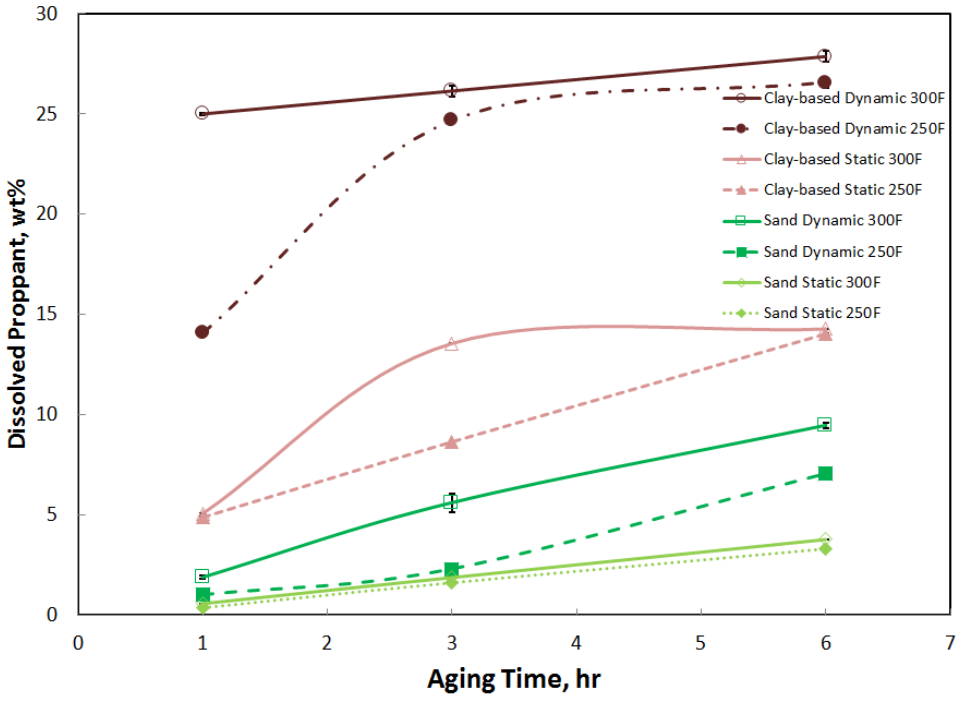

Fig. II- 6— Dissolved proppant over time after the aging cell experiments under static and dynamic conditions*.
*The lines represent the error bars for the experiments that were repeated.

Experiments Under Dynamic Conditions

The same procedures were repeated for sand and clay-based proppants at 250 and 300°F, but this time the oven rollers were running at 25 rpm. These tests were done to simulate injection conditions, where acid diffusion can affect its reactivity with different minerals. Some of the experiments were repeated as many as three times to ensure reproducibility of results. The average results are summarized in Tables II-6 and II-7.

For sand and clay-based proppants, acid soaking times of 1, 3, and 6 hours were used. Proppant weights before and after the experiments were tabulated in grams and a percentage of the weight dissolved was calculated.

Soaking Time, hrs	T, °F	Weight Before, g	Weight After, g	Dissolved Proppant, wt%
1	250	25	24.75	1.00
3		25	24.43	2.30
6		25	24.24	7.04
1	300	25	24.53	1.90
3		25	23.60	5.62
6		25	22.63	9.48

Table II- 6– Average results of aging cell experiments for sand proppant at different soaking times under dynamic conditions with regular mud acid.

Soaking Time, hrs	T, °F	Weight Before, g	Weight After, g	Dissolved Proppant, wt%
1	250	25	21.47	14.10
3		25	18.83	24.67
6		25	18.36	26.56
1	300	25	18.75	25.00
3		25	18.46	26.15
6		25	18.03	27.87

Table II- 7– Average results of aging cell experiments for clay-based proppant at different soaking times under dynamic conditions with regular mud acid.

The supernatant from the solubility tests was analyzed using ICP-OES. **Figs. II-7** through **II-9** show the key cations' concentration in the samples after each experiment at 250 and 300°F for sand and clay-based proppants, respectively. The samples showed higher concentrations of all cations present compared to the concentrations measured from experiments under static conditions.

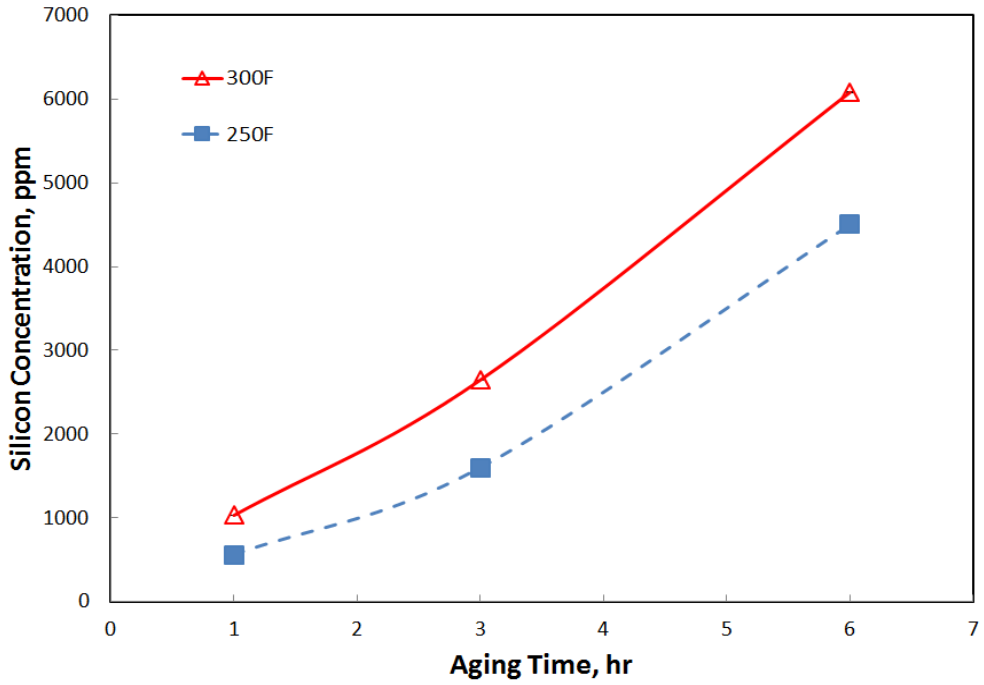

Fig. II- 7— Ion concentration in the supernatant of solubility tests after interaction with sand proppant for different soaking times under dynamic conditions at 250 and 300°F.

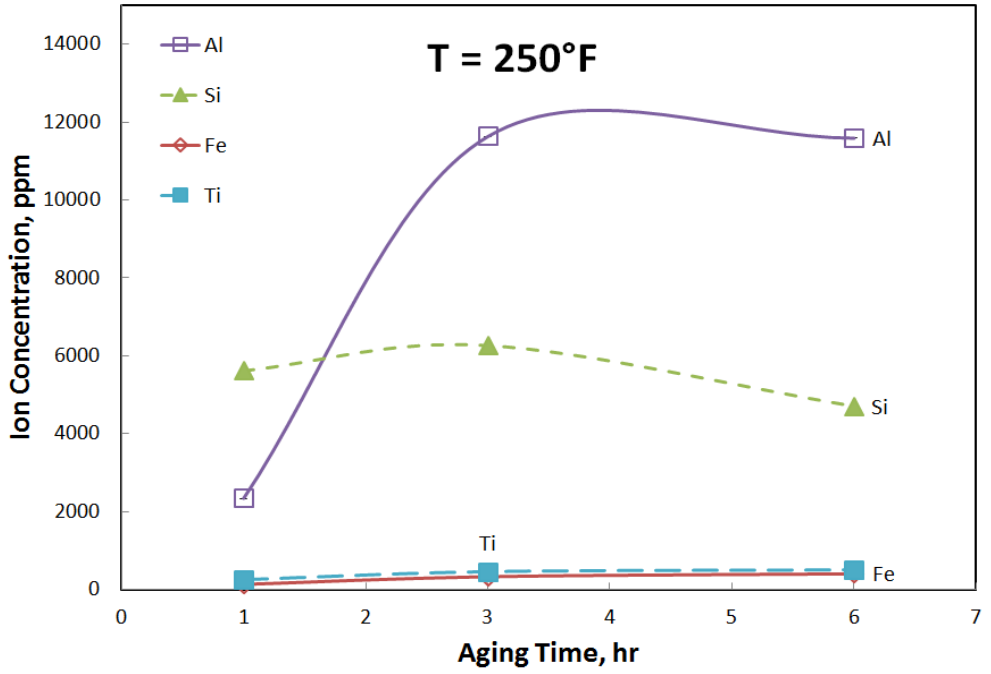

Fig. II- 8— Ion concentration in the supernatant of solubility tests after interaction with clay-based proppant for different soaking times at 250°F under dynamic conditions.

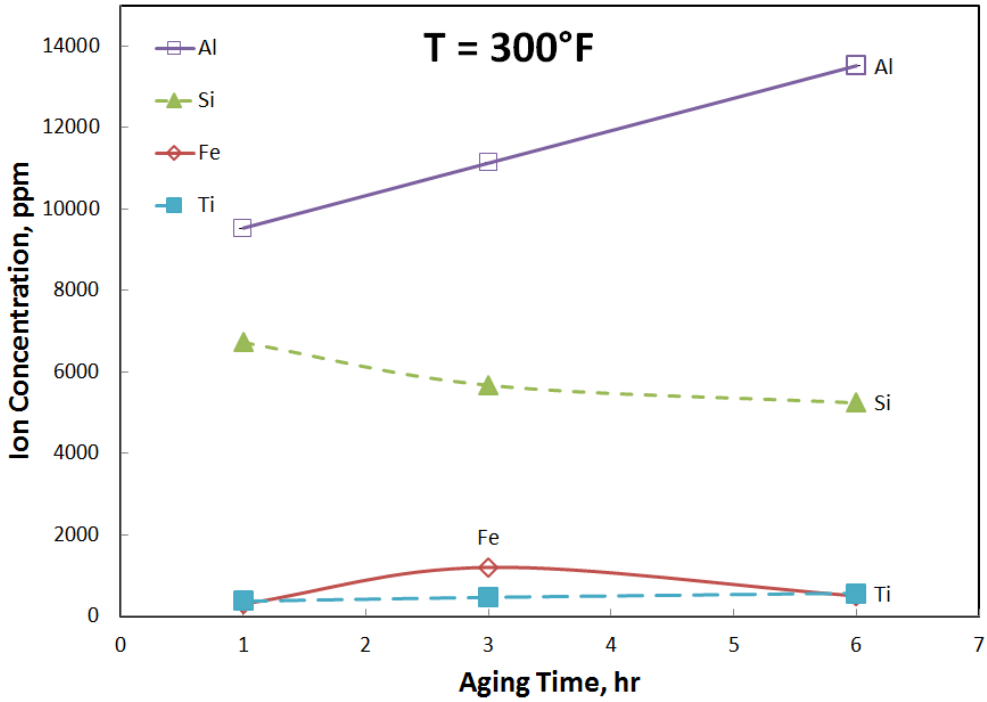

Fig. II- 9— Ion concentration in the supernatant of solubility tests after interaction with clay-based proppant for different soaking times at 300°F under dynamic conditions.

Fig. II-6, once again, plots proppant dissolution as a function of soaking time for sand and clay-based proppants. The dissolved proppant in these cases was also higher as agitation increases reaction rate (Tso and Pask 1982). The same trend was observed as the amount of dissolved proppant increased at a very low rate at 300°F, this time because of more silica precipitation at the higher temperature. However, the slow increase in dissolution was observed at 250°F after three hours, as silica precipitation is not as fast. The maximum solubility for sand proppant was less than 10.0 wt%; however, the clay-based proppant solubility reached 28.0 wt% at 300°F. The precipitation is evident in the SEM-EDS residue analysis shown later in this study. This precipitation can be due to secondary and tertiary reactions (Al-Dahlan et al. 2001) as follows.

First, the primary reaction of HF with sand and clays yields fluosilicic acid (Eqs. II-1 and II-2). At temperatures higher than 150°F, which is below our testing conditions, the fluosilicic acid undergoes a series of secondary and tertiary reactions. During secondary reactions, M-feldspars, where M can be Na^+ or K^+, can precipitate hydrated silica (Eq. II-3). In addition, fluosilicic and fluoaluminic acids can react with the cations leached precipitating fluosilicates and fluoaluminates (Eqs. II-4 and II-5). In tertiary reactions, aluminum ions can be extracted and silica gel is precipitated (Eq. II-6). Moreover, both aluminum fluoride (AlF_3) and aluminum hydroxide ($Al(OH)_3$) precipitate at high HF concentration and HF:HCl ratios (Eqs. II-7 and II-8), which can react later with aluminum silicate precipitating silica gel (Eq. II-9).

$$6HF + SiO_2 \leftrightarrow H_2SiF_6 + 2H_2O \quad \ldots \quad \text{(II-1)}$$

$$36HF + Al_2Si_4O_{10}(OH)_2 \rightarrow 4H_2SiF_6 + 2H_3AlF_6 + 12H_2O \quad \ldots \quad \text{(II-2)}$$

$$H_2SiF_6 + 6MAlSi_3O_8 + 18HCl \rightarrow 6AlF_2^+ + 6M^+ + 18H_2SiO_3 + SiO_2.2H_2O\downarrow + 18Cl^- \quad \ldots \quad \text{(II-3)}$$

$$H_2SiF_6 + 2M^+ \rightarrow M_2SiF_6\downarrow + 2H^+ \quad \ldots \quad \text{(II-4)}$$

$$H_3AlF_6 + 3M^+ \rightarrow M_3AlF_6\downarrow + 3H^+ \quad \ldots \quad \text{(II-5)}$$

$$AlF_2^+ + MAlSi_3O_8 + 4HCl + 4H_2O \rightarrow K^+ + 2AlF^{2+} + 3H_4SiO_2\downarrow \quad \ldots \quad \text{(II-6)}$$

$$3F^- + Al^{3+} \leftrightarrow AlF_3\downarrow \quad \ldots \quad \text{(II-7)}$$

$$Al^{3+} + 3OH^- \leftrightarrow Al(OH)_3\downarrow \quad \ldots \quad \text{(II-8)}$$

$$AlF_x + Al\text{-}Si + H^+ \rightarrow AlF_y + SiO_2.2H_2O\downarrow \quad \ldots \quad \text{(II-9)}$$

Images acquired by a Zeiss Axiophot optical microscope showed the effect of acid on the proppant particles. **Figs. II-10** and **II-11** depict the results of proppant particle solubility in acid. The proppants lost their smoothness, especially in the case of clay-based proppants. The dissolution of proppants resulted in the generation of fine particles that were separated from the solution after experiments. This process can decrease proppant pack conductivity.

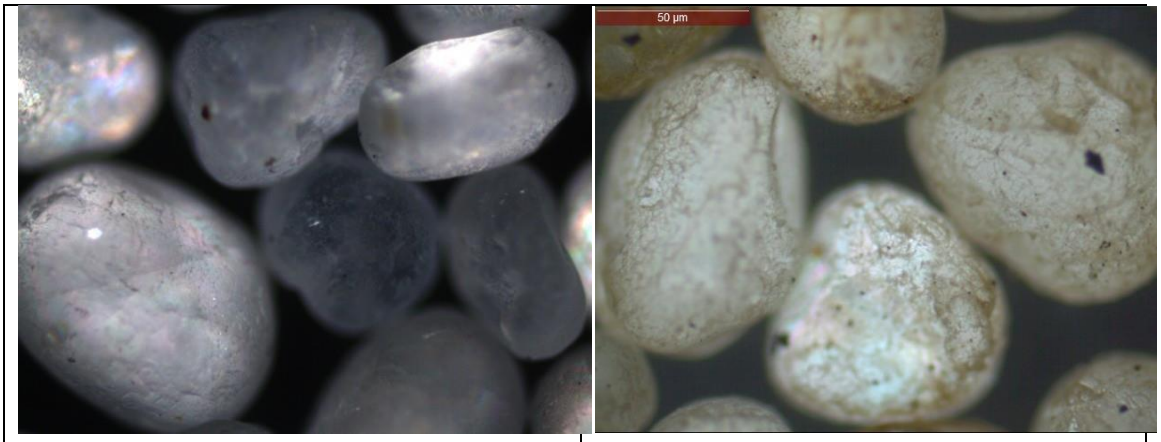

Fig. II- 10— Zeiss Axiophot optical microscope image at x50 magnification of sand proppant before and after acid solubility.

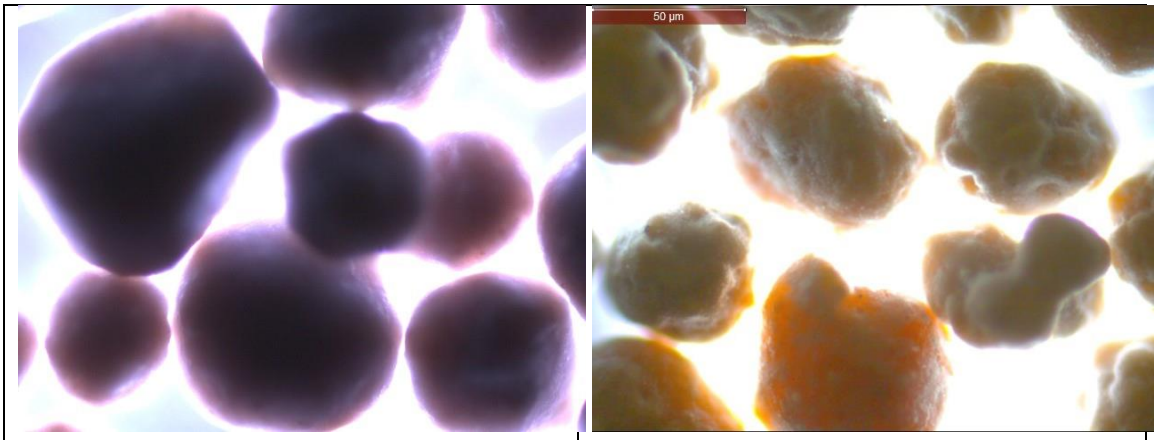

Clay-based before	Clay-based after

Fig. II- 11— Zeiss Axiophot optical microscope image at x50 magnification of clay-based proppant before and after acid solubility.

^{19}F-NMR Analysis

The ^{19}F-NMR analysis was conducted on some of the supernatants of acid solutions from the clay-based proppant experiments before and after the acid interactions. All ^{19}F chemical shifts were reported by use of trichlorofluoromethane ($CFCl_3$) as an internal reference, by means of an external reference of boron trifluoride etherate that was referenced at δ = -153 ppm (Zhou and Nasr-El-Din 2015). Unlike the chemical shifts that were reported by Shuchart and Buster (1995) relative to trifluoroacetic acid, $CFCl_3$ was used to convert the chemical shifts and compare the results in this study with reported values from the literature.

Fig. II-12 shows the ^{19}F-NMR spectra of the regular mud acid samples before and after three hours of reacting with clay-based proppant at 300°F under dynamic conditions. Before the reaction, ^{19}F-NMR showed a chemical shift for HF only (Shuchart and Buster 1995). After the reaction, ^{19}F-NMR showed three chemical shifts for SiF_5^-, AlF_4^-, and AlF_3 (Shuchart and Buster 1995; Sur and Bryant 1996) matching the results from ICP-OES

sample analysis that showed high concentrations of aluminum and silicon. However, iron did not form complexes with fluorine in the presence of aluminum as the affinity of fluorine to aluminum is high compared to that of iron (Crowe 1985; Sur and Bryant 1996). Iron has two forms: Fe^{2+} and Fe^{3+} ions. As clay-based proppants is composed of the latter type, Fe^{3+} ions remained soluble in the solutions because the pH was less than two as it precipitates between 1 and 2 (Taylor et al. 1999).

Based on these results, except for the silica gel precipitation, most of the cations remained soluble in the solution, which is optimal for the fracture conductivity.

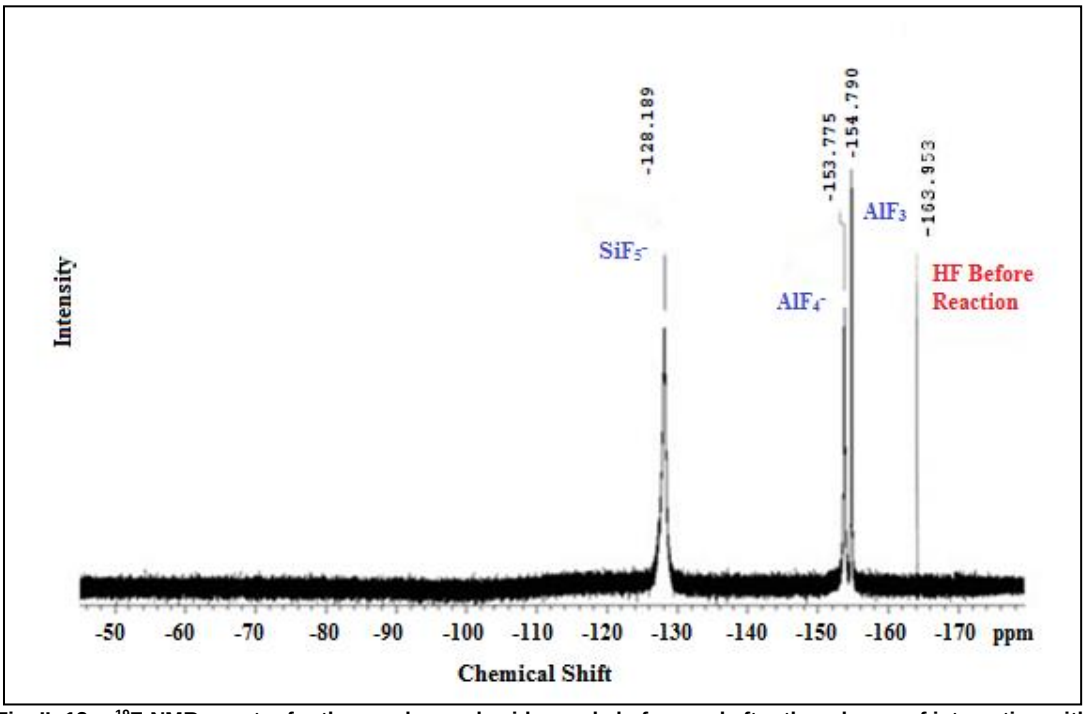

Fig. II- 12— ^{19}F-NMR spectra for the regular mud acid sample before and after three hours of interaction with clay-based proppant at 300°F under dynamic conditions.

XRD Analysis

XRD analysis was conducted on the crushed sand and clay-based proppants before and after a six-hour acid treatment under dynamic conditions. **Figs. II-13** and **II-14** show the analyses of the samples before and after the acid attack. The results show the presence of HF-soluble cristobalite (SiO_2) and mullite in clay-based proppants. Both minerals are the main reason for clay-based proppant weight loss after acid exposure. The concentration of mullite increased by 4.64% while the concentration of cristobalite decreased by 30.00%. The weight percentage of these minerals changed before and after the acid reaction, from 86.69 and 13.31 to 90.71 and 9.29 wt% for mullite and cristobalite, respectively. Cristobalite dissolved more than mullite as shown by the reduction in cristobalite peaks intensity which was later confirmed by XRF. On the contrary, sand proppants samples did not change, showing mainly quartz mineral (SiO_2) before and after the acid reaction. The presence of both cristobalite and mullite in clay-based proppant and its effect on the proppant weight loss will be further explained in the microstructure analysis section.

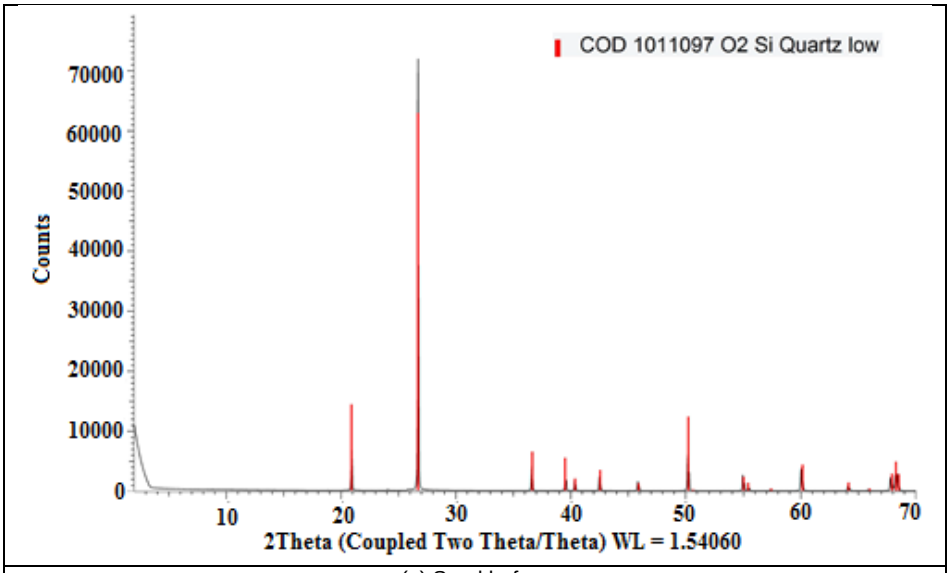

(a) Sand before

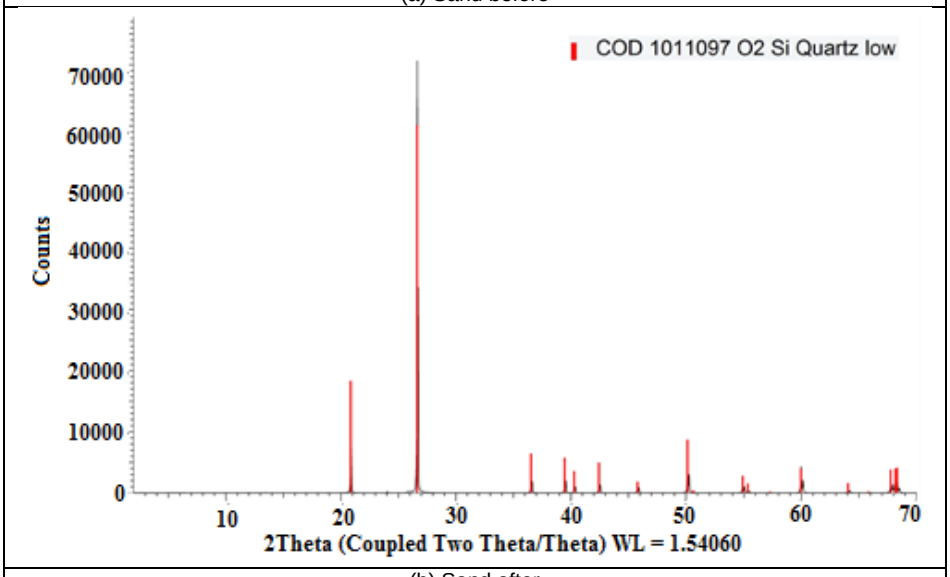

(b) Sand after

Fig. II- 13— XRD patterns for the sand proppant particles. (a) Before acid treatment, (b) after acid treatment at 300°F for six hours under dynamic conditions.

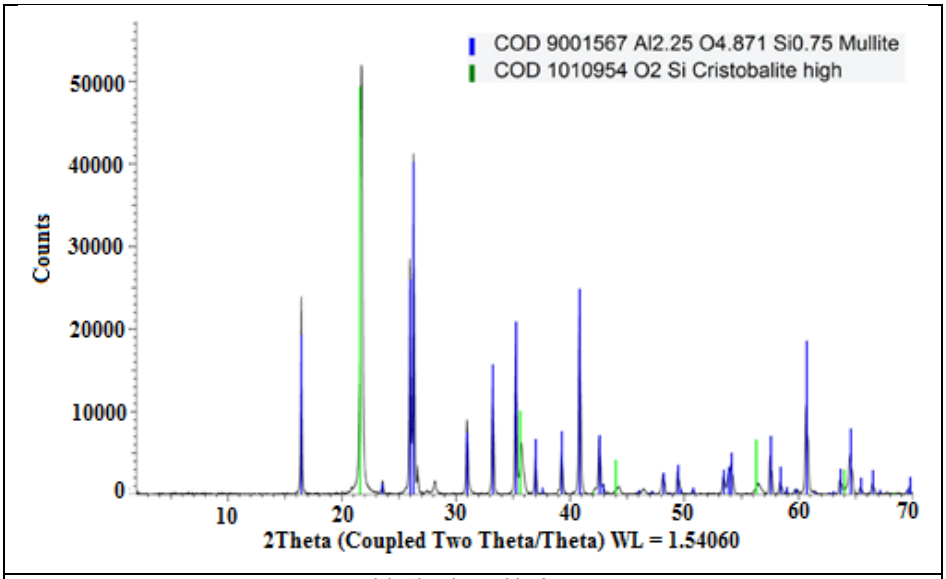

(a) Clay-based before

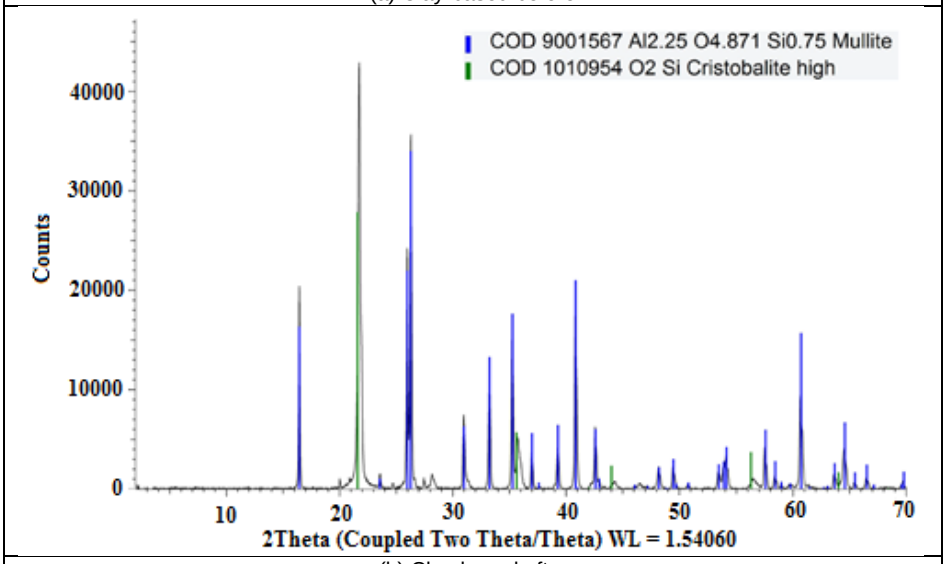

(b) Clay-based after

Fig. II- 14— XRD patterns for the clay-based proppant particles. (a) Before acid treatment, (b) after acid treatment at 300°F for six hours under dynamic conditions.

XRF Analysis

XRF analysis was conducted on the same crushed sand and clay-based proppant samples used for XRD. **Table II-8** summarizes the main oxides present in each sample before the experiments. Sand proppants showed mainly silicon oxide, as these proppants are mostly composed of quartz. However, the clay-based proppants showed aluminum and silicon

oxides, as they contain mullite and cristobalite, concentrations agrees with the results obtained by XRD analysis.

Oxide	Concentration, wt%	
	Sand Before	Clay-based before
Al_2O_3	0.17	47.62
SiO_2	99.79	48.54
TiO_2	-	2.38
Fe_2O_3	-	1.19

Table II- 8– Oxides analysis by XRF for different proppants used in the study.

Crushing Test

The crush resistance test described in ISO 13503-2 standard evaluates the degradation of the mechanical strength of each proppant sample before and after acid exposure. An MTS model Alliance RF/300 automated load frame was used in this study with a force resolution of ±1 lb. The MTS software captures the compaction distance and forces data over time. A machine compliance offset for the load frame excludes any exterior influences upon the measured compaction distance of the proppant specimen, such as the elastic deformation of the test cell and the motion from grips while under load. An empty test cell is used to measure this compliance offset (Stephens et al. 2007; Fuss et al. 2008). When the test cell with a specimen is in the load frame, the automated software preloads the specimen with 25 lbs of force to determine the initial proppant pack height. The compaction of the proppant sample is the ratio of the current pack height versus its initial value. The reported crush resistance value is equivalent to the weight of material finer than a 40-mesh sieve (425 microns), the lower end of the original size distribution.

The crush resistance tests were conducted at 8,000 psi for proppants before and after acid exposure for six hours under dynamic conditions at 300°F. **Figs. II-15** and **II-16** show the relative compaction of the proppant samples during the crush resistance.

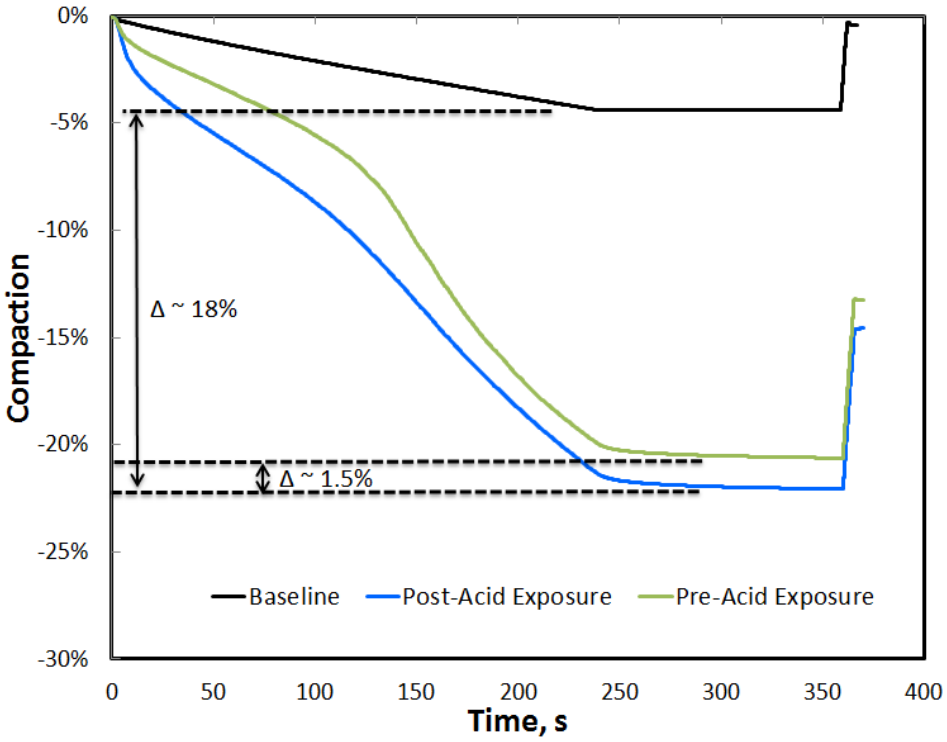

Fig. II- 15— Compaction of sand specimens at 8,000 psi before and after acid exposure.

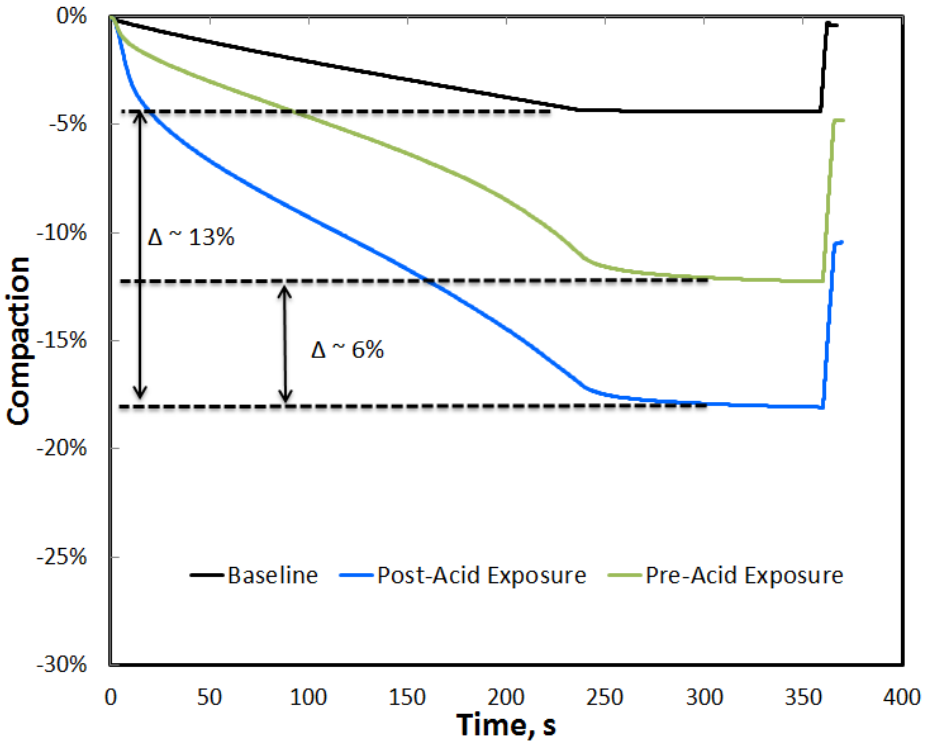

Fig. II- 16— Compaction of clay-based specimens at 8,000 psi before and after acid exposure.

The baseline represents compliance offset measured using the empty cell. Pack compaction of clay-based proppant is less compared to sand proppant at all conditions. At 8,000 psi, acid corrosion of clay-based proppant increases pack compaction by 6.0% while acid corrosion of sand proppant increases pack compaction by 1.5%. Higher proppant acid solubility, since significant materials were removed, may decrease the ability of the proppant structure to withstand the closure stress. Depending on the proppant selected, the loss in weight affected the mechanical integrity and, most likely, proppant conductivity. Because of the higher acid solubility, clay-based proppant did not maintain mechanical strength under acid exposure, and there was a big effect upon pack compaction.

Microstructure Analysis

Microstructure analysis can illustrate the effect of acid solubility on the proppant particles. **Figs. II-17** through **II-20** show these effects for some of the samples tested under dynamic conditions.

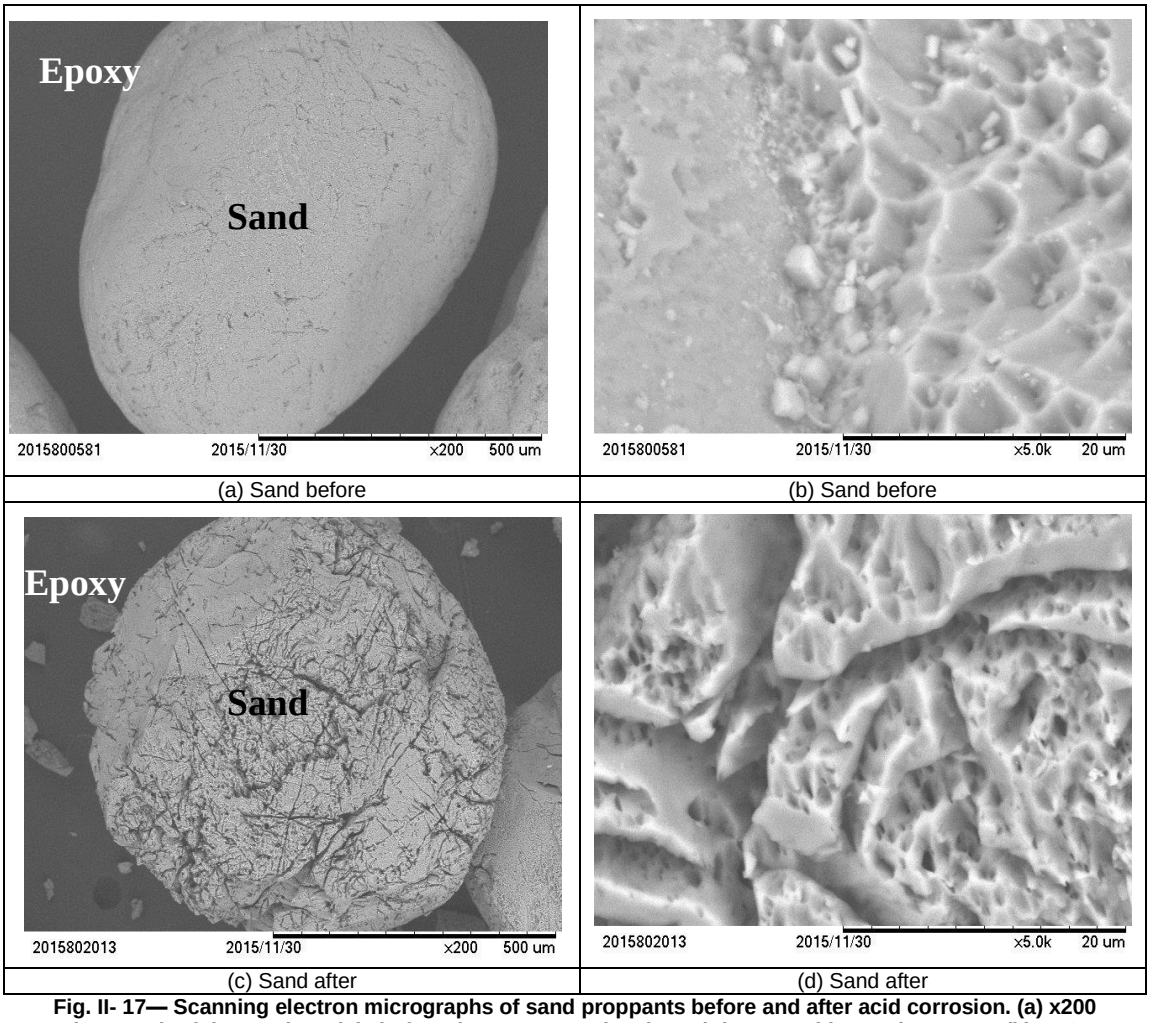

(a) Sand before (b) Sand before

(c) Sand after (d) Sand after

Fig. II- 17— Scanning electron micrographs of sand proppants before and after acid corrosion. (a) x200 micrograph of the sand particle before the treatment showing minimum etching and grooves, (b) x5.0K micrograph displaying a local enlargement for the same particle showing the irregular surface with lighter clay particles, (c) x200 micrograph of the sand particle after the treatment where the acid attack is clear on the surface as it generated microgrooves, (d) x5.0K micrograph depicting a local enlargement for the same particle showing the microgrooves on the sand particle surface where the acid attacked unevenly and the small clay particles disappeared.

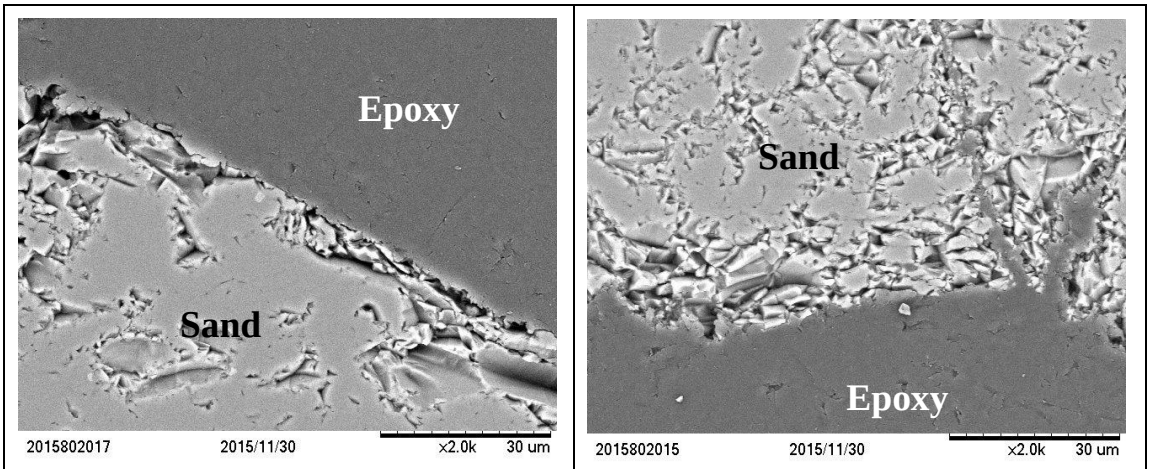

(a) Sand before | (b) Sand after

Fig. II- 18— Scanning electron micrographs of sand proppant cross-sections before and after acid corrosion. (a) x2.0K micrograph of the sand particle before the treatment again showing some grooves and irregularities, (b) x2.0K micrograph of the sand particle after the treatment showing more grooves and surface etching.

In Fig. II-17, the acid etches monocrystalline silica-rich sand proppant, creating microgrooves on the particles' surfaces. It also shows that post acid reaction, the small crystals disappeared because the acid leaches them first. **Fig. II-18** shows the same effect on the cross-sections taken before and after the acid exposure. The presence of grooves indicates that the acid does not attack the particles' surfaces evenly. As for clay-based proppant, the skeleton structure consists of cristobalite-bounded mullite, while amorphous SiO_2 remains in isolated "islands" that are consistent with the results reported by Fuss et al. (2008). As both amorphous and crystalline forms of SiO_2 are soluble in hydrofluoric acid, the presence of cristobalite is detrimental for proppants' mechanical strength after acid exposure. Microstructure analysis of clay-based proppant after acid corrosion reveals the presence of surface pits (**Fig. II-19**). Fig. II-20 shows how the cross-sections change before and after the acid exposure. There is a corrosion layer with slightly different morphology. Similar results were reported by Wu et al. (2015). With clay-based

proppants, the acid is detrimental to the structural matrix which, in turn, causes a significant compaction upon crushing the clay-based proppants versus that of sand.

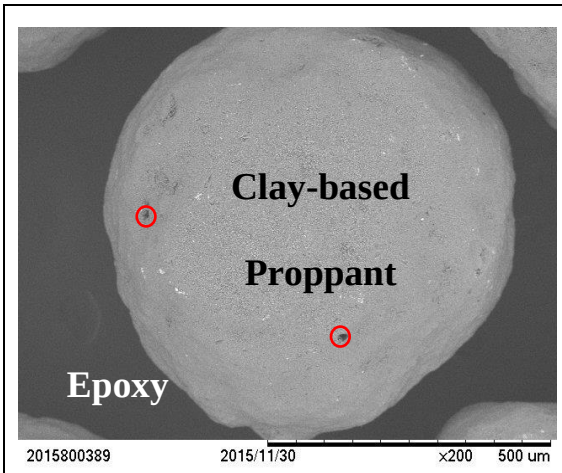

(a) Clay-based before

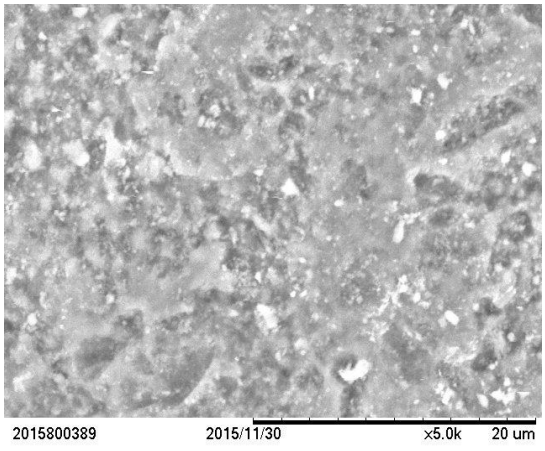

(b) Clay-based before

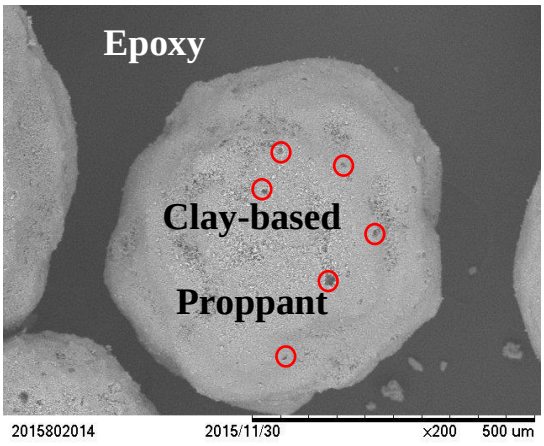

(c) Clay-based after

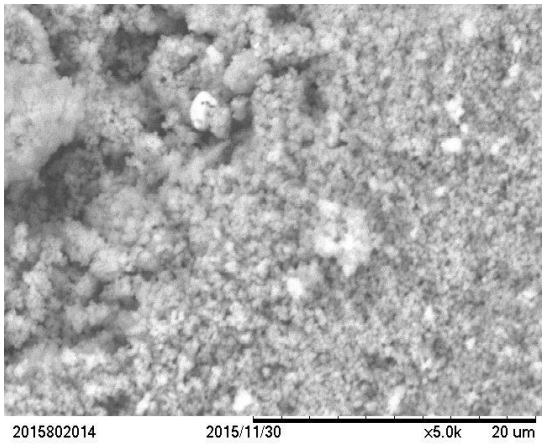

(d) Clay-based after

Fig. II- 19— Scanning electron micrographs of clay-based proppants before and after acid corrosion. (a) x200 micrograph of the clay-based particle before the treatment showing a little roughness, (b) x5.0K micrograph displaying a local enlargement showing the irregular surface of clay-based particles with different minerals, (c) x200 micrograph of the clay-based particle after the treatment where the acid attack is clear as the surface smoothness decreased, (d) x5.0K micrograph depicting a local enlargement for the same particle showing the disappearance of the lighter minerals as the acid attacked the surface, most likely cristobalite.

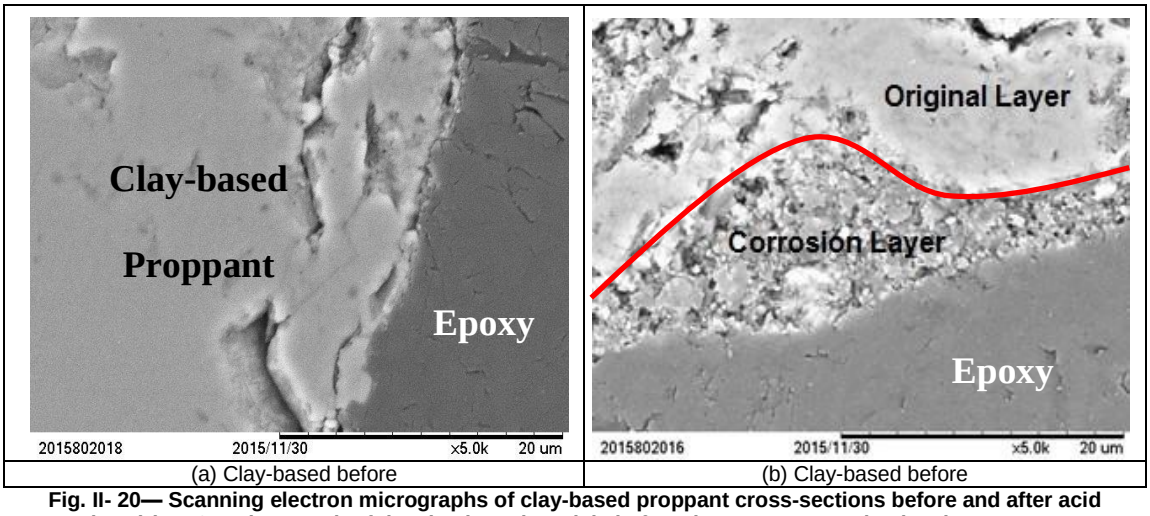

(a) Clay-based before (b) Clay-based before

Fig. II- 20— Scanning electron micrographs of clay-based proppant cross-sections before and after acid corrosion. (a) x5.0K micrograph of the clay-based particle before the treatment again showing some grooves and irregularities, (b) x5.0K micrograph of the clay-based particle after the treatment showing a corrosion layer that has a different morphology.

EDS was used to examine the elemental analysis for the residual solids that were filtered from the solution after the solubility tests. Because of the surface heterogeneity of the proppant, three samples were tested. Analyses of two samples were in agreement with the XRF analysis; therefore, the third result was discarded. **Table II-9** summarizes some of the results.

Element	Concentration, wt%	
	Sand Residue	Clay-based Residue
O	52.51	62.31
Si	47.49	35.37
Al	-	2.32

Table II- 9– Quantitative results by EDS for sand and clay-based residual solids after the reaction.

Figs. II-21 through **II-24** show the images of spectrum analyses for some samples of the residual solids after sand and clay-based proppants' interaction with regular mud

acid. Sand proppant residual solids showed silicon and oxygen elements as the main components. The weight percent differed between the residual solids and the original sand particles, indicating a different structure. Clay-based residual solids, on the contrary, showed high concentrations of silicon, oxygen, and aluminum with traces of iron and titanium. These findings are in agreement with the assumption of secondary and tertiary reaction precipitations. Furthermore, the amount of aluminum reduction can be attributed to its high affinity to fluorine.

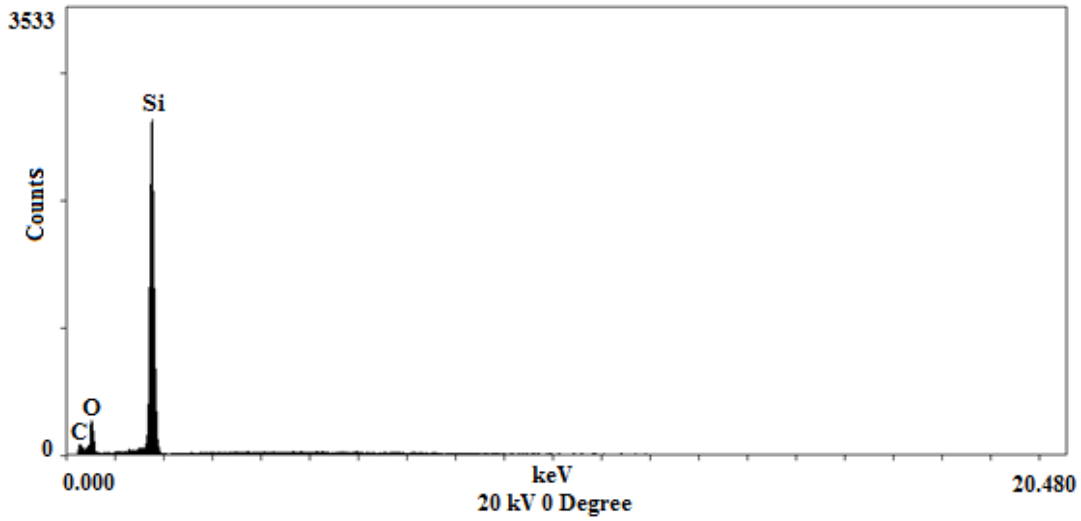

Fig. II- 21— Analysis for sample (A) of the sand residual solids after acid exposure.

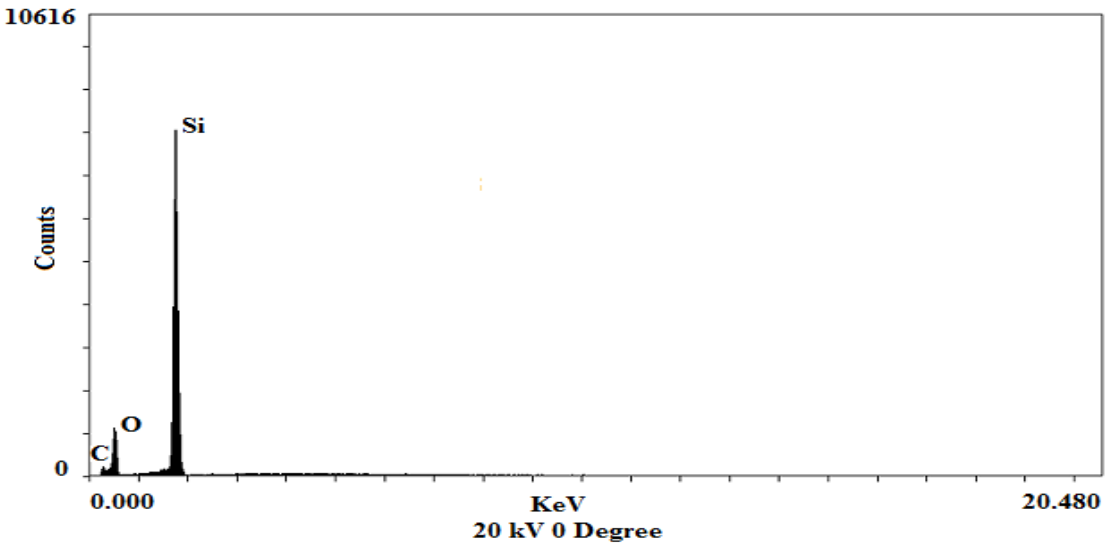

Fig. II- 22— Analysis for sample (B) of the sand residual solids after acid exposure.

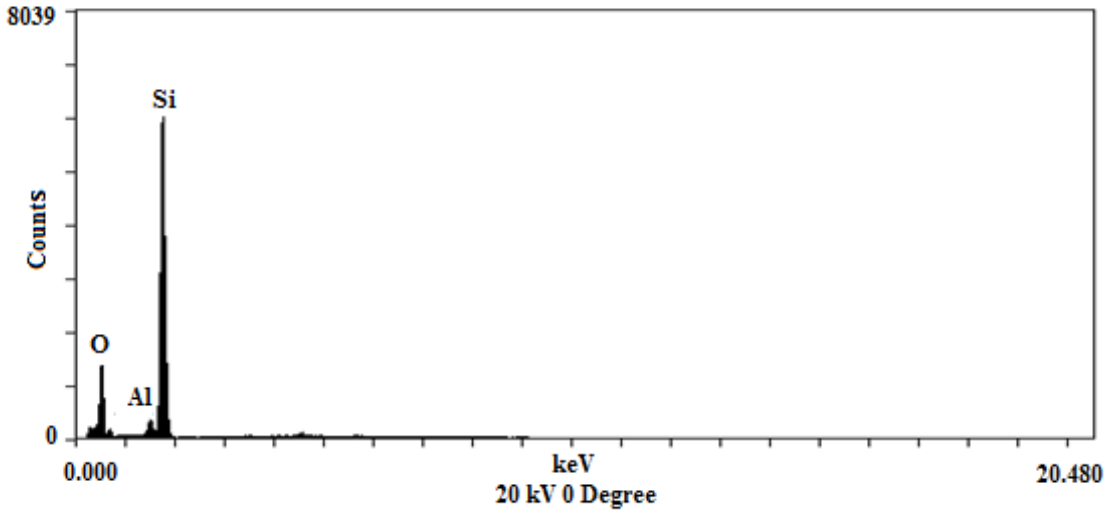

Fig. II- 23— Analysis for sample (A) of the clay-based residual solids after acid exposure.

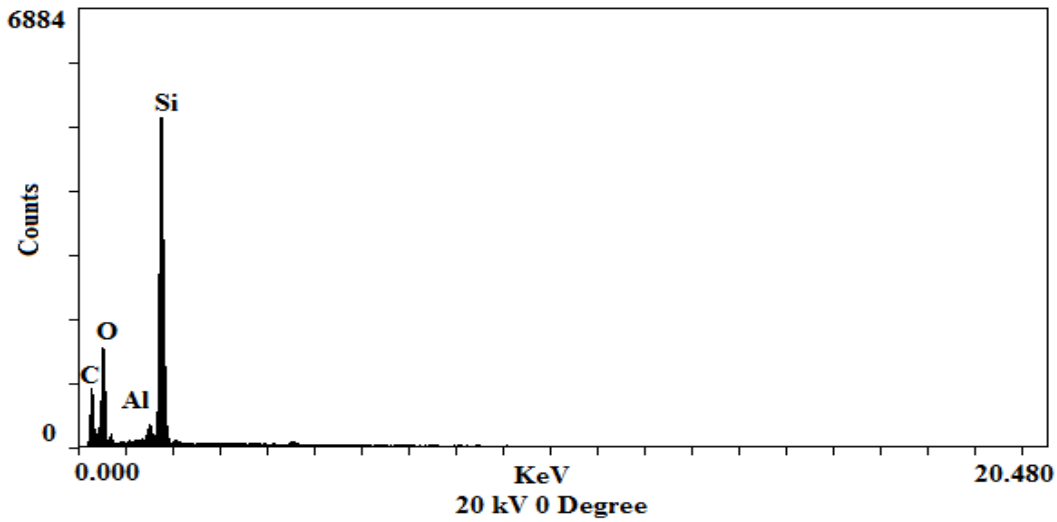

Fig. II- 24— Analysis for sample (B) of the clay-based residual solids after acid exposure.

Figs. II-25 and **II-26** show the residual solids filtered after sand and clay-based dissolutions in regular mud acid. Fig. II-25 shows the flaky-like residue filtered after the acid interaction. These fines were generated during the acid leaching of the monocrystalline, silica-rich proppants. Fig. II-26 shows the spongy-like residue filtered after acid dissolution. The fines generated from clay-based proppants come from the skeleton structure that consists of cristobalite-bounded mullite, and amorphous SiO_2 as previously explained. Both residues can cause damage and loss of conductivity for gravel-packed wells and fractures, respectively.

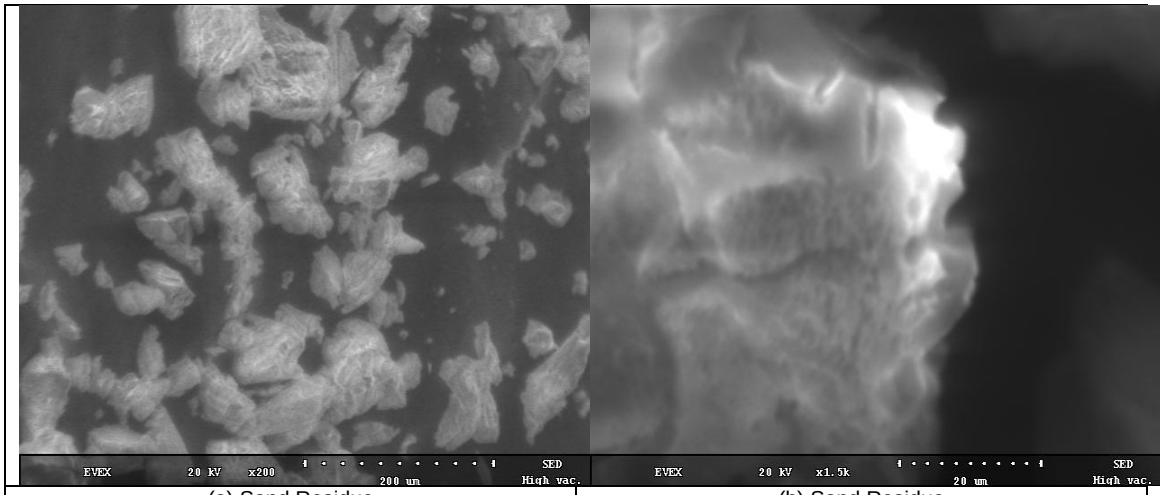

(a) Sand Residue | (b) Sand Residue

Fig. II- 25— Scanning electron micrographs of sand proppant residue filtered after acid corrosion. (a) x200 micrograph of the sand proppant residue after the treatment showing flaky-like precipitates, (b) x1.5K micrograph of the sand proppant residue after treatment showing the pores on the surfaces of these precipitates.

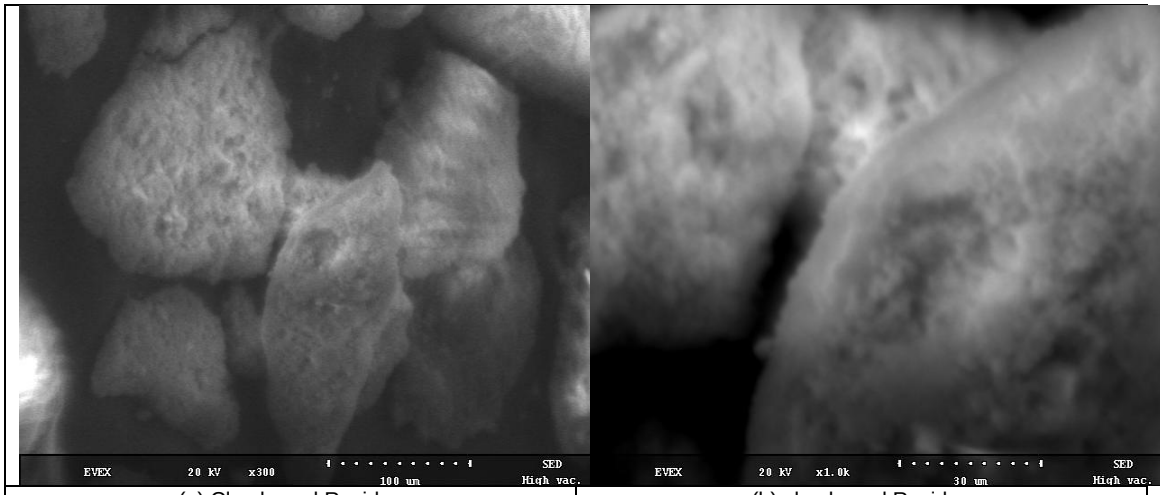

(a) Clay-based Residue | (b) clay-based Residue

Fig. II- 26— Scanning electron micrographs of sand proppant residue filtered after acid corrosion. (a) x300 micrograph of the clay-based proppant residue after the treatment showing spongy-like precipitates, (b) x1.0K micrograph of the clay-based proppant residue after treatment showing the pores on the surfaces of these precipitates.

Conclusions

Studying proppant acid solubility resistance is important because acids remove scale and clays from formations and equipment, but they can also affect proppants present in fractures. In this research, several tests were conducted to assess the effect of regular

mud acid on proppant solubility and mechanical properties. Based on the results obtained, the following conclusions can be drawn:

1. Clay-based proppants showed higher dissolution as HF attacked grain boundaries between cristobalite and mullite.
2. All proppant samples showed a high rate of dissolution with regular mud acid at 250 and 300°F. The dissolved proppant increased with the increase of temperature, soaking time, and dynamic conditions.
3. XRD and XRF analyses for clay-based proppants showed that cristobalite dissolved in the regular mud acid more than mullite, which can cause fines generation that might reduce proppant pack conductivity.
4. Microscopic images showed how proppant surfaces lose their smoothness as the acid attacks the surface unevenly.
5. ICP-OES and EDS analyses suggested that silica precipitated due to secondary and tertiary reactions, which slows the reaction rate.
6. ^{19}F-NMR analysis for acid supernatant samples after clay-based proppant solubility tests showed aluminum and silicon fluoride complexes due to their strong fluorine affinity compared to iron, which keeps most of these cations soluble in solution.
7. Clay-based proppant did not maintain mechanical strength under acid exposure.

Regular mud acid has a strong effect on the sand and clay-based proppants at high temperatures. API solubility test is not representative of the reservoir conditions. The

regular mud acid soaking time (static conditions) does not have as significant of an effect on proppants as the injection time (dynamic conditions). The latter can dissolve greater amounts of proppant, thus creating fines and reducing the proppant pack conductivity. If a regular mud acid treatment is needed, then minimizing acid/proppant contact time is recommended.

CHAPTER III

SOLUBILITY OF BAUXITE PROPPANTS IN DIFFERENT ACIDS

Experimental Studies

Materials

HCl of 10 wt% concentration, 9 wt% HCOOH, and 20 wt% of trisodium salt of N-(hydroxyethyl)-ethylenediaminetriacetic acid (Na_3-HEDTA) were used. The HCl, HCOOH, and Na_3-HEDTA acid solutions were prepared using 36.5, 88.0, and 43.0 wt% solutions, respectively. The corrosion inhibitor, which was quaternary ammonium compound-based, was obtained from a local service company. The mud acid solutions were prepared using HCl and NH_4HF_2. Proppant samples were obtained from a local service company. As previously explained, deionized water was used throughout the experiments.

Equipment

Besides the equipment mentioned in Chapter II, an HP/HT see-through cell was used to study the reaction between 10.0 wt% HCl and sintered bauxite. For details on the HP/HT see-through cell, refer to Al Moajil and Nasr-El-Din (2013). Additionally, a universal testing machine (hydraulic load frame), Instron 5583, was used for crush resistance tests.

Procedures

Acid Preparation

The 10.0 wt% HCl solution was prepared by mixing the corrosion inhibitor, deionized water, and HCl. Different mud acid solutions were prepared by mixing the corrosion inhibitor with the deionized water, NH_4HF_2, and the HCl for at least 15 minutes. In other acid systems, HCl was replaced with HCOOH or Na_3-HEDTA. In the case of Na_3-HEDTA, HCl was added to buffer the solution at a pH of 4 to maintain the acidity of the solution.

Proppant Preparation

Sieve analysis was conducted for all of the bauxite proppants. For consistency, particles of -20+30 mesh size were chosen for all aging cell experiments. The sphericity and roundness of proppants were examined in accordance with the API RP 19C/ISO 13503-2 standard. A Zeiss Axiophot optical microscope was used to acquire images of the proppant particles. These images were visually compared to the Krumbein/Sloss diagram. **Fig. III-1** shows a sample of these photos for two samples of the proppant. Both samples showed good sphericity and roundness according to API RP 19C/ISO 13503-2 standard. **Table III-1** gives the results of sphericity and roundness analyses.

Size, μm	Sphericity	Roundness
600-850	0.8	0.8

Table III- 1– Sphericity and roundness of bauxite proppant used in aging cell tests.

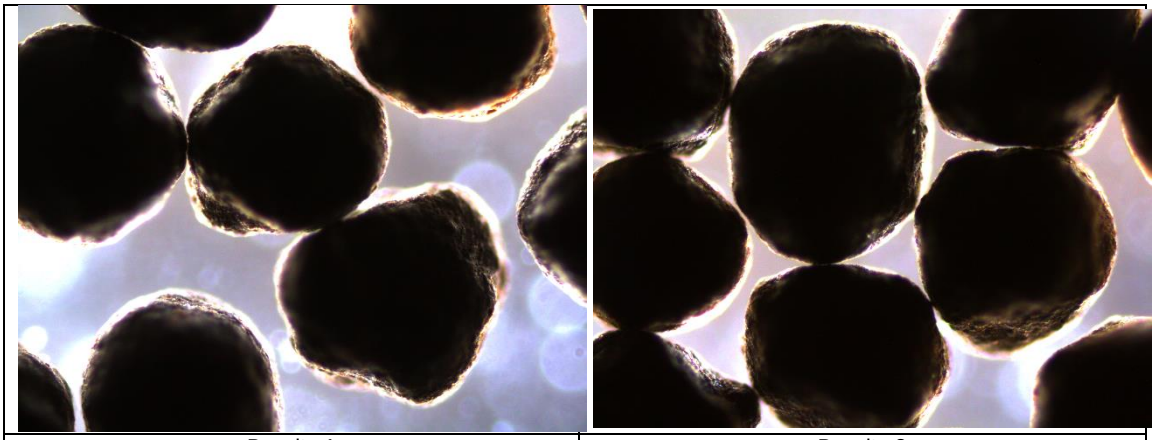

Bauxite 1	Bauxite 2

Fig. III- 1— Zeiss Axiophot optical microscope image at x50 magnification of examples of proppant samples (600–850 µm).

Results and Discussion

See-Through Cell

Two HCl solubility experiments were conducted. A bauxite disk was divided into four fragments. One of the four samples, weighing 4.94 g, was used. The soaking time was 24 hours at a temperature of 250°F. The sample was then dried and weighed again. There was no change in weight, which means the sample resists HCl attack at 250°F. The experiment was repeated using 20 g of proppant particles, which were added to the acid at the same conditions. The weight after the experiment was 19.9 g (0.5% dissolved). This confirmed the fact that HCl had almost no adverse effect on the bauxite samples. **Fig. III-2** shows the proppant samples before and after one of the experiments. By observation, the sample displayed no change in color after the experiments because of minimal dissolution.

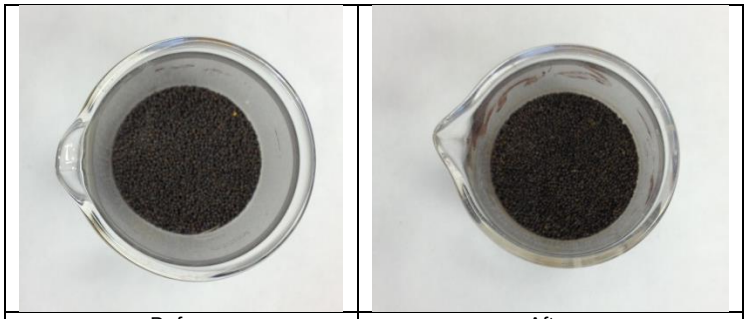

Fig. III- 2— Proppant before and after the see-through cell experiment.

API Solubility Test

Experiments Conducted with Corrosion Inhibitor Using Different Mud Acids

Four solubility experiments were conducted. Two five-gram samples of bauxite proppant were weighed and dried. At room temperature, the proppant was added to plastic beakers containing 100 cm^3 of different mud acid concentrations, regular i.e., (12:3) and (6:1), including 1 wt% corrosion inhibitor. The beaker was placed in a 66°C (150°F) water bath for 30 minutes without stirring. Proppant solubility increased with increasing acid concentration. The average results are summarized in **Table III-2**. With the regular mud acid, 3.65 wt% of bauxite was dissolved; while with the (6:1) mud acid, a value of 1.0 wt% dissolution was obtained. However, both acid systems showed less than 5.0 wt% weight loss, which meets the industry standards (The API RP 19C/ISO 13503-2 standard).

T, °F	Dissolved Proppant*, wt%	
	Mud Acid (6:1)	Mud Acid (12:3)
150	1.00	3.65

Table III- 2– Average results of API solubility test for bauxite proppant (corrosion inhibitor included).

*The experiments were repeated four times.

Experiments Conducted Without Corrosion Inhibitor Using Different Mud Acids

The experiments were repeated several times without using a corrosion inhibitor. Bauxite proppant was tested at both mud acid concentrations. The solubility of bauxite was 4.5 and 1.1 wt% for (12:3) and (6:1) mud acid systems, respectively. Proppant solubility increased with the lack of corrosion inhibition, as it coated the proppants, slowing their reaction with different acids. The average results are summarized in **Table III-3**.

T, °F	Dissolved Proppant*, wt%	
	Mud Acid (6:1)	Mud Acid (12:3)
150	1.10	4.50

Table III- 3– Average results of API solubility test for bauxite proppant (without corrosion inhibitor).

*The experiments were repeated at least thirty times.

Aging Cell Experiments

Experiments Under Static Conditions

Bauxite solubility tests in (6:1) mud acid solution were conducted using the aging cell. Twenty-five grams of the bauxite was used with two-hundred grams of (6:1) mud acid. Several experiments were conducted at different soaking times ranging between 1 and 6 hours at 250-300°F. These experiments were done to simulate soaking conditions where acid diffusion is neglected. Each experiment was repeated three times to ensure reproducibility of results. The solutions were then filtered; the bauxite remaining was washed thoroughly with deionized water to remove residual acid and dried at 250°F for at least 5 hours. The retained weight was measured. Sieve analysis was conducted on some of the bauxite particles after the experiments to measure the change in particles size. **Fig.**

III-3 shows an example of the proppant samples before and after one of the experiments. Evidently, the color of the sample after the experiments was lighter because of the acid dissolution of proppants.

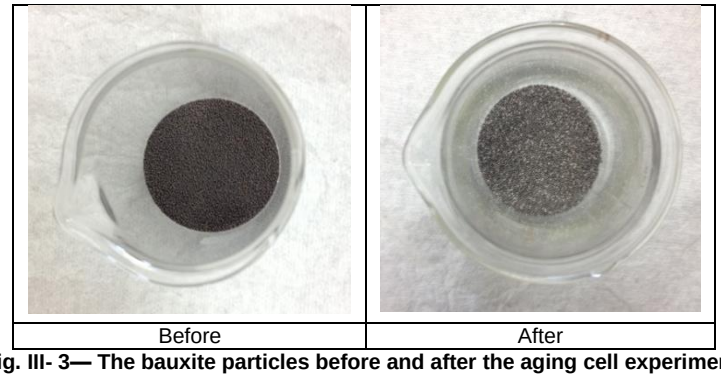

Fig. III- 3— The bauxite particles before and after the aging cell experiment.

The average results are summarized in **Table III-4**. More than 90.0 wt% of the proppant retained its size. These results are consistent with the results reported by Cheung (1988). **Fig. III-4** shows the dissolved proppant as a function of soaking time for bauxite proppant in (6:1) mud acid.

Soaking Time, hrs	T, °F	Weight Before, g	Weight After, g	Dissolved Proppant, wt%	Sieve Analysis After Experiment	
					30 Mesh, %	40 Mesh, %
1	250	25	24.67	1.32	92.03	7.97
2		25	24.34	2.65	98.37	1.60
3		25	23.85	4.59	94.67	5.32
4		25	23.65	5.40	99.20	0.76
5		25	23.58	5.69	94.89	5.02
6		25	23.51	5.97	96.05	3.75
1	300	25	24.56	1.76	90.87	9.11
2		25	23.81	4.77	98.26	1.71
3		25	23.45	6.19	96.60	3.26
4		25	22.95	8.21	96.92	3.04
5		25	22.59	9.64	96.51	3.41
6		25	22.62	9.53	95.91	3.99

Table III- 4– Average results of aging cell experiments for bauxite at different soaking times under static conditions with (6:1) mud acid system.

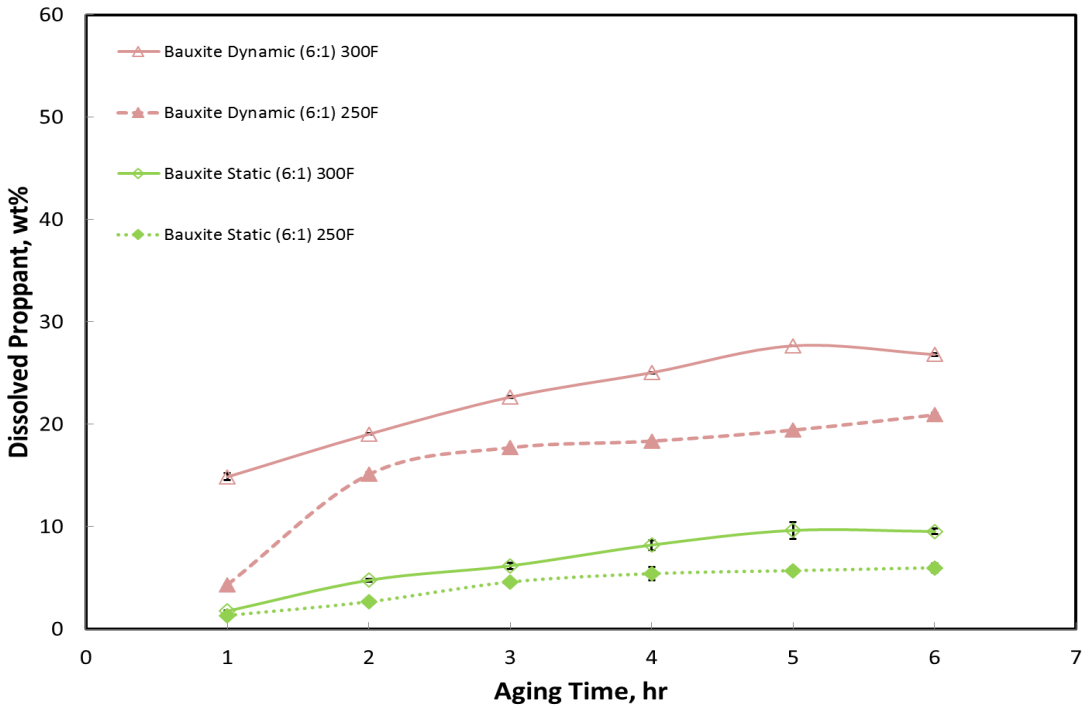

Fig. III- 4— Dissolved bauxite proppant over time after the aging cell experiments under both static and dynamic conditions at (6:1) mud acid system.

The supernatant of solubility tests was analyzed using ICP-OES. **Figs. III-5** and **III-6** show the concentrations of key elements (Al^{3+}, Si^{4+}, Fe^{3+}, and Ti^{4+}) in the samples after each experiment at 250 and 300°F, respectively. The sample showed high concentrations of aluminum, iron, and small amounts of titanium and silicon. The results show that the solubility increased with increasing temperature and soaking time. In bauxite proppant, although the crystals might be somewhat resistant to acid corrosion, HF attacked mullite, maghemite (Fe_2O_3), and corundum (Al_2O_3), especially at grain boundaries, causing the higher dissolution.

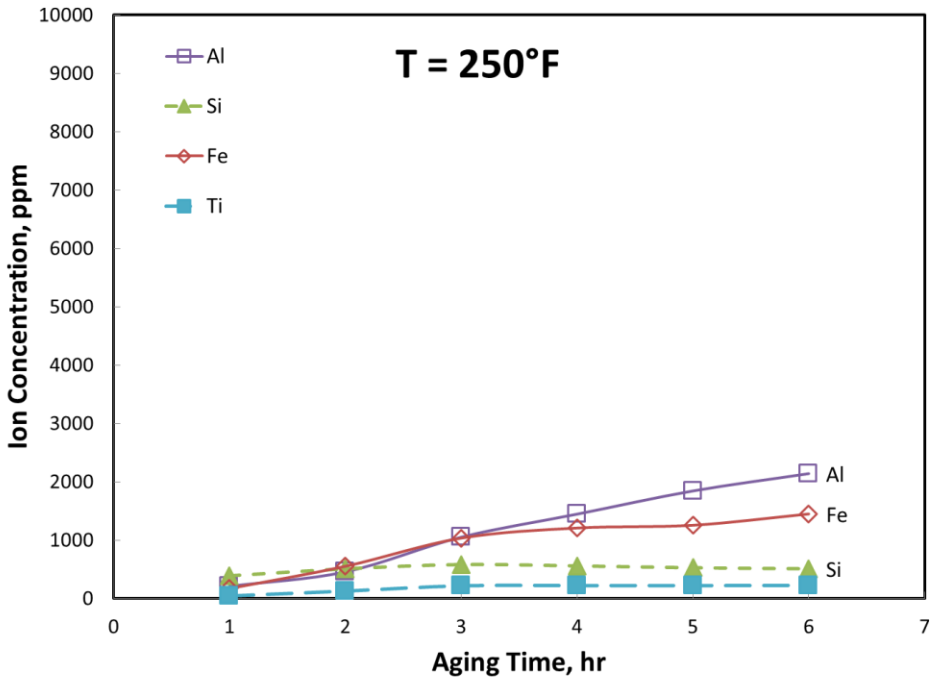

Fig. III- 5— Ion concentration in the supernatant of solubility tests after interaction with bauxite proppant for different soaking times at 250°F under static conditions, (6:1) mud acid system.

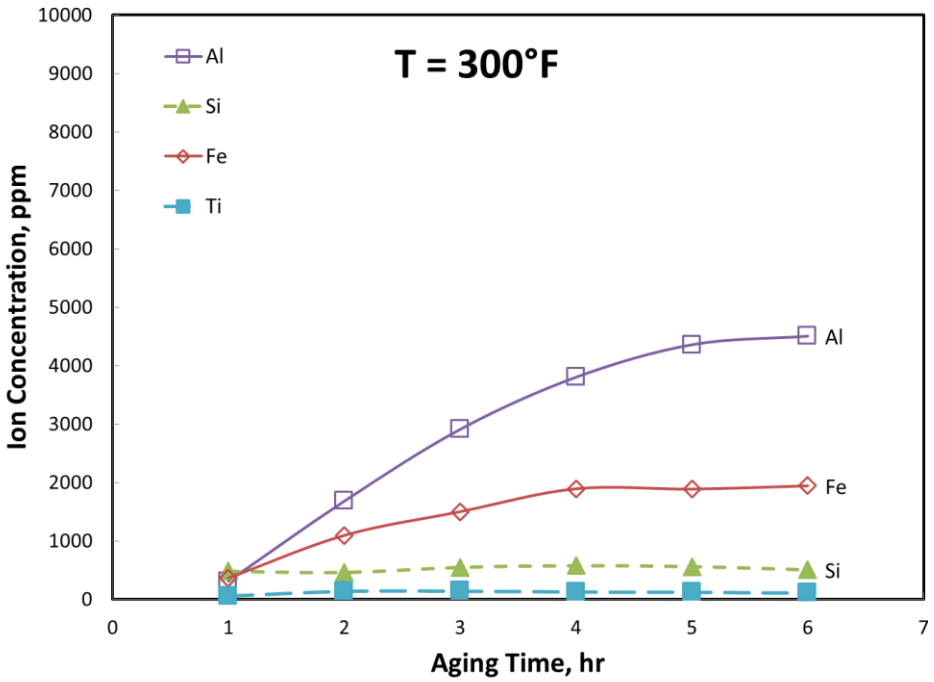

Fig. III- 6— Ion concentration in the supernatant of solubility tests after interaction with bauxite proppant for different soaking times at 300°F under static conditions, (6:1) mud acid system.

The experiments were repeated with bauxite using (12:3) mud acid, 9 wt% HCOOH, and 20 wt% Na_3-HEDTA acid systems at 250 and 300°F, respectively. The average results are summarized in **Tables III-5** through **III-7**.

Soaking Time, hrs	T, °F	Weight Before, g	Weight After, g	Dissolved Proppant, wt%
1	250	25	23.63	5.50
3		25	21.98	12.08
6		25	21.39	14.45
1	300	25	23.37	6.52
3		25	22.20	11.20
6		25	20.19	19.24

Table III- 5– Average results of aging cell experiments for bauxite proppant at different soaking times under static conditions with (12:3) mud acid system.

Soaking Time, hrs	T, °F	Weight Before, g	Weight After, g	Dissolved Proppant, wt%
1	250	25	24.50	2.02
3		25	23.56	5.78
6		25	23.26	6.95
1	300	25	24.17	3.34
3		25	23.58	5.67
6		25	23.49	6.04

Table III- 6– Average results of aging cell experiments for bauxite proppant at different soaking times under static conditions with (9:3) HCOOH:HF acid system.

Soaking Time, hrs	T, °F	Weight Before, g	Weight After, g	Dissolved Proppant, wt%
1	250	25	25.00	0.00
3		25	25.00	0.00
6		25	25.00	0.00
1	300	25	25.00	0.00
3		25	25.00	0.00
6		25	25.00	0.00

Table III- 7– Average results of aging cell experiments for bauxite proppant at different soaking times under static conditions with (20:1) Na_3-HEDTA:HF acid system.

Figs. III-7 and **III-8**, show the dissolved proppant as a function of soaking time for bauxite proppant with the first two acid systems, the dissolution with Na_3-HEDTA was negligible.

The supernatant of solubility tests was analyzed using ICP-OES. **Figs. III-9** through **III-12** show the cations' concentration in the samples after each experiment with (12:3) mud acid and HCOOH systems at 250 and 300°F, respectively. By increasing acid concentration, the solubility of bauxite increased. Additionally, its rate of dissolution increased at elevated temperatures. However, the solubility rates observed for HCOOH

were very close at 250 and 300°F. These rates actually declined slightly as temperature increased.

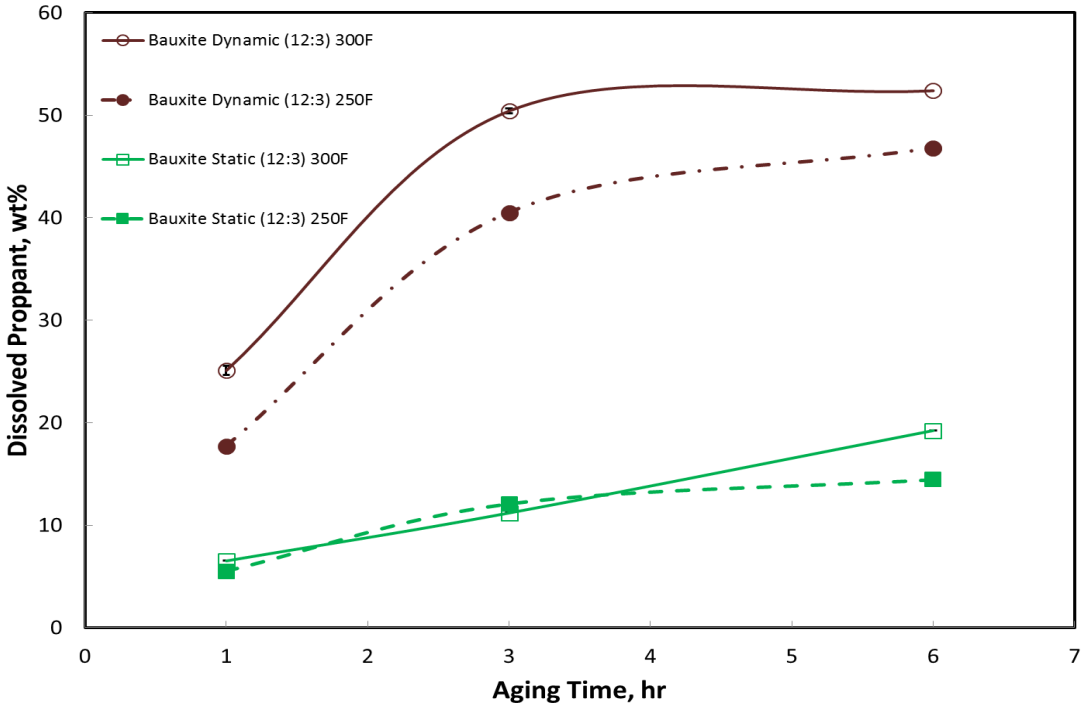

Fig. III- 7— Dissolved bauxite proppant over time after the aging cell experiments under both static and dynamic conditions at (12:3) mud acid system.

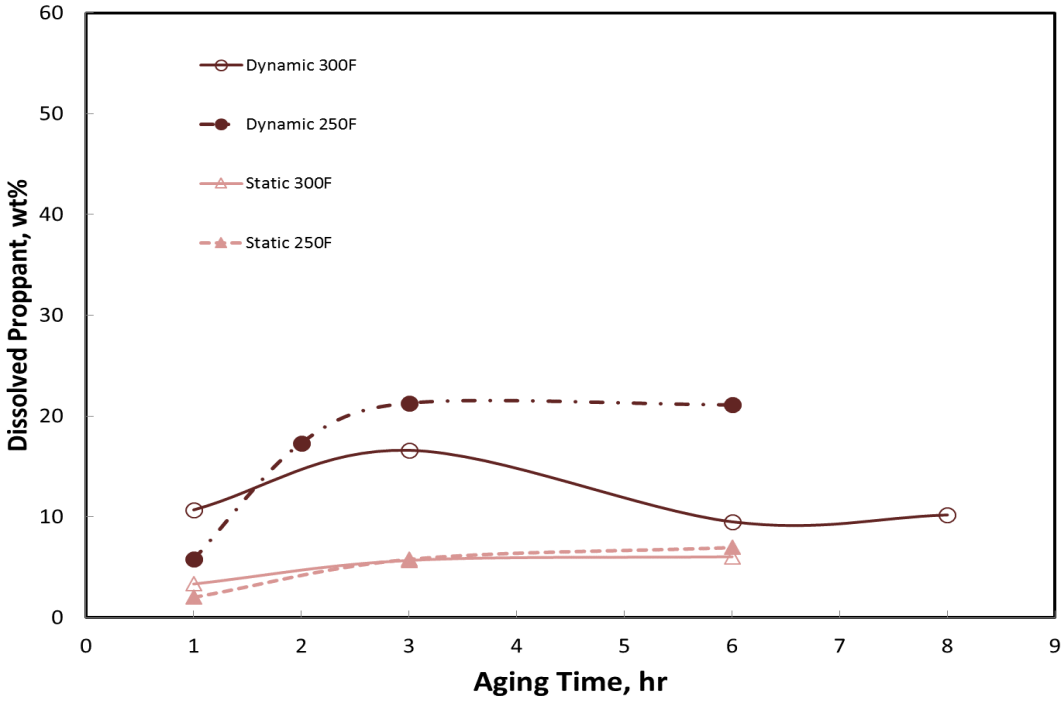

Fig. III- 8— Dissolved bauxite proppant over time after the aging cell experiments under both static and dynamic conditions at (9:3) HCOOH:HF acid system.

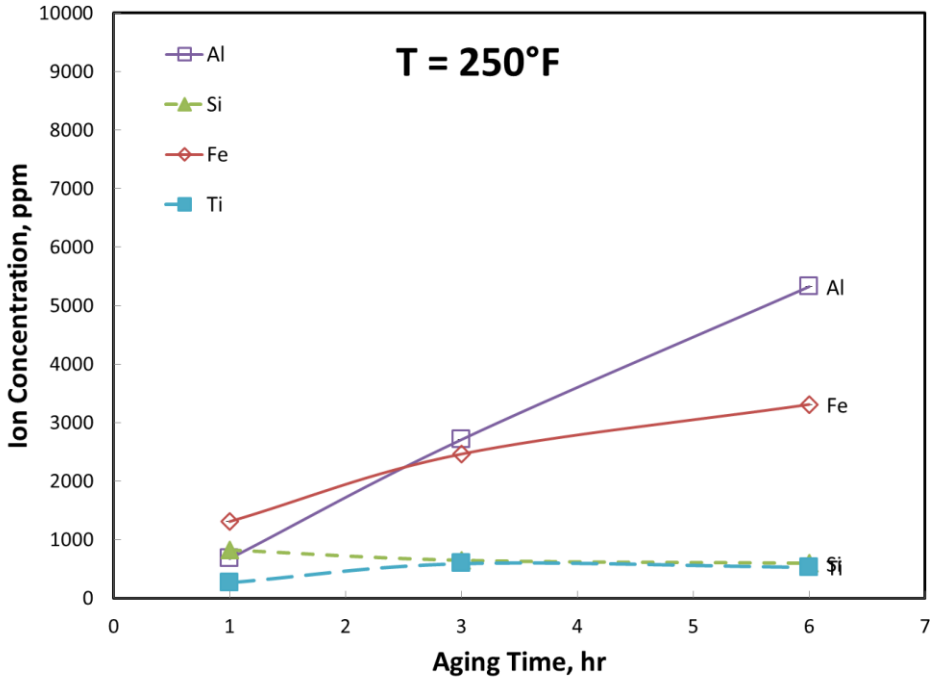

Fig. III- 9— Ion concentration in the supernatant of solubility tests after interaction with bauxite proppant for different soaking times at 250°F under static conditions, (12:3) mud acid system.

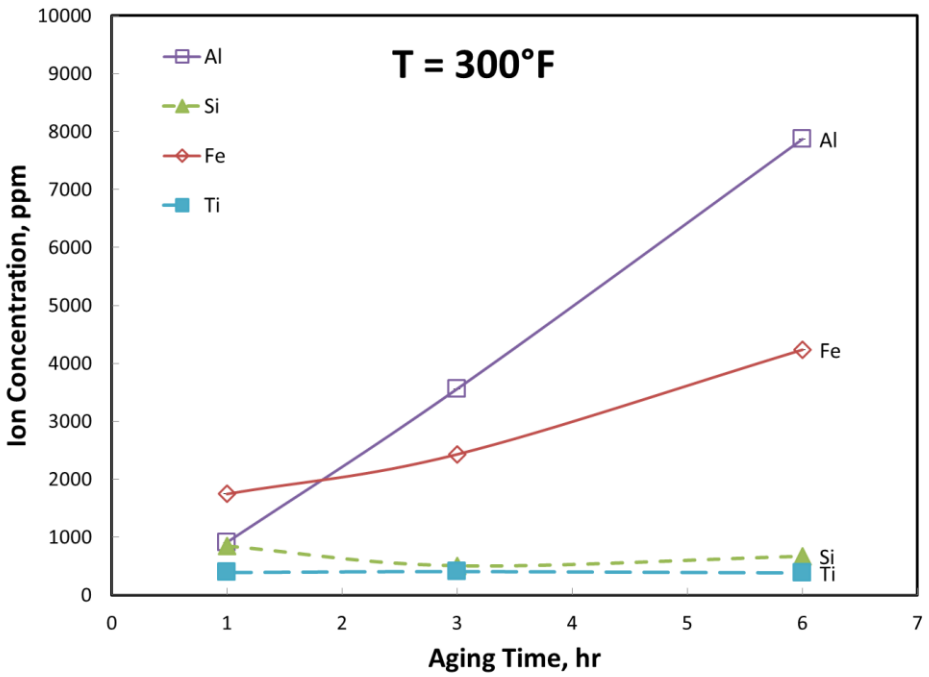

Fig. III- 10— Ion concentration in the supernatant of solubility tests after interaction with bauxite proppant for different soaking times at 300°F under static conditions, (12:3) mud acid system.

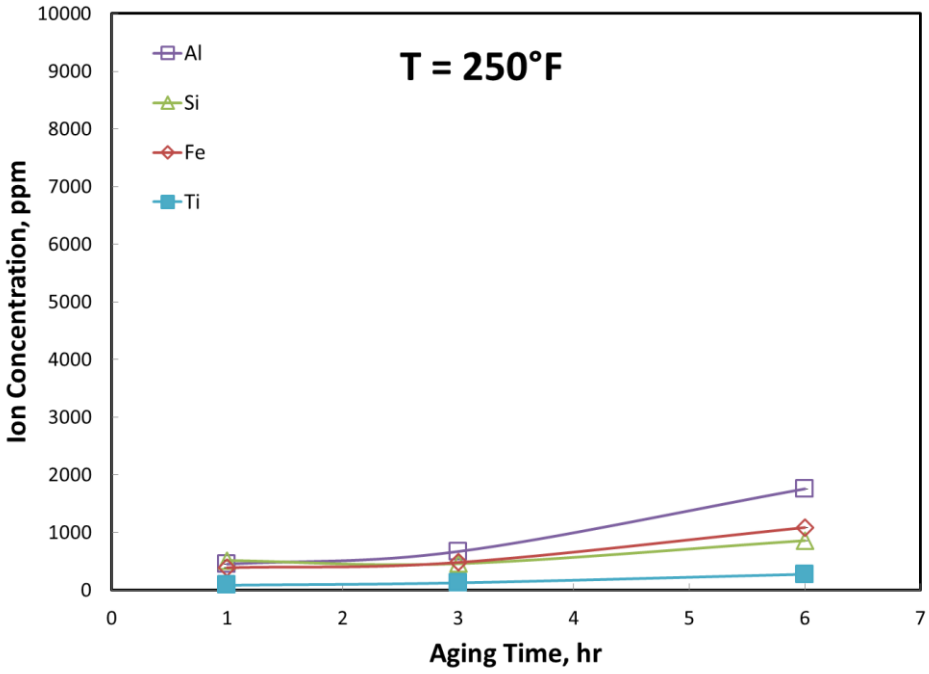

Fig. III- 11— Ion concentration in the supernatant of solubility tests after interaction with bauxite proppant for different soaking times at 250°F under static conditions, (9:3) HCOOH:HF acid system.

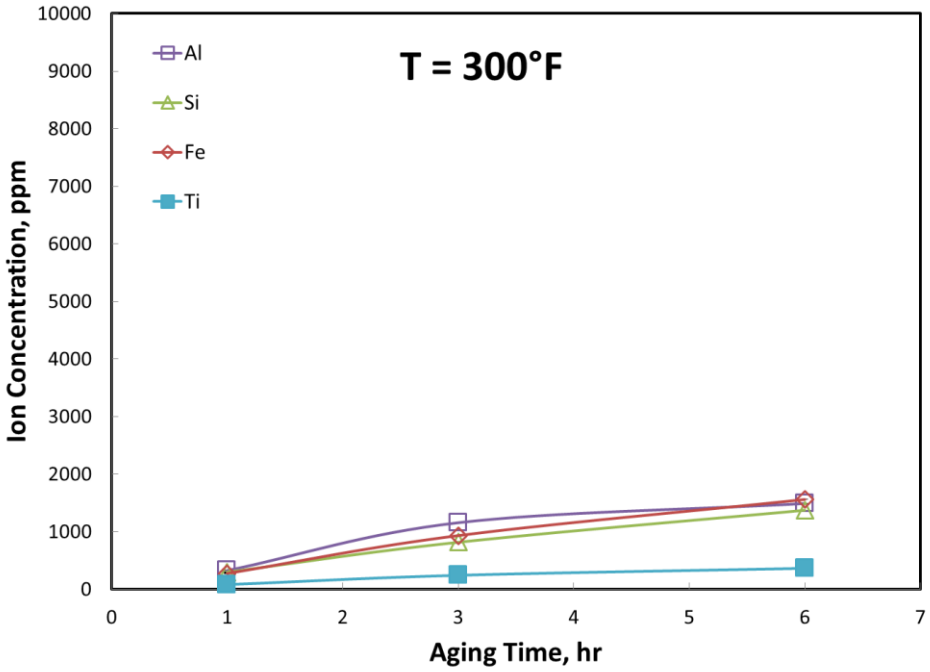

Fig. III- 12— Ion concentration in the supernatant of solubility tests after interaction with bauxite proppant for different soaking times at 300°F under static conditions, (9:3) HCOOH:HF acid system.

Experiments Under Dynamic Conditions

The same procedures were repeated at 250 and 300°F, but this time the oven rollers were running at 25 rpm. These tests were done to simulate injection conditions where acid diffusion can affect its reactivity with different minerals. Some of the experiments were repeated up to three times to ensure reproducibility of results. The average results for bauxite with different acid systems are summarized in **Tables III-8** through **III-11**.

Soaking Time, hrs	T, °F	Weight Before, g	Weight After, g	Dissolved Proppant, wt%	Sieve Analysis After Experiment	
					30 Mesh, %	40 Mesh, %
1	250	25	23.91	4.35	96.35	3.57
2		25	21.22	15.12	97.51	2.49
3		25	20.57	17.73	94.40	5.57
4		25	20.41	18.37	96.12	3.84
5		25	20.14	19.45	96.39	3.61
6		25	19.77	20.93	97.09	2.91
1	300	25	21.28	14.87	92.63	7.26
2		25	20.01	19.97	94.22	5.76
3		25	19.43	22.27	93.12	6.69
4		25	17.47	30.13	95.33	4.44
5		25	18.49	26.05	95.92	3.88
6		25	18.30	26.81	95.64	4.21

Table III- 8– Average results of aging cell experiments for bauxite proppant at different soaking times under dynamic conditions with (6:1) mud acid system.

Soaking Time, hrs	T, °F	Weight Before, g	Weight After, g	Dissolved Proppant, wt%
1	250	25	20.57	17.72
3		25	14.87	40.51
6		25	13.30	46.80
1	300	25	18.73	25.09
3		25	12.40	50.41
6		25	11.90	52.40
6*	350	37.5	16.42	56.2

Table III- 9– Average results of aging cell experiments for bauxite proppant at different soaking times under dynamic conditions with (12:3) mud acid system.

*The mud acid weight used was 300 g.

Soaking Time, hrs	T, °F	Weight Before, g	Weight After, g	Dissolved Proppant, wt%
1	250	25	23.56	5.77
2		25	20.68	17.30
3		25	19.69	21.26
6		25	19.73	21.08
1	300	25	22.33	10.68
3		25	20.85	16.60
6		25	22.62	9.50
8		25	22.454	10.18

Table III- 10– Average results of aging cell experiments for bauxite proppant at different soaking times under dynamic conditions with (9:3) HCOOH:HF acid system.

Soaking Time, hrs	T, °F	Weight Before, g	Weight After, g	Dissolved Proppant, wt%
1	250	25	24.66	1.36
3		25	25.00	0.00
6		25	25.00	0.00
1	300	25	25.00	0.00
3		25	25.00	0.00
6		25	24.88	0.46

Table III- 11– Average results of aging cell experiments for bauxite proppant at different soaking times under dynamic conditions with (20:1) Na_3-HEDTA:HF acid system.

Figs. III-4, III-7, and III-8 show the dissolved proppant as a function of soaking time for different acid systems with bauxite. **Figs. III-13** through **III-18** show the concentrations in the samples after each experiment with different acid systems at 250 and 300°F, respectively. The samples showed higher cations' concentration compared to the concentrations measured from experiments under static conditions. Also, the solubility increased with mud acids compared to the HCOOH system. The same trend was observed with HCOOH. Bauxite solubility—especially at longer soaking times—actually declined

with temperature. This phenomenon will be further analyzed in the microstructure analysis section.

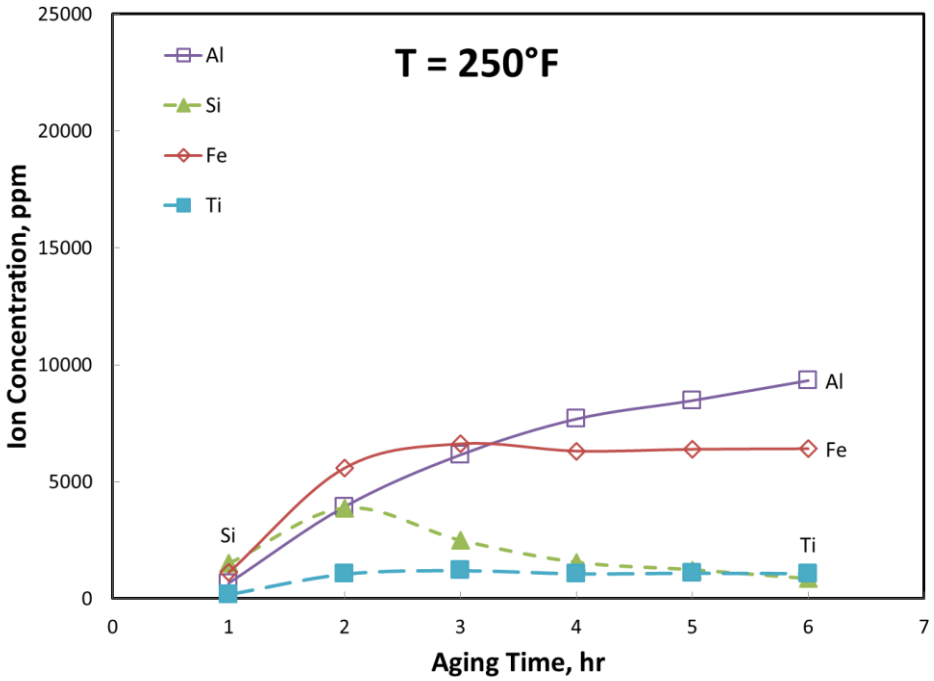

Fig. III- 13— Ion concentration in the supernatant of solubility tests after interaction with bauxite proppant for different soaking times at 250°F under dynamic conditions, (6:1) mud acid system.

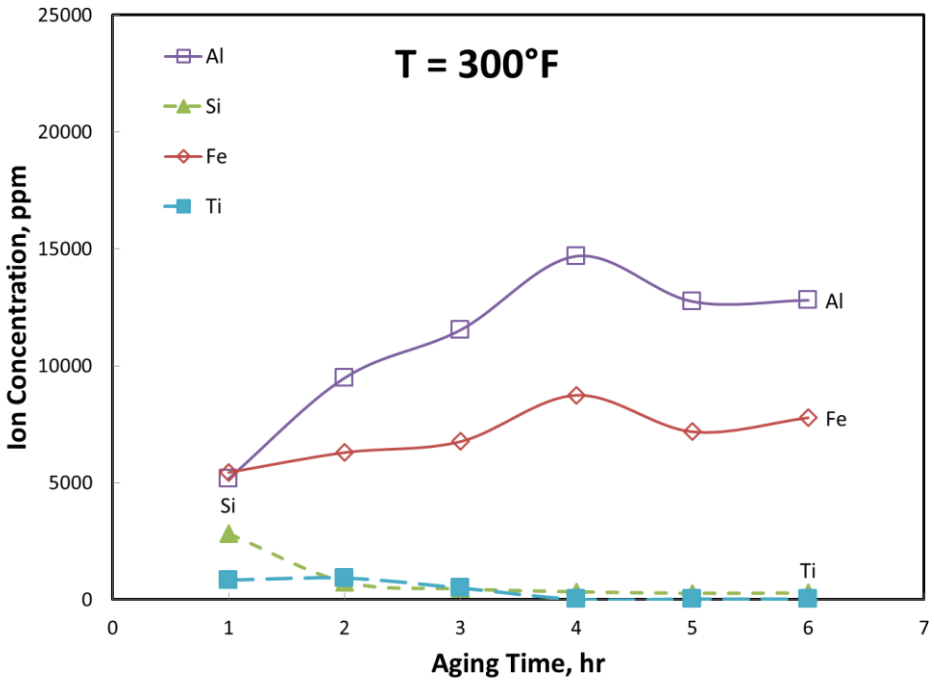

Fig. III- 14— Ion concentration in the supernatant of solubility tests after interaction with bauxite proppant for different soaking times at 300°F under dynamic conditions, (6:1) mud acid system.

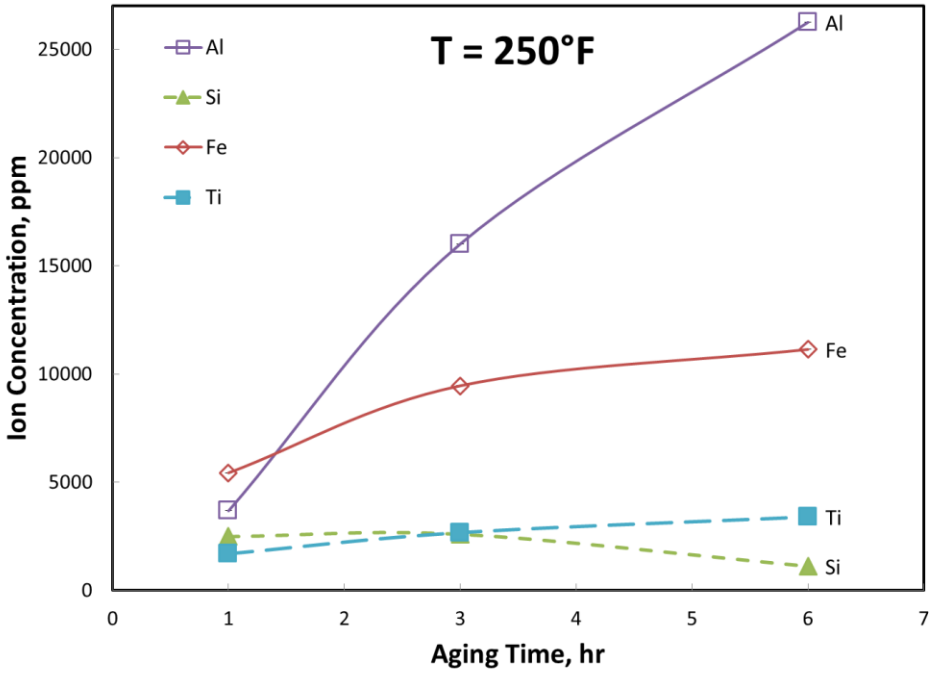

Fig. III- 15— Ion concentration in the supernatant of solubility tests after interaction with bauxite proppant for different soaking times at 250°F under dynamic conditions, (12:3) mud acid system.

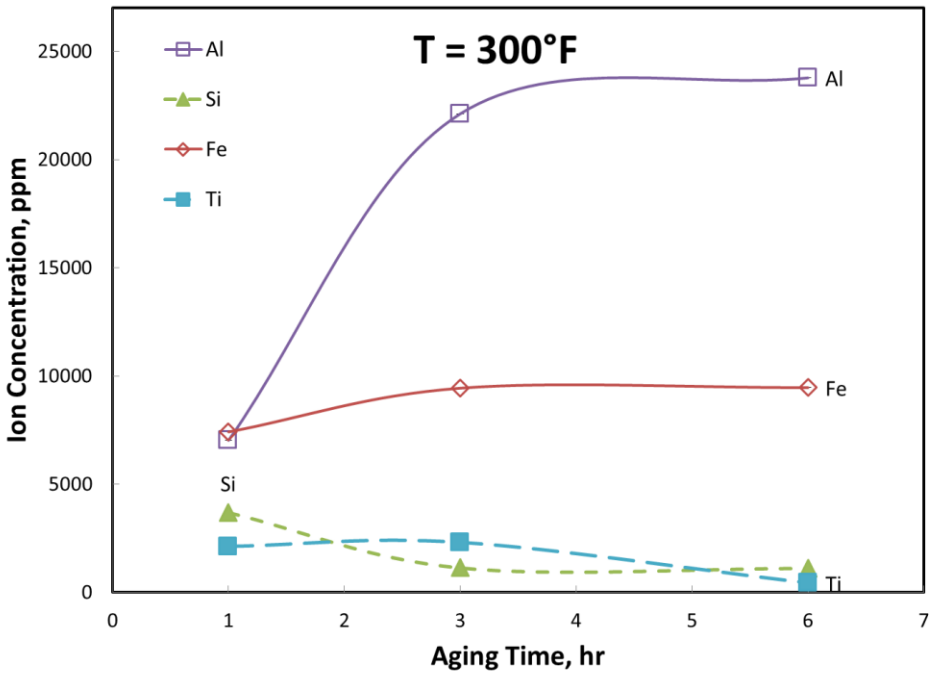

Fig. III- 16— Ion concentration in the supernatant of solubility tests after interaction with bauxite proppant for different soaking times at 300°F under dynamic conditions, (12:3) mud acid system.

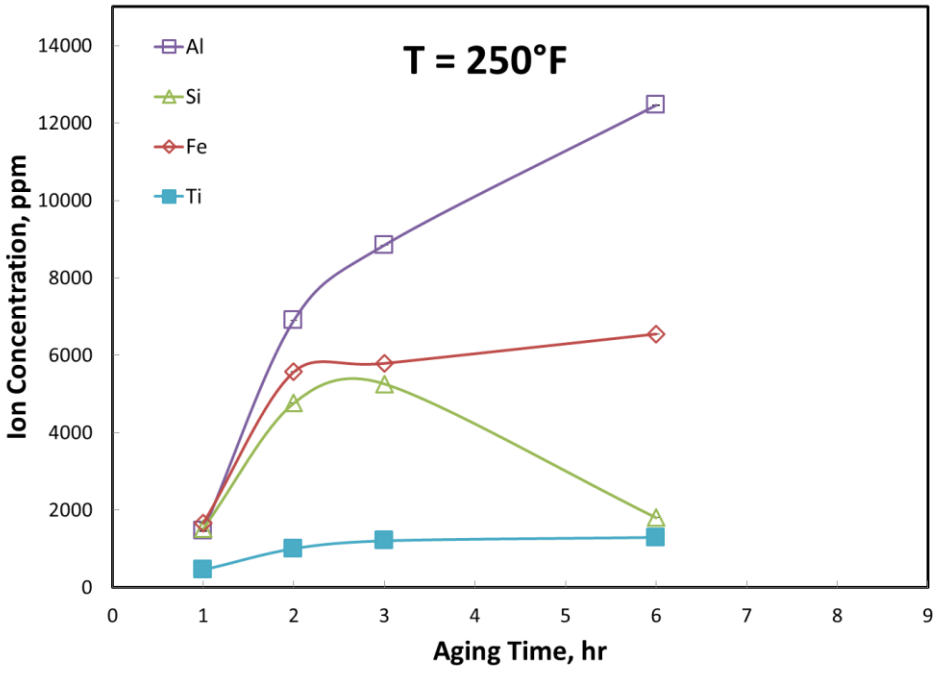

Fig. III- 17— Ion concentration in the supernatant of solubility tests after interaction with bauxite proppant for different soaking times at 250°F under dynamic conditions, (9:3) HCOOH:HF acid system.

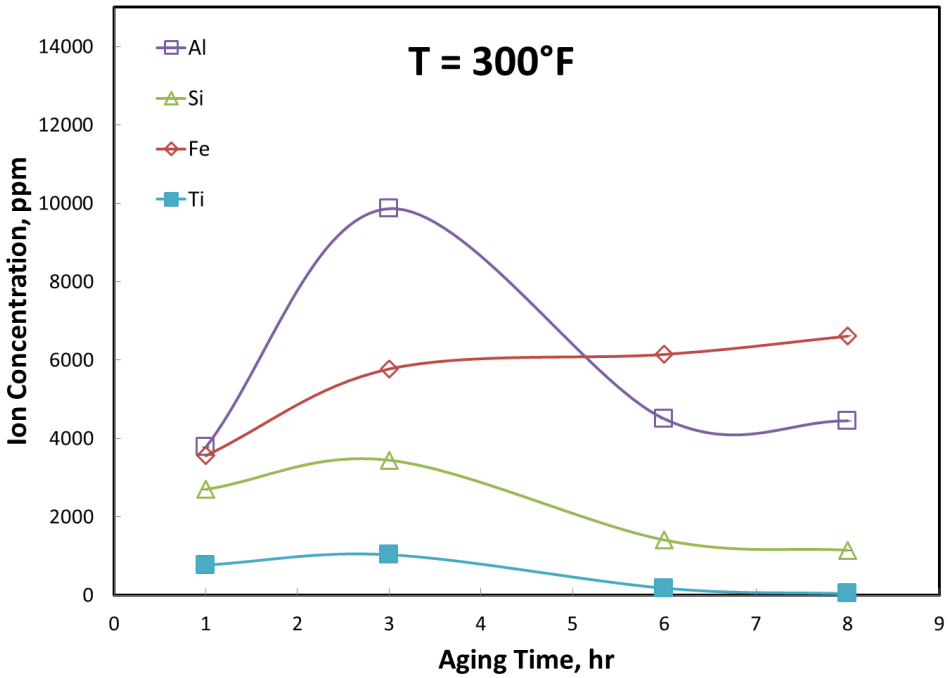

Fig. III- 18— Ion concentration in the supernatant of solubility tests after interaction with bauxite proppant for different soaking times at 300°F under dynamic conditions, (9:3) HCOOH:HF acid system.

Images acquired by a Zeiss Axiophot optical microscope showed the effect of acid solubility on the proppant particles. **Fig. III-19** depicts the results of proppant particle dissolution in regular mud acid. The proppant particles lost their smoothness showed porous surfaces. The dissolution of proppants resulted in the generation of fine particles that were separated from the solution after experiments. This process can decrease proppant pack conductivity.

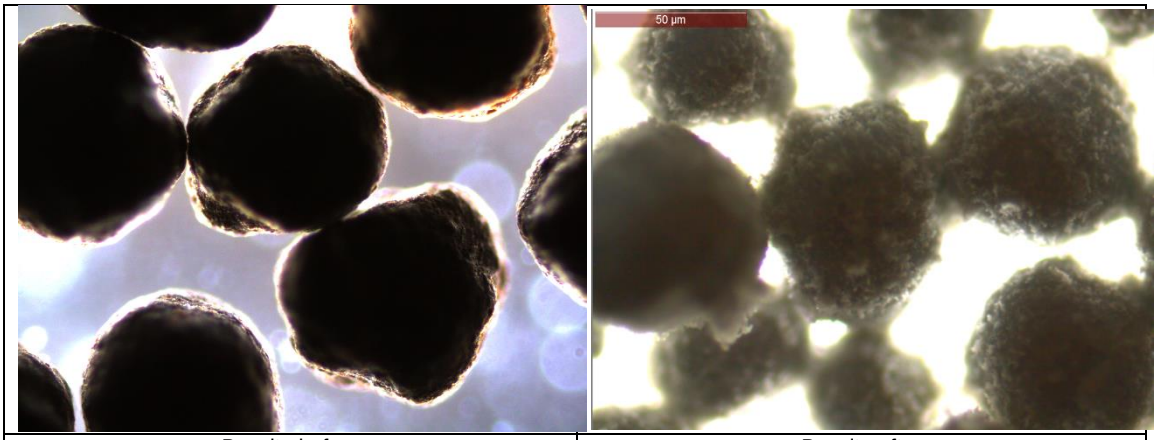

Fig. III- 19— Zeiss Axiophot optical microscope image at x50 magnification of bauxite proppant before and after acid solubility.

^{19}F-NMR Analysis

The ^{19}F-NMR analysis was conducted to some of the supernatants of acid solutions for the bauxite experiments prior to and after the acid interactions. **Fig. III-20** shows the ^{19}F-NMR spectra of the samples for three different solutions: fresh mud acid (6:1) and mud acids of (6:1 and 12:3) after 6 hours at 300°F under dynamic conditions. Fig. III-20 (a) shows a chemical shift for HF only (Shuchart and Buster 1995). From the ICP-OES sample analysis, after the experiments, the concentration of aluminum and iron are high in the samples. Yet, Fig. III-20 (b) shows a chemical shift for AlF^{2+} only (Sur and Bryant 1996). Fig. III-20 (c) shows two peaks for F^- and probably AlF_4O_2 (König et al. 2008). The affinity of fluorine to aluminum is high compared to that with iron (Crowe 1985; Sur and Bryant 1996). Iron may not have formed a complex with F^- in the presence of aluminum, but it is still soluble because of the low pH value of the acid solution after experiments.

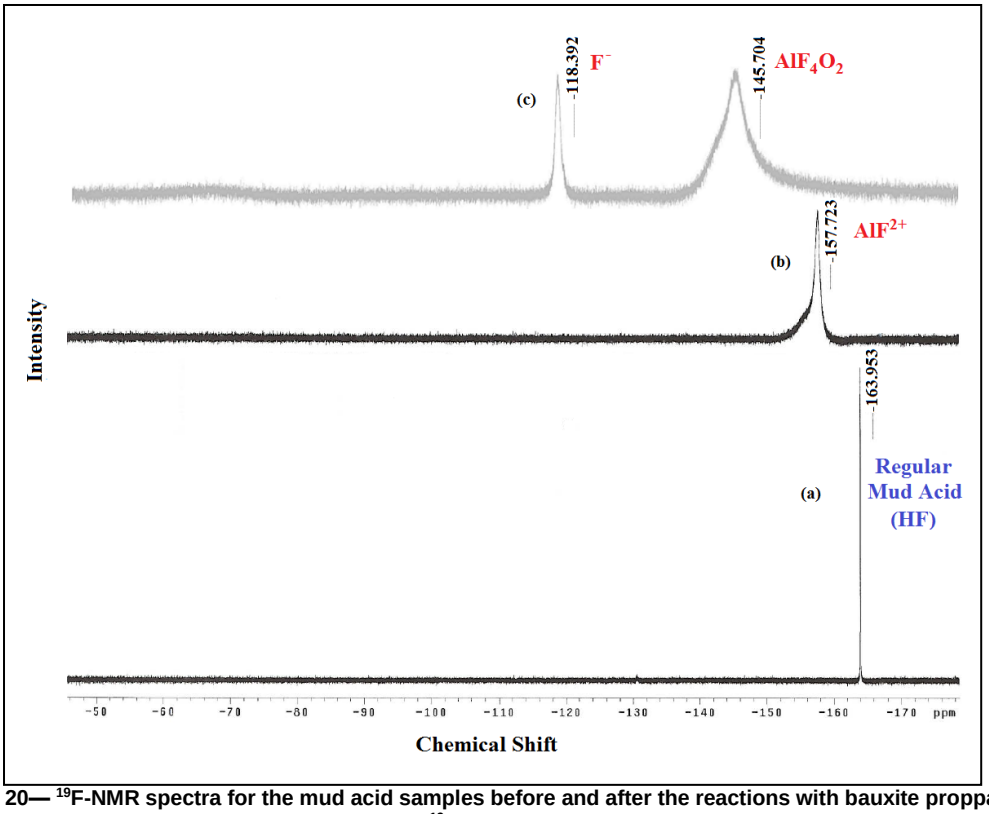

Fig. III- 20— ^{19}F-NMR spectra for the mud acid samples before and after the reactions with bauxite proppant. (a) ^{19}F-NMR spectrum for (6:1) mud acid system, (b) ^{19}F-NMR spectrum for the (6:1) mud acid system after 6 hours with bauxite proppant at 300°F under dynamic conditions, and (c) ^{19}F-NMR spectrum for the, regular, (12:3) mud acid system after 6 hours with bauxite proppant at 300°F under dynamic conditions.

XRD Analysis

XRD analysis was conducted on some of the bauxite particles prior to and after the acid interactions. **Fig. III-21** shows the analysis for the original proppant particles and the ones after interacting with different mud acid solutions for a period of 6 hours at 300°F under dynamic conditions. The results revealed that the minerals were almost unchanged. Only some of the mullite and maghemite peaks disappeared, and a minor quantity of minerals that were poorly crystallized was dissolved, which was the main reason for proppant weight loss after conducting the experiments. It is documented that the dissolution of

mullite in hydrofluoric acid is higher than that of corundum (Grosheva and Mironov 1974; Mikeska and Bennison 1999).

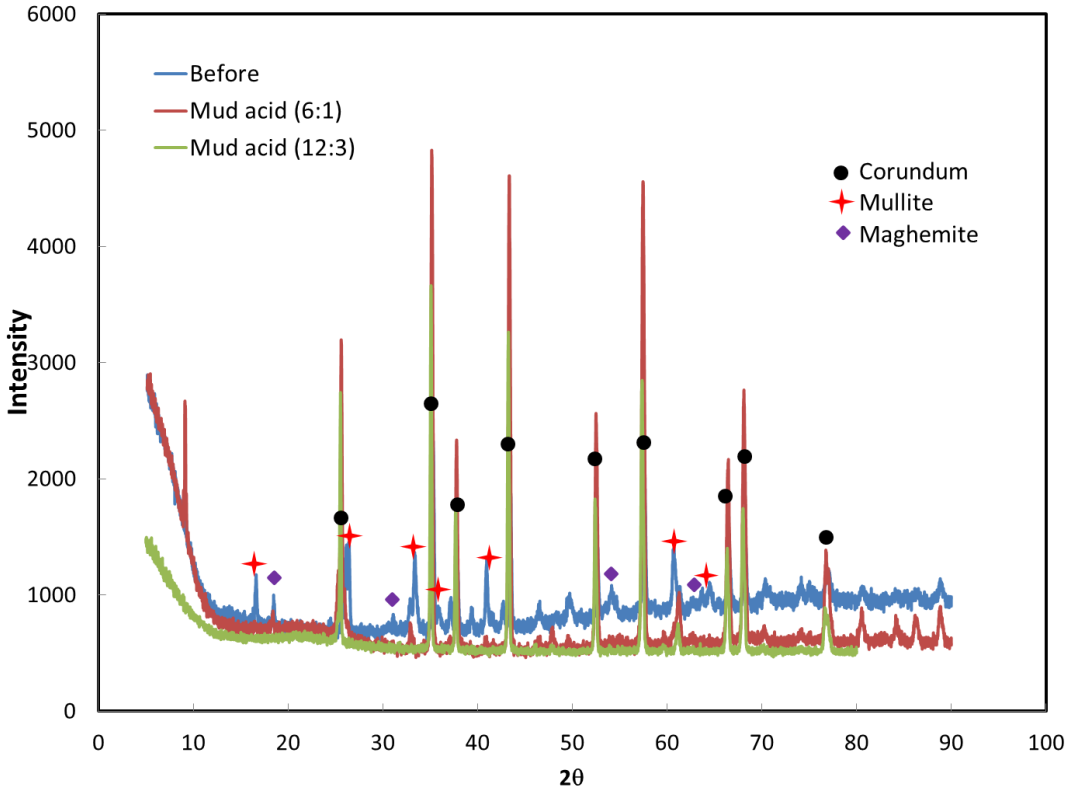

Fig. III- 21— XRD patterns for bauxite particles before and after interaction with mud acids for 6 hours at 300°F under dynamic conditions.

XRF Analysis

XRF analysis was conducted on the same samples used for XRD. **Table III-12** summarizes the key oxides present in the proppant samples prior to the experiments. Bauxite proppant showed aluminum, silicon, and iron oxides as they typically contain mullite, maghemite, and corundum. The concentrations agree with the results obtained by XRD.

Oxide	Concentration, wt%
Al_2O_3	79.70
SiO_2	7.38
TiO_2	4.88
Fe_2O_3	3.81
Other Oxides	<4.23

Table III- 12– Oxides analysis by XRF for bauxite proppant used in the study.

Microstructure Analysis

The analysis of bauxite residual solids was done using SEM. Several runs were performed. **Figs. III-22** through **25** show the images of the bauxite proppant spectrum for some residual solid samples; after proppants' interaction with (6:1) mud acid at different soaking times under dynamic conditions. The solids contain high concentrations of aluminum, silicon, iron, and titanium elements. The concentration of silicon increased with soaking time, which is consistent with the precipitation observed from ICP results. These figures show gold peaks because gold was used to coat the tested samples. Owing to the surface heterogeneity of the residual solids, all samples were tested several times to ensure good reproducibility of results. The results in agreement were considered, while others were discarded. The quantitative results for the elements are summarized in **Table III-13**.

Element	Concentration, wt%			
	2 hrs	3 hrs	4 hrs	5 hrs
O	23.63	31.68	34.56	37.00
Al	34.32	10.42	10.29	10.01
Si	21.99	26.56	34.13	32.53
Ti	2.96	13.35	11.41	14.76
Fe	17.11	12.62	3.70	2.86

Table III- 13– Quantitative results by EDS for bauxite residual solids after the reaction with (6:1) mud acid at different soaking times under dynamic conditions.

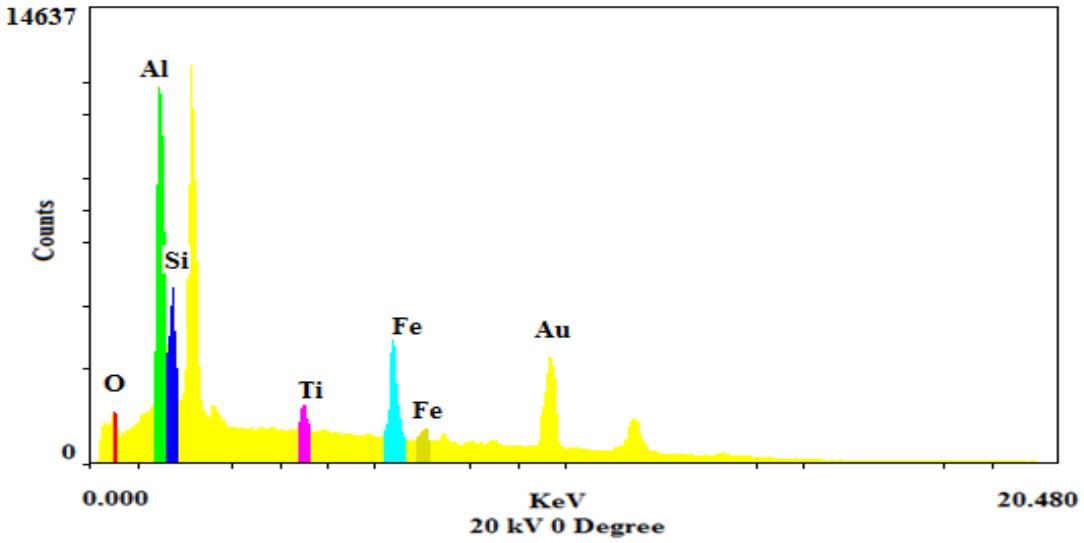

Fig. III- 22— Analysis for sample (A) of the bauxite residual solids after (6:1) mud acid exposure for 2 hours.

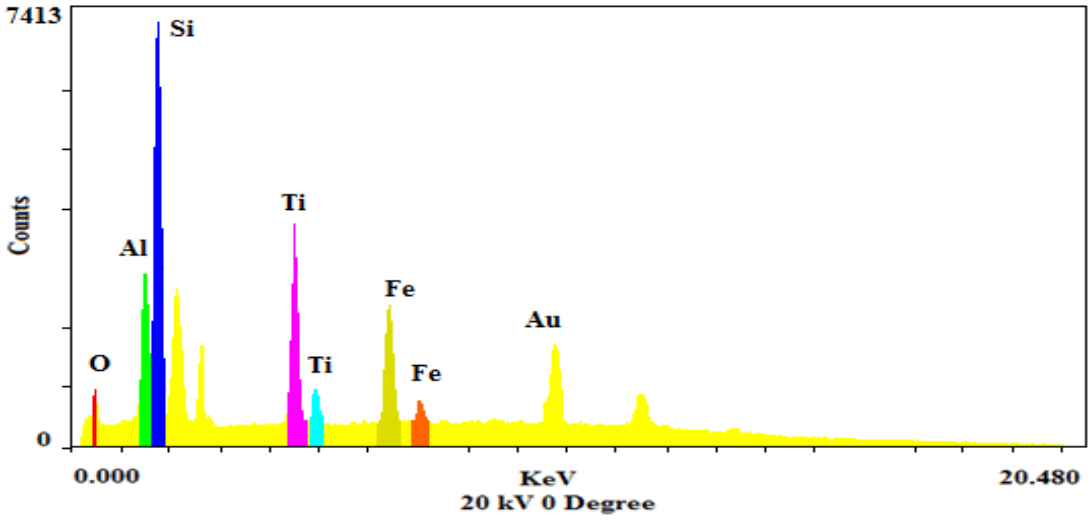

Fig. III- 23— Analysis for sample (B) of the bauxite residual solids after (6:1) mud acid exposure for 3 hours.

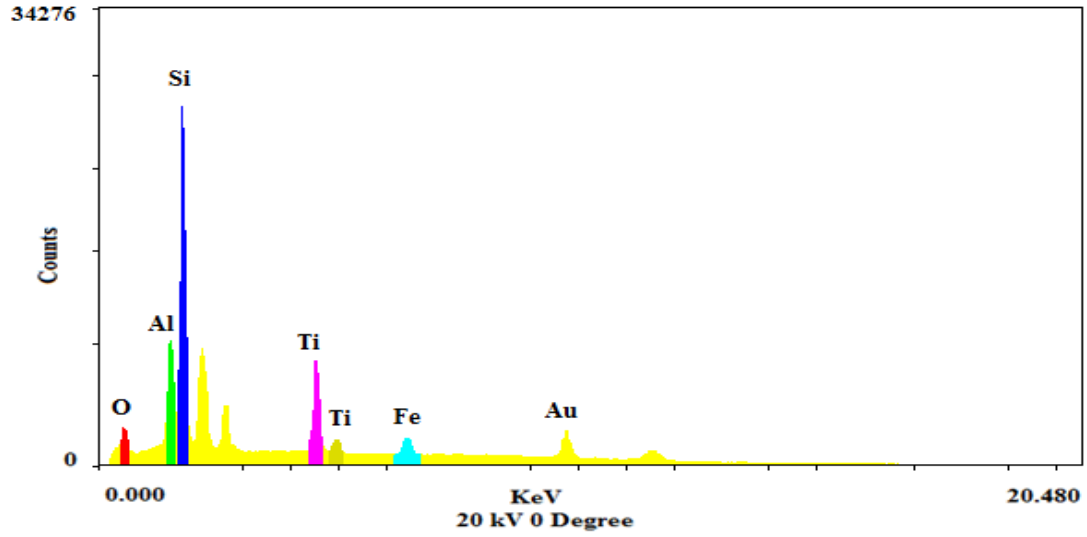

Fig. III- 24— Analysis for sample (C) of the bauxite residual solids after (6:1) mud acid exposure for 4 hours.

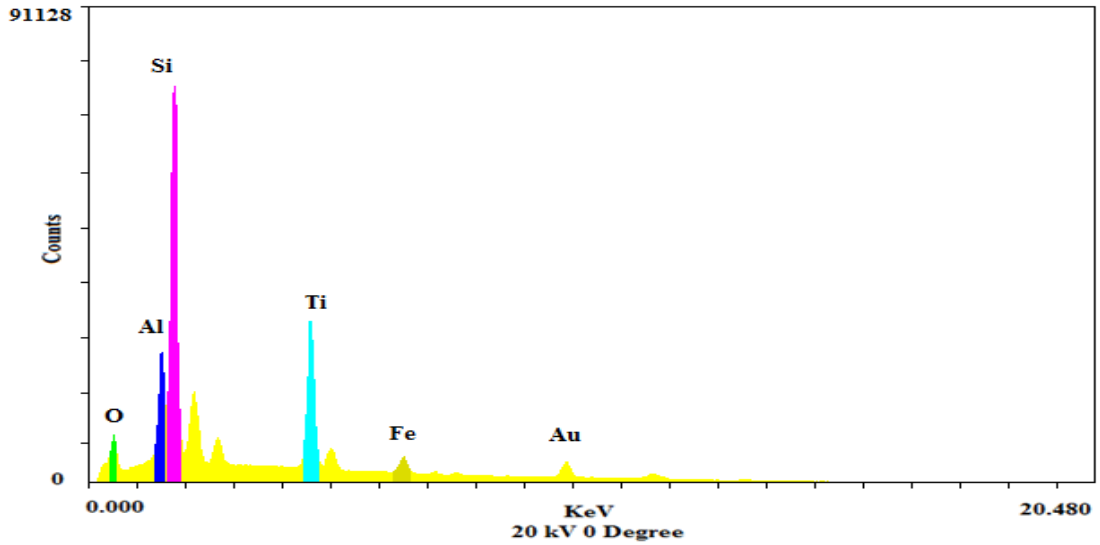

Fig. III- 25— Analysis for sample (D) of the bauxite residual solids after (6:1) mud acid exposure for 5 hours.

Fig. III-26 shows the residual solids filtered after bauxite dissolution in different mud acid solutions. Fig. III-26, including (a) and (b), illustrates the residue after exposure to (6:1) and (12:3) mud acids, respectively. Both micrographs show the agglomeration of fine particles with different crystalline structures. These fines were generated when acid dissolved mullite, maghemite, and other poorly crystallized minerals. The residues can be detrimental to both conductivity for gravel-packed wells and fractures.

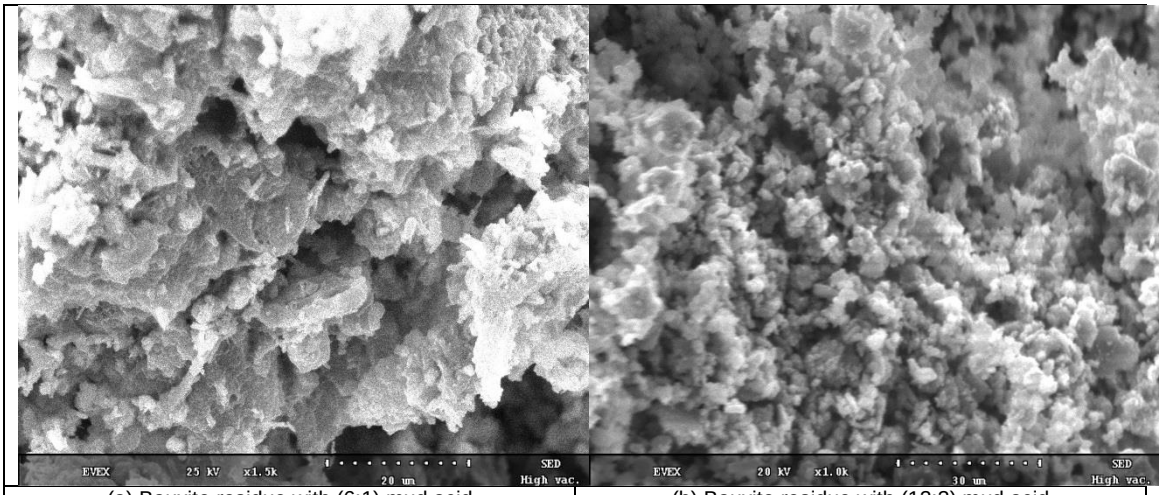

(a) Bauxite residue with (6:1) mud acid | (b) Bauxite residue with (12:3) mud acid

Fig. III- 26— Scanning electron micrographs of bauxite proppant residue filtered after different mud acid solutions' corrosion. (a) x1.5K micrograph of the bauxite proppant residue after treatment with (6:1) mud acid system, (b) x1.0K micrograph of the bauxite proppant residue after treatment with (12:3) mud acid system, both showing agglomeration of tiny precipitates.

The same analysis was performed for several residual solid samples after proppants' interaction with (9:3) HCOOH:HF acid at different soaking times under dynamic conditions. **Figs. III-27** and **28** show the images of the bauxite proppant spectrum analyses for some of these samples. The solids contain high concentrations of aluminum, iron/fluorine, and titanium/calcium elements. The concentration of aluminum increased with soaking time, which is consistent with the precipitation observed from ICP results. The quantitative results for the elements are summarized in **Table III-14**.

Element	Concentration, wt%	
	3 hrs	6 hrs
Al	28.15	38.61
Si	1.96	0
Ti/Ca	11.42	9.89
Fe/F	58.47	51.5

Table III- 14– Quantitative results by EDS for bauxite residual solids after the reaction with (9:3) HCOOH:HF acid system at 3 and 6 hours under dynamic conditions.

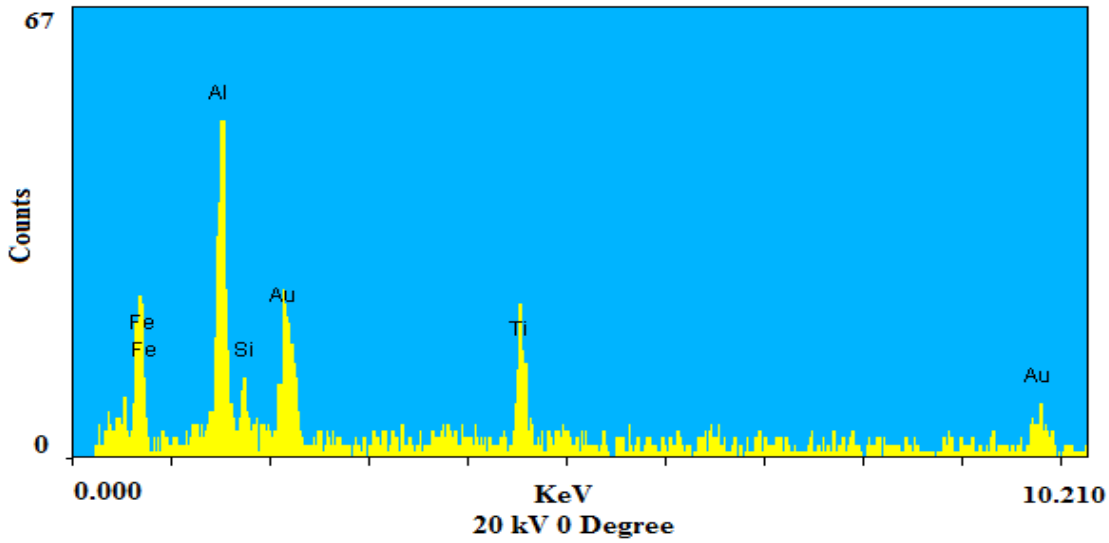

Fig. III- 27— Analysis for sample (A) of the bauxite residual solids (9:3) HCOOH:HF acid system exposure for 3 hours.

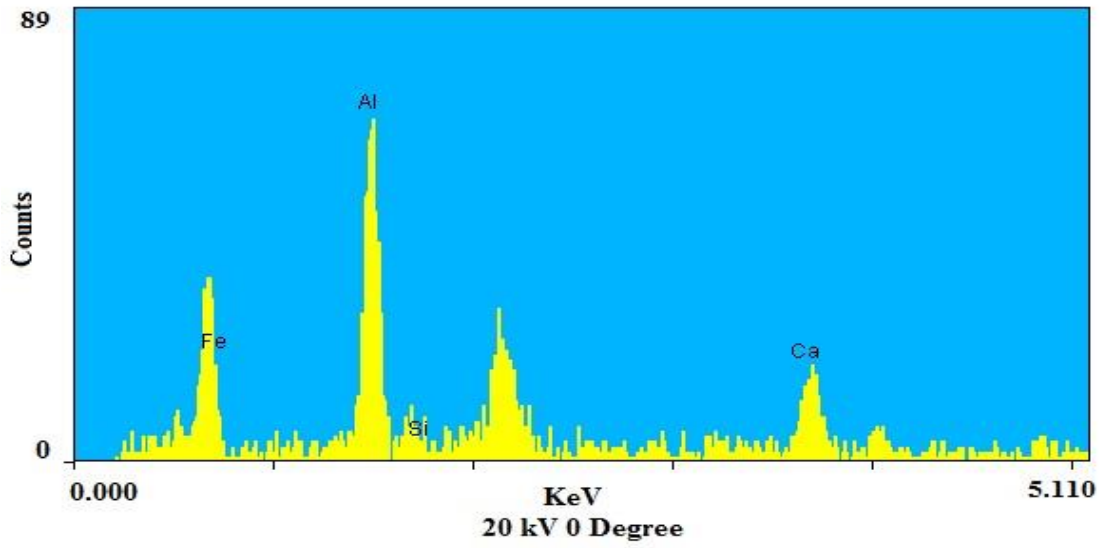

Fig. III- 28— Analysis for sample (B) of the bauxite residual solids (9:3) HCOOH:HF acid system exposure for 6 hours.

Crushing Test

In the following crush tests, a universal testing machine (Instron 5583) displayed in **Fig. III-29**, was used to apply the load required for accomplishing the stress levels up to 8,000 psi (103 MPa) and a cell for proppant crush-resistance test. 12 g of bauxite proppant were used in every test.

Crush tests were performed on both treated and untreated proppant samples. The treated samples simulated the harshest conditions presented in **Table III-15**. The experiments were performed at temperatures of 250 and 300°F under dynamic conditions.

Fig. III- 29— A universal testing machine, Instron 5583.

Prior to the crushing test, samples were sieved for 10 minutes. The cell was then loaded in order to obtain a consistent loose pack throughout the cell. The piston was inserted into the test cell containing the weighed sample of proppant, without applying any additional force and ensuring a level surface in the proppant pack. The test cell was carefully lifted and placed directly into the press, centered under the ram.

The diameter of the cell, d_{cell} = 2 in. and the stress was maintained at a constant rate of 2,000 psi/min (i.e., the force rate required (F_{tc}) = 6,280 lb_f/min) reaching 8,000 psi

in 4 minutes. The final stress level was held for 2 minutes then released, and the test cell was removed from the press. The content of the cell was carefully transferred into the same sieve stack used before and shaken for a comparable period of time. The crushed material in the pan was carefully weighed and recorded as m_{pan}. The amount of crushed material, particles finer than a 40-mesh sieve, was calculated and reported as a percentage, m'_{pan}, of the original mass of 12 g.

Table III-15 presents the average results of the bauxite proppant crush test. The results showed that there is a direct relationship between acid solubility and crushing resistance. Samples tested with Na_3-HEDTA exhibited the best mechanical properties followed by HCOOH and HCl-based mud acid solutions. Crushing resistance decreased with increasing mud acid concentration. Samples tested with Na_3-HEDTA showed up to a 10% increase in compaction compared to the untreated sample (the lowest). Conversely, (12:3) mud acid showed up to a 147% increase in compaction (the highest). Although the proppant mass used in the previous tests were not following standardized procedures, these tests can give us an idea about the severity of acid solubility on the mechanical properties of bauxite. **Fig. III-30** and **III-31** present the proppant samples' compressive extension as a function of crushing time. The untreated bauxite was used as a baseline for comparison purposes. Samples possessing high mechanical strength showed lower compression rates.

Acid Used	Conditions	Crushing Pressure	m'pan, %	Compression Increase*, %
No acid	-	5,000 psi	0	-
No acid	-	8,000 psi	1	0
(20:1) Na_3-HEDTA:HF	250°F/6 hrs	8,000 psi	0	10
(20:1) Na_3-HEDTA:HF	300°F/6 hrs	8,000 psi	0	6
(9:3) HCOOH:HF	250°F/6 hrs	8,000 psi	13	39
(9:3) HCOOH:HF	300°F/6 hrs	8,000 psi	19	51
(6:1) Mud acid	250°F/6 hrs	8,000 psi	12	54
(6:1) Mud acid	300°F/6 hrs	8,000 psi	21	101
(12:3) Mud acid	250°F/6 hrs	8,000 psi	48**	122
(12:3) Mud acid	300°F/6 hrs	8,000 psi	46	147

Table III- 15– Average results of the bauxite proppant crush test with different acid systems.

*% increase from an untreated sample.

**The average of 2 experiments with an average initial mass of 11.44 g.

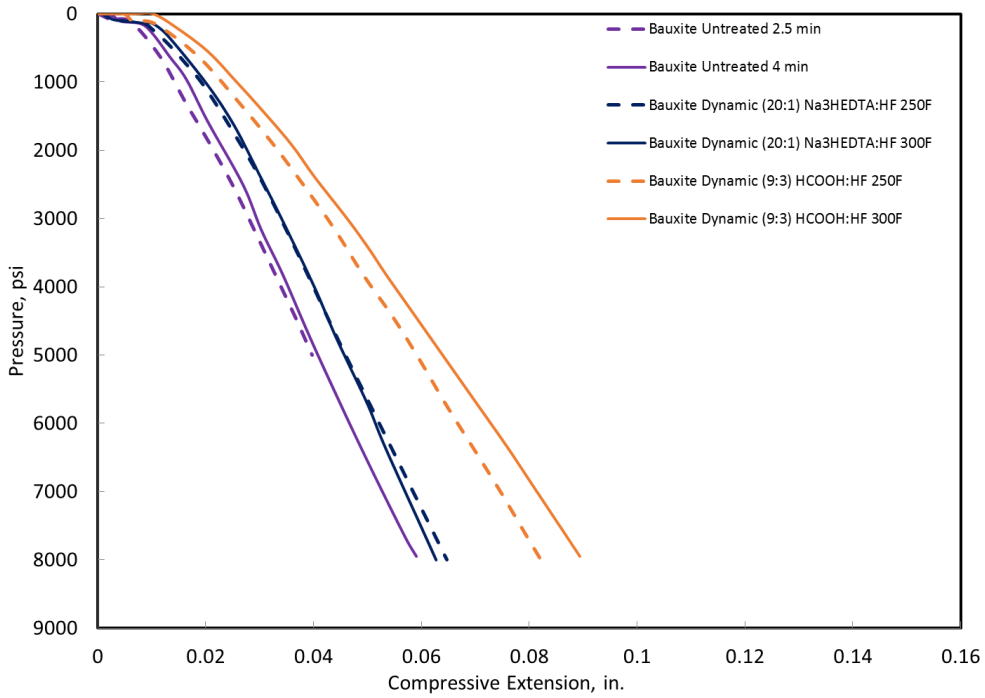

Fig. III- 30— Compaction of bauxite samples up to 8,000 psi at different conditions before and after the aging cell experiment with different acid systems.

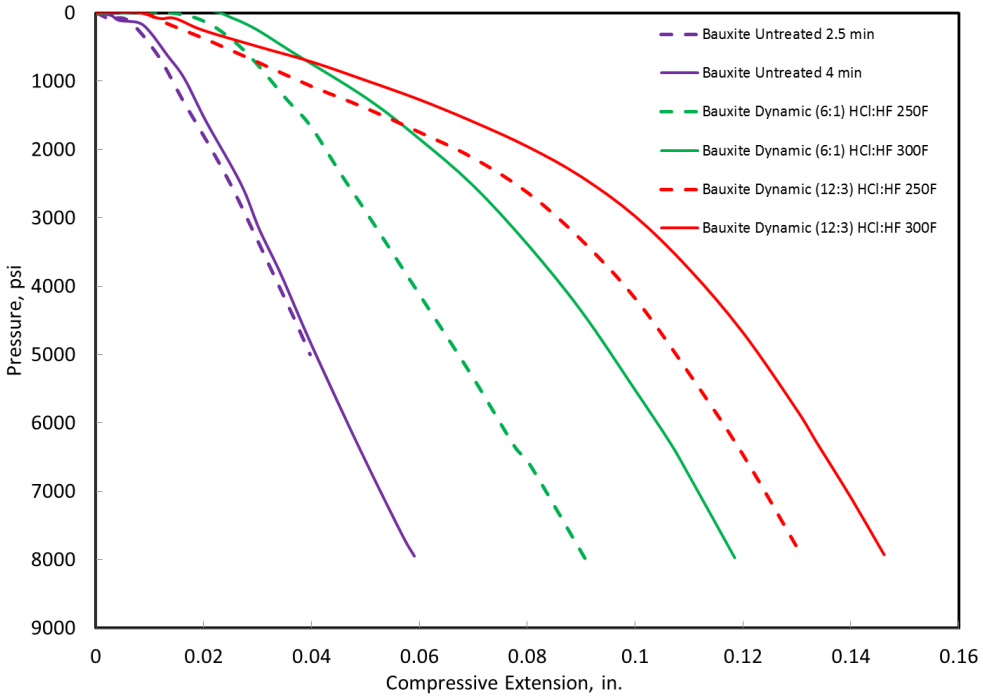

Fig. III- 31— Compaction of bauxite samples up to 8,000 psi at different conditions before and after the aging cell experiment with different HCl-based mud acid systems.

Conclusions

Studying proppant acid solubility is important because acids remove scale and clays from formations and gravel-packed wells, but they can also affect proppants present in fractures. In this part of the study, several tests were conducted to assess the effect of different acid systems on bauxite proppant solubility and mechanical properties. Based on the results obtained, the following conclusions can be drawn:

1. 10 wt% HCl and Na_3-HEDTA showed no adverse effect on bauxite proppant solubility.
2. Bauxite proppant showed less than 5 wt% loss at API conditions. Bauxite solubility also increased by increasing mud acid concentration and removing the corrosion inhibitor.

3. Bauxite proppant showed high dissolution with mud acids compared to HCOOH at 250 and 300°F, generally:
    - The amount of proppant dissolved increased under dynamic conditions and with the increase of soaking time and temperature, except for HCOOH.
4. When the mud acid concentration changed from (6:1) to (12:3), and the temperature reached 350°F, the following observations were noted:
    - The Dissolved proppant increased with acid concentration; the increase is negligible after soaking for a period of 3 hours.
    - The increase in dissolution is insignificant moving from 300 to 350°F.
    - At higher temperatures, silicon in solution decreased with time due to secondary and tertiary reactions. These reactions promote fines generation potentially hampering pack conductivity.
5. Sieve analysis of all samples tested with (6:1) mud acid showed that more than 90% of the particles retained their size.
6. The supernatant of solubility tests showed high concentrations of aluminum, iron, and relatively low concentrations of silicon and titanium due to their precipitation.
7. ^{19}F-NMR analysis for acid samples after solubility tests showed aluminum fluoride complexes.
8. XRD for particles after these experiments showed that some of the mullite and maghemite disappeared. Moreover, a small quantity of minerals that were poorly crystallized was dissolved. The dissolution increased with mud acid concentration.

9. Residual solids were rich in aluminum, silicon, iron, and titanium. The concentrations of silicon increased with soaking time because of precipitation.
10. The crushing tests showed a direct relationship between acid solubility and crush resistance, the following observations were noted:
    - The crush resistance depends on the type of acid used and decreased with the increase of mud acid concentration.
    - Compared to the untreated bauxite proppant, compaction varied between 10% for Na_3-HEDTA and 147% for (12:3) mud acid samples, respectively.

Different acids have a various substantial impact on bauxite proppants at elevated temperatures. As API solubility test is not representative of the reservoir conditions, caution should be exercised when considering these proppants for treatments. Minimizing contact time between bauxite proppant and mud acid solutions is recommended should the need for future treatment arises.

CHAPTER IV

CONCLUSIONS AND RECOMMENDATIONS

The objective of this work was to examine the different factors affecting the acid solubility for sand and ceramic proppants under downhole conditions and determine whether there is a relationship between acid solubility and crush resistance. In Chapter I, a brief introduction was given about hydraulic fracturing and gravel packing treatments. Different types of proppants used in the industry were also discussed including their main differences, how to choose the proper type of each treatment, and the best practices. Previous work showed that fines can migrate and get trapped in the gravel pack where permeability diminishes, resulting in lower formation productivity.

It is well documented that the composition and microstructure of proppants determine their chemical stability. Ceramic proppants consist of three major phases: corundum, mullite, and silica. These phases are chemically robust as they show different affinities towards acids.

Previous work should some contradictions. Some studies investigated the solubility of different proppants at relatively low temperatures but ignored its effects on crush resistance. Others studied both the solubility and compressive strength of gravel pack. Out of the latter, some showed a direct relationship between solubility and compressive strength while others stated that the solubility did not produce a concerning compressive strength loss. Moreover, some results showed that the other HF systems showed promising results in removing fines without negatively affecting the gravel pack.

In Chapter II, the solubility of sand and clay-based ceramic proppants was studied in regular mud acid. Clay-based proppants showed higher dissolution as HF attacked grain boundaries between cristobalite and mullite. Both proppants showed a high rate of dissolution at 250 and 300°F. The Dissolved proppant increased with the increase of temperature, soaking time, and dynamic conditions. API solubility test was not representative of the reservoir conditions. The regular mud acid soaking time (static conditions) does not have as significant of an effect on proppants as the injection time (dynamic conditions). Moreover, clay-based proppant did not maintain mechanical strength under acid exposure.

In Chapter III, the solubility of bauxite proppants was studied in in different acid systems. Bauxite proppant showed minimal solubility in HCl and Na_3-HEDTA acid systems. The proppant showed high dissolution with mud acid solutions compared to HCOOH at 250 and 300°F. Moreover, the crushing tests showed a direct relationship between acid solubility and crush resistance where compaction varied between 10% for Na_3-HEDTA and 147% for (12:3) mud acid samples.

Having studied the solubility of these proppants in different acid systems, we recommend the following:

i. Regular mud acid treatment should be avoided if ceramic proppants are present in the fracture.

ii. If an HCl-based mud acid treatment is needed, then minimizing acid/proppant contact time is essential.

iii. Weaker organic acids and chelating agents treatments can be used especially with bauxite proppant should the need for future treatment arises.

REFERENCES

Al-Dahlan, M. N., Nasr-El-Din, H. A., and Al-Qahtani, A. A. 2001. Evaluation of Retarded HF Acid Systems. Presented at the SPE International Symposium on Oilfield Chemistry, Houston, Texas, USA, 13–16 February. SPE-65032-MS. http://dx.doi.org/10.2118/65032-MS.

Al Moajil, A. M. and Nasr-El-Din, H. A. 2013. Formation Damage Caused by Improper Mn_3O_4-Based Filter-Cake-Cleanup Treatments. *J Can Pet Technol* **52** (1): 64–74. SPE-144179-PA. http://dx.doi.org/10.2118/144179-PA.

API RP 19C, Recommended Practice for Measurement of Proppants Used in Hydraulic Fracturing and Gravel Packing Operations, first edition (ISO 13503-2:2006, identical). 2008. Washington, DC: American Petroleum Institute.

API RP 60, Recommended Practices for Testing High Strength Proppants Used in Hydraulic Fracturing Operations. 1995. Washington, DC: American Petroleum Institute.

Belyadi, H., Fathi, E., and Belyadi, F. 2016. Proppant Characteristics and Application Design. In *Hydraulic Fracturing in Unconventional Reservoirs: Theories, Operations, and Economic Analysis*, first edition, ed. K. Hammon and K. Washington, Chap. 6, 73–96. Cambridge, Massachusetts, USA: Gulf Professional Publishing.

Brown, E., Thrasher, R. W., and Behrmann, L. A. 2000. Fracturing Operations. In *Reservoir Stimulation*, third edition, ed. M. J. Economides and K. G. Nolte, Chap. 11, 11-1–11-33. Chichester, West Sussex, England: John Wiley & Sons.

Browne, D. J. and Wilson, B. A. 2003. Proppant Flowback Control in Deviated Shallow Gas Wells. *J Can Pet Technol* **42** (11): 29–34. PETSOC-03-11-02. http://dx.doi.org/10.2118/03-11-02.

Cheung, S. K. 1988. Effects of Acids on Gravels and Proppants. *SPE Prod Eng* **3** (2): 201–204. SPE-13842-PA. http://dx.doi.org/10.2118/13842-PA.

Crowe, C. W. 1985. Evaluation of Agents for Preventing Precipitation of Ferric Hydroxide from Spent Treating Acid. *J Pet Technol* **37** (4): 691–695. SPE-12497-PA. http://dx.doi.org/10.2118/12497-PA.

Davis, S. and Devereux, T. 2007. Polyurethane Proppant Particle and Use Thereof. U.S. Patent No. 20070204992 A1.

Freeman, E. R., Anschutz, D. A., Renkes, J. J. et al. 2009. Qualifying Proppant Performance. *SPE Drill & Compl* **24** (1): 210–216. SPE-103623-PA. http://dx.doi.org/10.2118/103623-PA.

Fuss, T., Snyder, E. M., Herndon, D. C. et al. 2008. Influence of Acid Exposure upon Mechanical Strength of Ceramic Proppants, Margarita Island, Venezuela, SEFLUCEMPO.

Gaurav, A., Dao, E. K., and Mohanty, K. K. 2012. Evaluation of Ultra-Light-Weight Proppants for Shale Fracturing. *Journal of Petroleum Science and Engineering* **92–93** (0): 82–88. http://dx.doi.org/10.1016/j.petrol.2012.06.010.

Gidley, J. L., Holditch, S. A., Nierode, D. E., and Veatch, R. W. *Recent Advances in Hydraulic Fracturing*, Monograph Series, SPE, Richardson, Texas, December 1989, 1.

Grosheva, V. M. and Mironov, I. M. 1974. Solubility of Synthetic Mullite in Hydrofluoric Acid. *Refractories and Industrial Ceramics* **15** (3): 248–250. http://dx.doi.org/10.1007/BF01286274.

Gulbis, J. and Hodge, R. M. 2000. Fracturing Fluid Chemistry and Proppants. In *Reservoir Stimulation*, third edition, ed. M. J. Economides and K. G. Nolte, Chap. 7, 7-1–7-23. Chichester, West Sussex, England: John Wiley & Sons.

Hartman, R. L., Lecerf, B., Frenier, W. et al. 2006. Acid Sensitive Aluminosilicates: Dissolution Kinetics and Fluid Selection for Matrix Stimulation Treatment. *SPE Prod & Oper* **21** (2): 194–204. SPE-82267-PA. http://dx.doi.org/10.2118/82267-PA.

Hellmann, J. R., Scheetz, B. E., Luscher, W. G. et al. 2014. Proppants for Shale Gas and Oil Recovery: Engineering Ceramics for Stimulation of Unconventional Energy Resources. *American Ceramic Society Bulletin* **93** (1): 28–35.

Holditch, S. A. 2006. Tight Gas Sands. *J Pet Technol* **58** (6): 86–93. SPE-103356-JPT. http://dx.doi.org/10.2118/103356-JPT.

ISO 13503-2:2006, Petroleum and Natural Gas Industries—Completion Fluids and Materials—Part 2: Measurement of Properties of Proppants Used in Hydraulic Fracturing and Gravel Packing Operations. Geneva, Switzerland: ISO.

König, R., Scholz, G., Bertram, R. et al. 2008. Crystalline Aluminium Hydroxy Fluorides—Suitable Reference Compounds for ^{19}F Chemical Shift Trend Analysis of Related Amorphous Solids. *Journal of Fluorine Chemistry* **129** (7): 598–606. http://dx.doi.org/10.1016/j.jfluchem.2008.04.015.

Lacy, L. L., Rickards, A. R., and Bilden, D. M. 1998. Fracture Width and Embedment Testing in Soft Reservoir Sandstone. *SPE Drill & Compl* **13** (1): 25–29. SPE-36421-PA. http://dx.doi.org/10.2118/36421-PA.

Lehman, L. and Cannan, C. 2015. Compositions and Methods for Improving Proppant Conductivity. U.S. Patent No. 20160186050 A1.

Liang, D. T. and Readey, D. W. 1987. Dissolution Kinetics of Crystalline and Amorphous Silica in Hydrofluoric-Hydrochloric Acid Mixtures. *Journal of the American Ceramic Society* **70** (8): 570–577. http://dx.doi.org/10.1111/j.1151-2916.1987.tb05708.x.

Liang, F., Sayed, M., Al-Muntasheri, G. A. et al. 2016. A Comprehensive Review on Proppant Technologies. *Petroleum* **2** (1): 26–39. http://dx.doi.org/10.1016/j.petlm.2015.11.001.

Mahmoud, M. A., Nasr-El-Din, H. A., De Wolf, C. A. et al. 2011. Sandstone Acidizing Using A New Class of Chelating Agents. Presented at the SPE International Symposium on Oilfield Chemistry, The Woodlands, Texas, USA, 11–13 April. SPE-139815-MS. http://dx.doi.org/10.2118/139815-MS.

Mikeska, K. R. and Bennison, S. J. 1999. Corrosion of Alumina in Aqueous Hydrofluoric Acid. *Journal of the American Ceramic Society* **82** (12): 3561–3566. http://dx.doi.org/10.1111/j.1151-2916.1999.tb02279.x.

Nasr-El-Din, H. A. 2016. Additives for Acidizing Fluids: Their Function, Interactions, and Limitations. In *Acid Stimulation*, ed. S. A. Ali, L. J. Kalfayan, and C. T. Montgomery, Chap. 9, 203–238. Richardson, Texas, USA: Society of Petroleum Engineers.

Nguyen, P. D., Dusterhoft, R. G., Dewprashad, B. T. et al. 1998. New Guidelines for Applying Curable Resin-Coated Proppants. Presented at the SPE Formation Damage Control Conference, Lafayette, Louisiana, USA, 18–19 February. SPE-39582-MS. http://dx.doi.org/10.2118/39582-MS.

Nitters, G., Roodhart, L., Jongma, H. et al. 2000. Structured Approach to Advanced Candidate Selection and Treatment Design of Stimulation Treatments. Presented at the SPE Annual Technical Conference and Exhibition, Dallas, Texas, USA, 1–4 October. SPE-63179-MS. http://dx.doi.org/10.2118/63179-MS.

Palisch, T. T., Duenckel, R. J., and Wilson, B. 2015. New Technology Yields Ultrahigh-Strength Proppant. *SPE Prod & Oper* **30** (1): 76–81. SPE-168631-PA. http://dx.doi.org/10.2118/168631-PA.

Palisch, T. T. and Saldungaray, P. 2013. Understanding Ceramic Proppants: Are They All Created Equal? Paper presented at the SPE Middle East Unconventional Gas Conference and Exhibition, Muscat, Sultanate of Oman, 28–30 January. SPE-164042-MS. http://dx.doi.org/10.2118/164042-MS.

Penberthy, W. L. and Cope, B. L. 1980. Design and Productivity of Gravel-Packed Completions. *J Pet Technol* **32** (10): 1679–1686. SPE-8428-PA. http://dx.doi.org/10.2118/8428-PA.

Penberthy, W. L. and Echols, E. E. 1993. Gravel Placement in Wells. *J Pet Technol* **45** (7): 612–674. SPE-22793-PA. http://dx.doi.org/10.2118/22793-PA.

Ravensbergen, J., Misselbrook, J. G., and Portman, L. N. 2004. Method for cleaning gravel packs. U.S. Patent No. 6,832,655.

Raysoni, N. and Weaver, J. 2013. Long-Term Hydrothermal Proppant Performance. *SPE Prod & Oper* **28** (4): 414–426. SPE-150669-PA. http://dx.doi.org/10.2118/150669-PA.

Rickards, A. R., Lacy, L., Brannon, H. et al. 1998. Need Stress Relief? A New Approach to Reducing Stress Cycling Induced Proppant Pack Failure. Presented at the SPE Annual Technical Conference and Exhibition, New Orleans, Louisiana, USA, 27–30 September. SPE-49247-MS. http://dx.doi.org/10.2118/49247-MS.

Roberts, S. S., Binder, M. S., and Lane, R. H. 1990. Strength, Volume and Weight Loss of Gravels and Proppants due to HF-Based Acids. Presented at the SPE Formation Damage Control Symposium, Lafayette, Louisiana, USA, 22–23 February. SPE-20168-MS. http://dx.doi.org/10.2118/20168-MS.

Saucier, R. J. 1974. Considerations in Gravel Pack Design. *J Pet Technol* **26** (2): 205–212. SPE-4030-PA. http://dx.doi.org/10.2118/4030-PA.

Shuchart, C. E. and Buster, D. C. 1995. Determination of the Chemistry of HF Acidizing with the Use of ^{19}F NMR Spectroscopy. Presented at the SPE International

Symposium on Oilfield Chemistry, San Antonio, Texas, USA, 14–17 February. SPE-28975-MS. http://dx.doi.org/10.2118/28975-MS.

Sinclair, A. R., Graham, J. W., and Sinclair, C. P. 1983. Improved Well Stimulation with Resin-Coated Proppants. Presented at the SPE Production Operations Symposium, Oklahoma City, Oklahoma, USA, 27 February–1 March. SPE-11579-MS. http://dx.doi.org/10.2118/11579-MS.

Stanley, F. O., Troncoso, J. C., Martin, A. N. et al. 2000. An economic, Field-Proven Method for Removing Fines Damage from Gravel Packs. Presented at the SPE International Symposium on Formation Damage Control, Lafayette, Louisiana, USA, 23–24 February. SPE-58790-MS. http://dx.doi.org/10.2118/58790-MS.

Stephens, W. T., Schubarth, S. K., Dickson, K. R. et al. 2007. Behavior of Proppants Under Cyclic Stress. Presented at the SPE Hydraulic Fracturing Technology Conference, College Station, Texas, USA, 29–31 January. SPE-106365-MS. http://dx.doi.org/10.2118/106365-MS.

Stephens, W. T., Schubarth, S. K., Rivera, D. I. et al. 2006. Statistical Study of the Crush Resistance Measurement for Ceramic Proppant. Presented at the SPE Annual Technical Conference and Exhibition, San Antonio, Texas, USA, 24–27 September. SPE-102645-MS. http://dx.doi.org/10.2118/102645-MS.

Stephenson, C. J., Rickards, A. R., and Brannon, H. D. 2003. Is Ottawa Still Evolving? API Specifications and Conductivity in 2003. Presented at the SPE Annual Technical Conference and Exhibition, Denver, Colorado, USA, 5–8 October. SPE-84304-MS. http://dx.doi.org/10.2118/84304-MS.

Sur, S. K. and Bryant, R. G. 1996. ^{19}F and ^{27}Al NMR Spectroscopic Study of the Fluoro Complexes of Aluminum in Aqueous Solution and in Zeolites: Dealumination of Zeolites by Fluoride Ions. *Zeolites* **16** (2): 118–124. http://dx.doi.org/10.1016/0144-2449(95)00108-5.

Svendsen, O. B., Kleven, R., Hartley, I. P. R. et al. 1992. Stimulation of High-Rate Gravel-Packed Oil Wells Damaged by Clay and Fines Migration: A Case Study, Gullfaks Field, North Sea. Presented at the European Petroleum Conference, Cannes, France, 16–18 November. SPE-24991-MS. http://dx.doi.org/10.2118/24991-MS.

Taylor, K. C., Nasr-El-Din, H. A., and Al-Alawi, M. J. 1999. Systematic Study of Iron Control Chemicals Used During Well Stimulation. *SPE J.* **4** (3): 19–24. SPE-54602-PA. http://dx.doi.org/10.2118/54602-PA.

Terracina, J. M., Turner, J. M., Collins, D. H. et al. 2010. Proppant Selection and its Effect on the Results of Fracturing Treatments Performed in Shale Formations. Presented at the SPE Annual Technical Conference and Exhibition, Florence, Italy, 19–22 September. SPE-135502-MS. http://dx.doi.org/10.2118/135502-MS.

Thomas, R. L. and Suhy, F. A. 1979. Method of Treating a Well Using Fluoboric Acid to Clean a Propped Fracture. U.S. Patent No. 4,160,483.

Tso, S. T. and Pask, J. A. 1982. Reaction of Glasses with Hydrofluoric Acid Solution. *Journal of the American Ceramic Society* **65** (7): 360–362. http://dx.doi.org/10.1111/j.1151-2916.1982.tb10471.x.

Underdown, D. R., Sparlin, D. D., and Day, J. C. 1980. A Plastic Pre-Coated Gravel for Controlling Formation Sand. Presented at the Offshore South East Asia Show, Singapore, 26–29 February. SPE-8850-MS. http://dx.doi.org/10.2118/8850-MS.

Weaver, J. D. and Nguyen, P. D. 2010. Hydrophobic Filming Reduces Frac Gel and Mineral Scale Damage. Presented at the SPE Eastern Regional Meeting, Morgantown, West Virginia, USA, 13–15 October. SPE-138314-MS. http://dx.doi.org/10.2118/138314-MS.

Weaver, J. D., Parker, M., van Batenburg, D. W. et al. 2007. Fracture-Related Diagenesis May Impact Conductivity. *SPE J.* **12** (3): 272–281. SPE-98236-PA. http://dx.doi.org/10.2118/98236-PA.

Weaver, J. D., Rickman, R. D., and Luo, H. 2010. Fracture-Conductivity Loss Caused by Geochemical Interactions Between Man-Made Proppants and Formations. *SPE J.* **15** (1): 116–124. SPE-118174-PA. http://dx.doi.org/10.2118/118174-PA.

Welch, J. C. and Hossaini, M. 1996. Effect of Cleanup Acids on Compressive Strength of Proppants Used in Gravel Packing. Presented at the SPE Formation Damage Control Symposium, Lafayette, Louisiana, USA, 14–15 February. SPE-31133-MS. http://dx.doi.org/10.2118/31133-MS.

Wu, T., Wu, B., and Zhao, S. 2013. Acid resistance of silicon-free ceramic proppant. *Materials Letters* **92** (0): 210–212. http://dx.doi.org/10.1016/j.matlet.2012.10.124.

Wu, T., Zhou, J., and Wu, B., 2015. Effect of TiO_2 Content on the Acid Resistance of a Ceramic Proppant. *Corrosion Science* **98**: 716–724. http://dx.doi.org/10.1016/j.corsci.2015.06.012.

Yang, F., Nasr-El-Din, H. A., and Harbi, B. A. 2012. Acidizing Sandstone Reservoirs Using HF and Formic Acids. Presented at the SPE International Symposium and Exhibition on Formation Damage Control, Lafayette, Louisiana, USA, 15–17 February. SPE-150899-MS. http://dx.doi.org/10.2118/150899-MS.

Zahid, S., Bhatti, A. A., Khan, H. A. et al. 2007. Development of Unconventional Gas Resources: Stimulation Perspective. Presented at the Production and Operations Symposium, Oklahoma City, Oklahoma, USA, 31 March–3 April. SPE-107053-MS. http://dx.doi.org/10.2118/107053-MS.

Zhou, L. and Nasr-El-Din, H. A. 2015. Phosphonic-Based Hydrofluoric Acid: Interactions with Clay Minerals and Flow in Sandstone Cores. *SPE J.* **21** (1): 264–279. SPE-164472-PA. http://dx.doi.org/10.2118/164472-PA.

Ziauddin, M. 2016. Acidizing Chemistry. In *Acid Stimulation*. ed. S. A. Ali, L. J. Kalfayan, and C. T. Montgomery, Chap. 3, 43–84. Richardson, Texas, USA: Society of Petroleum Engineers.

Zoveidavianpoor, M. and Gharibi, A. 2015. Application of Polymers for Coating of Proppant in Hydraulic Fracturing of Subterraneous Formations: A Comprehensive Review. *Journal of Natural Gas Science and Engineering* **24**: 197–209. http://dx.doi.org/10.1016/j.jngse.2015.03.024.